2007-06-20

Identification and Characterization of Agv1, a Pre-Metazoan Arf GAP: A Dissertation

Kimberly Renee Long
University of Massachusetts Medical School

Identification and characterization of Agv1, a pre-metazoan Arf GAP

A Dissertation Presented

By

Kimberly Renee Long

Submitted to the Faculty of the University of Massachusetts Graduate School of Biomedical Sciences, Worcester

DOCTOR OF PHILOSOPHY

(June 20, 2007)

Molecular Genetics and Microbiology

COPYRIGHT

IDENTIFICATION AND CHARACTERIZATION OF AGV1P, A PRE-METAZOAN ARF GAP ANCESTRAL PARALOG

A Dissertation Presented
By
Kimberly Renee Long

Approved as to style and content by:

_____
Allan Jacobson Ph.D., Chair of Committee

_____
Reid Gilmore, Ph.D., Member of Committee

_____
Dannel McCollum, Ph.D., Member of Committee

_____
Peter Pryciak, Ph.D., Member of Committee

_____
Charles Hoffman, Ph.D., Member of Committee

_____
Maria L. Zapp, Ph.D., Thesis Advisor

_____
Anthony Carruthers, Ph.D.
Dean of the Graduate School of Biomedical Sciences

Program in Molecular Genetics and Microbiology

June 20, 2007

ACKNOWLEDGEMENTS

I am fortunate to have so many mentors, teachers, colleagues, and friends to thank for their contributions to my graduate work. I would foremost like to thank my mentor, Maria Zapp, for her total support, endless patience, and constructive criticism during my time in her laboratory. Her passion for science not only caught my attention immediately, but also fostered an all encompassing environment that was nurturing for both personal and professional growth.

I would not have been successful in my thesis work without the help and support of past and present members of the Zapp laboratory; Ellen Kittler, Enyeneama Udofia, Irina Catrina, Zhong Yu, Adonia Lee, Tracy Schmidt, Lynn Kerr, Juan Sánchez-Torres, and Seth Shatkin-Margolis. I would especially like to thank Ellen Kittler for encouragement and support of my research, answers to my many scientific questions, help with bioinformatics, valuable advice about life in general, and tough love whenever I needed a reality check. I would also like to specifically thank Irina Catrina and Tracy Schmidt for reading and constructive criticism of this written thesis. What became my thesis project was initiated in the lab prior to my arrival. In order to best present the complete project, I have included some of the work of collaborating laboratory members in my thesis. In Chapter 2, Ellen Kittler is responsible for the cloning of the *agv1*$^{+}$ gene from *S. pombe* and Seth Shatkin-Margolis is responsible for the generation of the *agv1* heterozygous diploid and for the *agv1* mutagenesis PCR.

There are multiple UMASS CORE facilities that were instrumental in completing my thesis research. I would specifically like to thank Greg Hendricks and John Nunnari of the University of Massachusetts Core Electron Microscopy Facility for technical advice and assistance with transmission electron microscopy; Stephen Baker and David Lapointe of the University of Massachusetts Bioinformatics Group for help with statistical analysis and phylogenetic analysis, respectively; and Ellen Kittler and Lynn Kerr of the University of Massachusetts Center For AIDS Research Molecular Biology Core for oligonucleotides and automated DNA sequencing. Elisabet Mandon, Nick Rhind and Mary Munson also offered valuable advice and critical evaluation of my research.

I would like to thank the members of my thesis research advisory committee, Allan Jacobson, David Lambright, Dannel McCollum, Peter Pryciak, and Reid Gilmore for their insight and critical evaluation of my research. I would also like to thank Charles Hoffman for his time and effort in completion of this thesis.

Finally, I would like to thank my family and friends whose love and support helped me through my entire graduate career.

ABSTRACT

Human immunodeficiency virus type 1 (HIV-1) is a member of the lentivirus subfamily of retroviruses. HIV-1 expresses multiple genes from a single provirus by alternative splicing. Early in viral expression, fully spliced 2-kb viral RNA is exported from the nucleus and encodes the viral regulatory protein, Rev, which is essential for nuclear transport of partially spliced and unspliced genomic-length RNA. Rev binds to an RNA structural element called the Rev response element (RRE) and mediates nuclear export through the leucine-rich nuclear export signal (NES) pathway. The human Rev Interacting Protein (hRIP) interacts specifically with the Rev NES. Rev NES mutants that are unable to export Rev-dependent RNAs are also unable to bind to hRIP. The hRIP cDNA encodes a 562 amino acid protein containing an N-terminal zinc finger with homology to Arf GAP domains, a central serine and threonine rich region, and C-terminal phenylalanine-glycine (FG) repeats characteristic of nucleoporins.

To identify an hRIP ortholog in a genetically tractable organism, we performed database searches using the N-terminal zinc finger of hRIP. Using this approach, we identified a novel gene in *Schizosaccharomyces pombe*. Alignment of the entire reading frame of the putative ortholog with hRIP indicates similarity with the serine/threonine rich region and with the FG repeats,

suggesting that *S. pombe* could be a good model system to study the cellular function of hRIP.

We find that the *S. pombe* ORF is an essential gene, which encodes a 483 amino acid protein that is also able to interact with the NES of HIV-1 Rev. Based on being an essential gene, and the presence of a putative Arf GAP domain, the ORF was named an Arf GAP essential for viability, *agv1*$^{+}$. We show that Agv1 is not directly involved in the nuclear export of poly(A^{+}) RNA or 5S rRNA, nuclear export of leucine-rich NES-containing proteins, or nuclear import of nuclear localization signal (NLS)-containing proteins. However, Agv1 does appear to play a role in the cytoplasmic localization of 5S rRNA.

We demonstrate that loss of Agv1 alters the localization of endoplasmic reticulum (ER) membrane and Golgi membrane resident proteins, accumulates intracellular membrane, and blocks processing of carboxypeptidase Y. Furthermore, the *S. cerevisiae* ADP-ribosylation factor (Arf) GTPase activating protein (GAP) Glo3, but not a catalytically inactive Glo3 mutant [R59K], is able to partially compensate for the loss of Agv1 function in temperature sensitive strains, indicating that Agv1 is an *S. pombe* Arf GAP with some functional features similar to *S. cerevisiae* Glo3.

TABLE OF CONTENTS

LIST OF TABLES

LIST OF FIGURES

LIST OF ABBREVIATIONS

5-FOA	5-Fluoroorotic Acid
ADP	Adenosine Diphosphate
AGE2	Arf GAP Effector 2
AGV1	ArfGAP Essential for Viability 1
ALP	Alkaline Phosphatase
ALPS	ArfGAP1 Lipid Packing Sensor
AP-1	Adaptor Protein Complex 1
AP-2	Adaptor Protein Complex 2
ARF	ADP Ribosylation Factor
ARM	Arginine Rich Motif
ATP	Adenosine Triphosphate
BAR	Bin/Amphiphysin/Rvs Domain
BFA	Brefeldin A
BLAST	Basic Local Alignment Search Tool
BSA	Bovine Serum Albumin
CA	Capsid
CAT	Chloramphenicol Acetyltransferase
cDNA	Complementary Deoxyribonucleic Acid
CMV	Cytomegalovirus
COP	Coatomer Protein
CPY	Carboxypeptidase Y
CRM1	Chromosomal Region Maintenance 1
DAPI	4',6-diamidino-2 phenylindole
DMEM	Dulbecco's Modified Eagle's Medium
DNA	Deoxyribonucleic Acid
ECL	Enhanced Chemiluminescence
EGFP	Enhanced Greed Fluorescent Protein
EGFR	Epidermal Growth Factor Receptor
EH	Eps15 Homology Domain
EMM	Edinburgh Minimal Medium
ER	Endoplasmic Reticulum
ERD2	ER Retention Defective Complementation Group 2
ERGIC	ER-Golgi Intermediate Compartment
Eps15	EGFR pathway Substrate Protein Clone no. 15
FBS	Fetal Bovine Serum
FG	Phenylalanine – Glycine Repeat Motif
FM4-64	N-(3-triethylammoniumpropyl)-4-(ρ-diethylaminophenyl-hexatrienyl) pyridium dibromide
GAP	GTPase Activating Protein

GCS1	Growth Cold Sensitive
GDP	Guanosine Diphosphate
GEF	GTPase Exchange Factor
GFP	Green Fluorescent Protein
GLO3	Gcs1-like ORF
GMA12	Galactomannan, alpha 1,2
GPI	Glycosylphosphatidylinositol
GST	Glutathione S-Transferase
GTP	Guanosine Triphosphate
HA	Hemagglutinin A
HIV-1	Human Immunodeficiency Virus Type 1
HRB	Human Rev Binding Protein
hRIP	Human Rev Interacting Protein
HRO1	Human RIP Ortholog
IκB	Inhibitor of nuclear factor κB
IN	Integrase
kb	Kilobase
kDa	Kilodalton
KDEL	Lysine – Aspartate – Glutamate – Leucine Signal Motif
LMB	Leptomycin B
LTR	Long Terminal Repeat
MA	Matrix
MAPKK	Mitogen Activated Protein Kinase Kinase
ME	Malt Extract
MLV	Murine Leukemia Virus
NC	Nucleocapsid
NES	Nuclear Export Signal
NFκB	Nuclear Factor κB
NLS	Nuclear Localization Signal
NMT	No Message in Thiamine
NPF	Aspartate– Proline – Phenylalanine Repeat Motif
NRE	Negative Regulatory Element
NUP	Nucleoporin
OD	Optical Density
ORF	Open Reading Frame
PAB1	Poly A Binding Protein 1
PBS	Phosphate Buffered Saline
PCR	Polymerase Chain Reaction
P_i	Inorganic Phosphate
PI	Phosphoinositide
PKI	Protein Kinase Inhibitor
PM	Plasma Membrane

PR	Protease
PROMALS	PROfile Multiple Alignment with predicted Local Structure
PSI-BLAST	Position-Specific Iterated BLAST
PSIPRED	Protein Secondary Structure Prediction
PTAP	Proline-Threonine-Alanine-Proline Motif
RAB	Rev/Rex Activation Domain Binding
RAE1	Ribonucleic Acid Export 1
RIP1	Rev-Interacting Protein 1
RNA	Ribonucleic Acid
RRE	Rev Response Element
RT	Reverse Transcriptase
SAR1	Secretion-Associated and Ras-Related
SC	Sodium Cacodylate Buffer
SNARE	Soluble NSF Attachment Receptor
SNS	Septated Not in S Phase
TBST	Tris/Sodium Chloride/Tween 20 Buffer
TEM	Transmission Electron Microscopy
TGN	*trans* Golgi Network
TS	Temperature Sensitive
TSG101	Tumor Susceptibility Gene
VPS	Vacuolar Protein Sorting
VSV	Vesicular Stomatitis Virus
VTC	Vesicular-Tubular Clusters
WT	Wild-type
XPO1	Exportin 1
YES	Yeast Extract with Supplements
YNB	Yeast Nitrogen Base

CHAPTER I

GENERAL INTRODUCTION

Human Immunodeficiency Virus Type 1

Human immunodeficiency virus type 1 (HIV-1) is a complex retrovirus, which infects a cell by the binding of its surface glycoprotein, gp120, to cell surface receptors. The virion fuses with the membrane releasing the viral core into the cytoplasm. Genomic viral RNA is reverse transcribed in the cytoplasm and the resulting proviral DNA is imported into the nucleus where it integrates into the host cell chromosome, forming a proviral DNA template for transcription (reviewed in Frankel and Young, 1998). HIV-1 expresses multiple genes from a single provirus by alternative splicing (reviewed in Pollard and Malim, 1998). Fully spliced viral RNA is exported to the cytoplasm via the cellular mRNA export pathway (reviewed in Frankel and Young, 1998). The fully spliced RNA transcript encodes the regulatory protein Rev, which is imported into the nucleus. Rev binds to an RNA structural element called the Rev Response element (RRE) present in all partially spliced or unspliced genomic length viral RNA (Malim *et al*, 1998a). Rev contains a nuclear export signal (NES), which is required for nuclear export of partially spliced and unspliced viral RNA (Felber *et al*, 1989) via the CRM1-dependent export pathway normally used by cellular proteins as well as 5S rRNA (Fridell *et al*, 1996; Fischer *et al*, 1995). Env is translated in the

endoplasmic reticulum and transported to the plasma membrane resulting in its glycoproteins, gp120 and gp41, becoming embedded on the cell surface. Gag and Gag-Pol polyproteins are translated in the cytoplasm and through protein-protein and protein-RNA interactions assemble into the virion core particle at the cell surface causing the membrane to bend and form a viral bud. After the bud is released, protease cleaves the Gag and Gag-Pol polyproteins generating a mature virion capable of infecting another cell (Figure 1-1; reviewed in D'Souza and Summers, 2005; Frankel and Young, 1998; and Pollard and Malim, 1998).

Rev

Rev is a 116 amino acid protein with two distinct domains. The N-terminal portion is an arginine-rich RNA-binding domain as well as a nuclear localization signal (NLS). The C-terminal domain contains a leucine-rich nuclear export signal (NES) and is known as the effector/activation domain (reviewed in Pollard and Malim, 1998). A mutation in the leucine rich Rev NES (M10) has a completely nuclear localization (Malim *et al*, 1989b) and fails to export RNA (Meyer and Malim 1994). Due to the fact that leucine-rich NES domains from cellular proteins can functionally substitute for the Rev NES (Fritz and Green 1996) and that Rev can shuttle between the nucleus and the cytoplasm, the Rev NES was predicted to interact with cellular cofactors involved in receptor-mediated export pathways (Pollard and Malim 1998).

human Rev Interacting Protein

A yeast two-hybrid screen to identify cellular factors that interact with the Rev NES, identified the human Rev Interacting Protein [hRIP; also known as the Rev/Rex activation domain binding protein (Rab) or the HIV-1 Rev Binding Protein (HRB); the official Entrez gene name is HRB; the official GeneID is 3267; (Fritz *et al*, 1995; Bogerd *et al* 1995)]. The isolated hRIP cDNA encodes a 562 amino acid protein containing an N-terminal zinc finger with homology to *S. cerevisiae* proteins Gcs1 and Sps18, a central serine-threonine rich region, C-terminal FG repeats characteristic of nucleoporins, and C-terminal NPF repeat motifs, which interact with EH domains (Bogerd *et al*, 1995, Fritz *et al*, 1995, Salcini *et al*, 1997). Previously described Rev-activation domain mutants (Malim *et al*, 1991) were tested for binding to hRIP and a correlation was found between the loss of binding to hRIP and loss of Rev function (Fritz *et al*, 1995; Bogerd *et al*, 1995). Additional yeast two-hybrid analyses using truncated versions of hRIP narrowed the interaction site to the C-terminal portion of hRIP containing the FG repeats (Fritz *et al*, 1995) but did not determine whether the interaction was direct or indirect.

Recent data has shown that an overexpression of a *trans* dominant-negative hRIP mutant (hRIPΔN360) lacking the N-terminal zinc finger and a portion of the central serine/threonine rich region results in an accumulation of

Rev-directed RNAs at the nuclear periphery. Depletion of endogenous hRIP by RNA interference also causes an accumulation of Rev-directed RNAs at the nuclear periphery and a failure to support Rev function suggesting a role for hRIP in movement of RNA from the perinuclear region into the cytoplasm (Sánchez-Velar *et al*, 2004). Additionally, hRIPΔN360 overexpression as well as depletion of hRIP by RNA interference promotes the accumulation of viral RNA at the nuclear periphery and inhibits HIV-1 production in human T cell lines and primary macrophages, confirming that hRIP is required for HIV-1 viral replication (Yu *et al*, 2005). These studies indicate that hRIP plays a role in movement of HIV-1 viral RNA from the nuclear periphery to the cytoplasm.

hRIP has also been shown to interact with a component of the endocytic pathway, the epidermal growth factor receptor (EGFR) pathway substrate protein clone no. 15 (Eps15). Eps15 contains a protein-protein interaction domain called the Eps15 homology (EH) domain, which interacts with the aspartate-proline-phenylalanine (NPF) motifs at the C-terminus of hRIP (Salcini *et al*, 1997). Additionally, hRIP co-localizes with Eps15 in punctate spots in the cytoplasm suggesting a link between nucleocytoplasmic transport and the endocytic pathway (Doria *et al*, 1999).

Additionally, male hRIP$^{-/-}$ mice are sterile and have round-headed spermatid with no visible acrosome structures. Ultrastructural analysis shows a normal accumulation of small proacrosomal vesicles, which are unable to fuse

with each other to form a single large acrosomic vesicle, suggesting a defect in docking or fusion of proacrosomic vesicles. Immunogold labeling of hRIP in wild-type mice shows hRIP localizes on the cytosolic surface of proacrosomic vesicles and on the outer membrane of the acrosomic vesicle. Proacrosomic vesicles in wild-type mice were found to contain hRIP, Eps15 and the heterotetrameric adaptor protein (AP) AP-1. However, hRIP$^{-/-}$ mice do not show any overlap of Eps15 and AP-1 on the proacrosomic vesicles, suggesting that Eps15 positive vesicles and AP-1 positive vesicles are unable to fuse (Kang-Decker *et al*, 2001).

These more recent findings, in addition to the similarity of the hRIP zinc finger to the zinc finger of *S. cerevisiae* Gcs1 (Fritz *et al*, 1995), which has been shown to be a GTPase activating protein (GAP) for adenosine diphosphate (ADP)- ribosylation factor (Arf1; Poon *et al*, 1996), suggest a possible role for hRIP in intracellular membrane trafficking. In fact, the structure of the hRIP zinc finger domain has been recently determined and found to be an Arf GAP domain (http://www.pdb.org/pdb/explore/explore.do?structureId=2OLM).

Western blot analysis of cellular protein extracts of mammalian, avian, amphibian, and invertebrate origin using affinity purified rabbit antiserum to hRIP shows a predominant band of approximately 60kDa in all species examined (Bogerd *et al*, 1995), indicating that an hRIP ortholog is evolutionarily conserved across species. This conservation suggests the possibility of finding a genetically tractable model system, which can also express HIV-1 genes, in order

to study the molecular mechanisms and cellular factors involved in the post-transcriptional regulation of HIV-1 gene expression. *S. cerevisiae* was originally thought to have an hRIP ortholog. A Rev interacting protein (Rip1) was identified in a yeast two-hybrid screen of *S. cerevisiae* proteins. However, unlike hRIP, Rip1 does not contain an N-terminal zinc finger domain and has a punctate nuclear rim localization, suggesting an association with the nuclear pore (Stutz *et al*, 1995). Further studies revealed that mutations in the nuclear pore protein Nup85 are lethal in the absence of Rip1, indicating that Rip1 is a component of the nuclear pore (Stutz *et al*, 1997). Rip1 has officially been named Nucleoporin 42 (Nup42; reviewed in Fabre and Hurt, 1997).

S. pombe as a possible model system

Due to the lack of an hRIP ortholog in budding yeast, it was necessary to identify another genetically tractable organism as a model system. Our database searches for putative homologs of hRIP using the N-terminal zinc finger domain identified a possible ortholog in the fission yeast *Schizosaccharomyces pombe*. *S. pombe* is a unicellular eukaryote that exists as a haploid organism, allowing for easy genetic manipulation and the generation of mutants. *S. pombe* has cellular properties that make it more reminiscent than *S. cerevisiae* of metazoans. *S. pombe* divides by medial fission and maintains an intact nuclear envelope throughout mitosis (Moreno *et al*, 1991). Fission yeast have also been shown to

properly splice mammalian introns (Kaufer *et al*, 1985), suggesting conservation of cellular processes. In addition, *S. pombe* has fewer predicted genes than *S. cerevisiae*, contains introns in many genes, and has no apparent genome duplication event, reducing the possibility of functional redundancy (Wood *et al*, 2002).

Fission yeast has also been used in the study of nuclear protein export or RNA export due to the identification of *S. pombe* homologs of key factors implicated in these processes in both budding yeast and mammalian cells. For example, the chromosomal region maintenance (*crm1*) gene was originally isolated as a cold-sensitive *S. pombe* mutant with visible fibrous or rod like condensed chromosome segments. *Crm1*$^{+}$ was cloned and encodes a 1,077 amino acid protein with a predominantly nuclear and perinuclear localization (Adachi and Yanagida, 1989). Crm1 has been shown to interact with the NES of cellular proteins and loss of Crm1 function in a cold-sensitive strain (*crm1-809*) at restrictive temperature results in an accumulation of a cellular NES-containing protein (Dsk1) in the nucleus (Fukuda *et al*, 1997). These findings were extended by localization studies of GST-NES_{Rev}-GST and GST-NLS_{SV40}-GST fusion proteins in fission yeast. GST-NES_{Rev}-GST and GST-NLS_{SV40}-GST localize to the cytoplasm and nucleus, respectively, in wild-type fission yeast, suggesting the constructs are functional reporters. Growth of the *crm1-809* mutant strain at restrictive temperature causes an accumulation of GST-NES_{Rev}-GST in the

nucleus. Localization of GST-NLS_{SV40}-GST remains nuclear, suggesting the *crm1-809* mutant is defective in nuclear protein export but not nuclear protein import in fission yeast (Kudo *et al*, 1998).

Screening of a collection of *S. pombe* conditional mutants for defects in nucleocytoplasmic transport of poly(A)$^+$ RNA, identified ribonucleic acid export (*rae1*$^+$). Within 30 minutes at the restrictive temperature of 36°C, 100% of the *rae1-1* cells accumulate poly(A)$^+$ RNA in the nucleus (Brown *et al*, 1995). Expression of a CMV-promoter driven human RAE1 cDNA in a *rae1-1* temperature sensitive strain, partially suppresses the temperature sensitivity and increases poly(A)$^+$ RNA export (Bharathi *et al*, 1997). These studies suggest that nuclear protein import and export as well as mRNA export function similarly in fission yeast and mammalian cells and provide established reagents necessary for studying these pathways in fission yeast.

Additionally, fission yeast has been used to study the function of other HIV-1 encoded proteins and to assay *cis*- and *trans*-acting requirements for HIV-1 viral gene expression. Study of HIV-1 *Vpr* expression in fission yeast determined similar functions for Vpr compared with those established for Vpr in human cells, suggesting *S. pombe* is a good model system for study of HIV-1 encoded proteins (Zhao *et al*, 1996). Studies assaying for chloramphenicol acetyltransferase (CAT) activity have also established that the HIV-1 LTR is functional for transcription in fission yeast (Toyama *et al*, 1992).

Taken together, these studies suggest that *S. pombe* makes an attractive model organism for the study of cellular factors required for HIV-1 viral replication. The existence of an hRIP ortholog in *S. pombe* would significantly enhance the ability to analyze the cellular function of hRIP. Furthermore, establishment of an assay for Rev-directed RNA export in fission yeast would generate a useful system for studying transport in a genetic system more similar to mammals than is budding yeast.

Intracellular Trafficking/ Adenosine diphosphate (ADP)-ribosylation factors (Arfs)

Cells must coordinate traffic of macromolecules among a network of membrane bound organelles. Intracellular trafficking, which is necessary for secretion of proteins, endocytosis, and biogenesis of plasma membranes, endosomes, and lysosomes, is mediated by the budding and fusion of transport vesicles. Using a cell-free biochemical approach, transport of the G protein of vesicular stomatitis virus (VSV) between Golgi cisternae can be reconstituted *in vitro* by incubating Golgi membranes with cytosol and adenosine triphosphate (ATP). Electron microscopy analysis suggested that coated vesicles, which contain VSV-G and only appear when cytosol and ATP were added to the Golgi membranes, mediate transport. The non-hydrolyzable guanosine triphosphate (GTP) analog, GTPγS, blocks transport between Golgi cisternae in this assay and

electron microscopy shows the accumulation of coated vesicles suggesting that the vesicles must uncoat before fusing to an acceptor membrane. Purification of the coated vesicles generated eight polypeptides: Adenosine diphosphate (ADP)-ribosylation factor (Arf1), and seven subunits of the coat protein (COP) complex. Arf and coatomer are cytosolic proteins, suggesting they must co-assemble on the Golgi membrane to form vesicles (reviewed in Rothman, 1994).

ADP-ribosylation factor (Arf) was originally identified as a membrane-bound cofactor for cholera toxin-dependent ADP ribosylation of the stimulatory regulatory component (G_s) of adenylate cyclase. Arf binds guanine nucleotides but does not hydrolyze measurable amounts of GTP in optimal conditions (Kahn and Gillman, 1986). Early studies indicate that Arf can bind to membranes in the absence of coatomer in a GTP dependent manner. However, coatomer is unable to bind to membranes in the absence of membrane bound Arf-GTP, suggesting that Arf provides binding sites for coatomer. An Arf mutant, which is able to bind but not hydrolyze GTP, also inhibits transport and accumulates coated vesicles in the cell free reconstitution assay, suggesting that GTP hydrolysis is required for the uncoating of vesicles. The coated vesicles are also unable to fuse with acceptor Golgi membranes, further suggesting that uncoating of vesicles is required for fusion with target membranes (reviewed in Rothman 1994).

Identification of Arf regulatory proteins confirmed that controlled binding and hydrolysis of GTP are required for Arf function. A guanine nucleotide

exchange factor (GEF) catalyzes the exchange of GDP for GTP converting the Arf to an active membrane associated GTP-bound state. A GTPase-activating protein (GAP) catalyzes the hydrolysis of GTP, returning the Arf to an inactive cytosolic GDP-bound state (Figure 1-2; Moss and Vaughan, 1998).

Arfs are highly conserved, ubiquitously expressed, and have been found in all eukaryotes examined. Six mammalian Arfs have been identified and divided into three classes based on amino acid sequence identity. Arf1, Arf2, and Arf3 are Class I Arfs, which have been shown to localize to the Golgi and to play a role in assembly of COPI coat complexes on the Golgi, clathrin-AP1 complexes on the TGN, and clathrin AP3 complexes on endosomes. Arf4 and Arf5 are Class II Arfs, which are not well characterized but have a similar localization and function as Class I Arfs. Arf6 is a Class III Arf, which functions in endocytosis and exocytosis at the plasma membrane (Nie *et al*, 2003; D'Souza-Schorey and Chavrier, 2006). Multicellular organisms have at least one member of each class of Arfs. The protist *Giardia lamblia* also has six Arf proteins suggesting an early eukaryotic origin for Arf family members (D'Souza-Schorey and Chavrier 2006). Both *S. cerevisiae* and *S. pombe* contain Class I and Class III, but not Class II Arfs (Donaldson and Honda 2005). *S. cerevisiae* has three characterized Arf proteins, of which Arf1 and Arf2 are Class I Arfs and constitute an essential pair (Stearns *et al.*, 1990). *S. cerevisiae* Arf3 is a Class III Arf. *S. pombe* Arf1 is a

Class I Arf (Erickson *et al*, 1993). The completed *S. pombe* genome predicts a second Arf, Arf2, which would be a Class III Arf (Wood *et al*, 2002).

Arf GTPase Activating Proteins (Arf GAPs)

GTPase-activating proteins (GAPs) catalyze the hydrolysis of GTP, returning Arf to an inactive GDP-bound state and, in the classic model of membrane traffic, regulate the disassembly and dissociation of vesicle coats. All identified Arf GAPs contain a conserved zinc finger motif, $C\text{-}X_2\text{-}C\text{-}X_{16\text{-}17}\text{-}C\text{-}X_2\text{-}C$, which was first shown to be essential for GAP function in rat Arf1GAP/ArfGAP1 (Cukierman *et al*, 1995). The characteristic Arf GAP catalytic domain also contains an invariant arginine residue positioned five residues after the 4th cysteine generating the more specific zinc finger motif of $C\text{-}X_2\text{-}C\text{-}X_{16\text{-}17}\text{-}C\text{-}X_2\text{-}C\text{-}X_3\text{-}HR\text{-}X_4\text{-}H$. Mutation of this invariant arginine residue to a lysine residue in mammalian and *S. cerevisiae* Arf GAPs results in a significant decrease in GTPase activity, indicating the invariant arginine is essential for Arf GAP activity (Mandiyan *et al*, 1999; Randazzo *et al*, 2000; Yanagisawa *et al,* 2002; Lewis *et al,* 2004).

Multiple proteins containing Arf GAP domains have been identified and can be divided into families based on their secondary structure and functional domains: ArfGAP1; GIT; ASAP; ACAP; ARAP; and AGAP. The known mammalian members of these families are diagrammed in Figure 1-3 (reviewed

in Nie and Randazzo, 2006). The presence of additional catalytic domains and protein-protein interaction domains suggest additional Arf independent functions for Arf GAPs. hRIP shares sequence homology and putative structural domains with the ArfGAP1 family of Arf GAPs (Figure 1-3). In addition to the mammalian ArfGAP1 and ArfGAP3 proteins, the *S. cerevisiae* proteins, Gcs1, Glo3, and Age2 also belong to the ArfGAP1 family. Many members of the ArfGAP1 family of Arf GAPs have been well studied.

S. cerevisiae Arf GAP, Gcs1

The growth cold sensitive (*gcs1*) mutant was first isolated in a screen for cold-sensitive *S. cerevisiae* cell cycle mutants. The *gcs1-1* mutant was found to be conditionally defective for reentry into the cell cycle from stationary phase (Drebot *et al*, 1987). Sequence analysis of the *gcs1-1* mutant showed a cysteine to tyrosine mutation in the zinc finger motif suggesting the finger is essential for Gcs1 function. Cloning of the *GCS1* gene indicated a 352 amino acid protein containing a zinc finger structure in the N-terminal portion of the protein (Ireland *et al*, 1994). Purified wild-type Gcs1 stimulates the GTPase activity of *S. cerevisiae* Arf1 and Arf2 in an *in vitro* GAP assay (Poon *et al*, 1996) and has been shown to have overlapping function with two other *S. cerevisiae* Arf GAPs, Glo3 and Age2 (Poon *et al*, 1999; Poon *et al*, 2001). Gcs1 does not interact with COPI coat components and its GAP activity is not stimulated by the addition of

coatomer in GAP assays using full-length Golgi-membrane bound Arf1 (Eugster *et al*, 2000; Szafer *et al*, 2001). However, Gcs1 does interact with post-Golgi v-SNAREs that mediate endocytosis and exocytosis, in a GAP domain independent manner. The v-SNAREs also co-localize with Gcs1 at the late Golgi and endosomal compartments, suggesting that in addition to post-Golgi sorting, Gcs1 plays a role in recycling from the endosome back to the Golgi (Robinson *et al*, 2006).

Mammalian Arf GAP, ArfGAP1

An Arf1 GAP was first isolated through purification from rat liver cytosol by chromatography resulting in a 49kDa protein, which retains *in vitro* Arf GAP activity (Makler *et al*, 1995). The cloned cDNA sequence determined the Arf1 GAP encodes a 415 amino acid protein, which contains an N-terminal $CX_2CX_{16}CX_2C$ zinc finger motif with a high degree of similarity to *S. cerevisiae* Gcs1, Glo3, and Sps18. N-terminal truncation of the zinc finger motif or substitution of conserved cysteine residues with alanine residues result in loss of Arf GAP activity, suggesting the zinc finger is the 'catalytic' domain (Cukierman *et al*, 1995). Based on reconstitution experiments that block GTP hydrolysis using GTPγS or a mutant form of Arf1, Arf GAPs are classically believed to antagonize coat recruitment during vesicle formation, suggesting that Arf GAPs trigger vesicle uncoating. However, recent data suggests a larger role for ArfGAP1

(renamed from Arf1 GAP) in coat recruitment, vesicle formation, cargo sorting, and membrane curvature sensitivity.

Two-stage reconstitution assays using GTP produce COPI coated vesicles, which quickly lose their coat after formation. Use of GTPγS in the two-stage reconstitution assay results in a block in vesicle formation, suggesting that in addition to uncoating, GTP hydrolysis is also necessary for vesicle formation (Yang at el, 2002). Additionally, studies indicate that ArfGAP1 plays a role in cargo sorting by interacting directly with the cytoplasmic domain of the receptor for the lysine-aspartate–glutamate–leucine (KDEL) soluble protein ER retention signal motif. Two-stage reconstitution assays using Golgi membranes isolated from cells stably expressing a myc-tagged KDEL receptor and GTPγS, display an inhibition in cargo sorting to vesicles and indicate that ArfGAP1 is required for efficient cargo sorting. Moreover, vesicles isolated from the two-stage reconstitution assay using GTP and ArfGAP1 do not contain Arf1, but do contain ArfGAP1, suggesting the possibility that ArfGAP1 deactivates Arf1 during vesicle formation releasing it from the membrane leaving ArfGAP1 as a member of the coat (Yang at el, 2002).

Other recent studies using ArfGAP1 indicate that membrane lipid composition and membrane curvature also influence Arf GAP activity. Investigation of GTP hydrolysis in the presence of different synthetic lipids determined that ArfGAP1 activity increases with a decrease in the size of the

polar head group (Antonny *et al*, 1997), suggesting that lipid packing plays a role in Arf GAP activity. Additional studies using liposomes with constant lipid composition, but varying radii, show that Arf GAP activity increases with a decrease in radii to typical coated vesicle size (<50nm; Bigay *et al*, 2003). This sensitivity to membrane curvature suggests that as the membrane curvature of a vesicle increases, ArfGAP1 hydrolyzes GTP and causes the release of the inactivated Arf1 from the tip of the budding vesicle. Experiments using truncation mutants of ArfGAP1 reveal that the central region of the protein is essential for sensitivity to membrane curvature (Bigay *et al* 2005). This phenotype also extends to the *S. cerevisiae* homolog of ArfGAP1, Gcs1. The conserved central region in both ArfGAP1 and Gcs1 is highly hydrophobic, serine-threonine rich, and forms amphipathic helices in membrane, which are termed the ArfGAP1 lipid packing sensors (ALPS1 & ALPS2). Mutations of the most conserved hydrophobic residues reduce sensitivity to membrane curvature (Bigay *et al* 2005; Mesmin *et al*, 2007).

S. cerevisiae Arf GAP, Glo3

The Gcs1-like ORF (*GLO3*) gene was first identified in a *gcs1* copy-suppressor screen in *S. cerevisiae* and contains the same zinc finger motif and similar C-terminal region as Gcs1 (Ireland *et al*, 1994). Recombinant Glo3 stimulates the GTP hydrolysis activity of *S. cerevisiae* Arf1 and Arf2,

demonstrating that it is an Arf GAP. Deletion of Glo3 results in a transient accumulation of the ER P1 form of CPY in a pulse-chase immunoprecipitation assay and an impairment in invertase processing, suggesting involvement in ER-Golgi transport. However, deletion of both Gcs1 and Glo3 is not viable, indicating that Gcs1 and Glo3 have an overlapping essential function. Moreover, *glo3Δgcs1-28* double mutant cells contain highly elaborated ER at the restrictive temperature of 37°C. *Glo3Δgcs1-28* cells also secrete hypoglycosylated invertase and show a complete block in carboxypeptidase Y (CPY) processing, accumulating the ER P1 form in a pulse-chase immunoprecipitation experiment, indicating a disruption in ER-Golgi transport (Poon *et al*, 1999). Glo3 was also identified in a screen to complement defects in ER retrieval of dilysine-tagged proteins and loss of Glo3 results in a lack of secretion of a subset of proteins (Dogic *et al*, 1999).

In addition to ER-Golgi transport, recent findings indicate that Glo3 could play a role in COPI recruitment and vesicle formation. Specifically, experiments demonstrate that Glo3 interacts with constitutively active ΔN17-Arf1-Q71L, with v-SNAREs, and with coatomer components (Poon *et al*, 1999; Eugster *et al*, 2000; Lewis *et al*, 2004; Watson *et al*, 2004). Other studies using a microsomal binding assay, show that SNAREs bind ΔN17-Arf1-Q71L and coatomer in a Glo3 dependent manner, indicating that Glo3 is necessary for v-SNARE-COPI interactions. In these studies, it was determined that only when Glo3 was added

before a v-SNARE, were both ΔN17-Arf1-Q71L and coatomer recruited to the membrane, suggesting that Glo3 may play a role in inserting v-SNAREs into COPI vesicles (Rein *et al*, 2002). Mutation of the invariant arginine residue 59 in the zinc finger of Glo3 to a lysine residue results in loss of Arf GAP activity. Glo3-R59K is still able to co-precipitate with Sec21, indicating that this mutation does not disrupt association with the COPI coat. Additionally, Golgi membranes from *glo3Δ* cells induced to express catalytically inactive Glo3-R59K fail to produce COPI vesicles in an *in vitro* vesicle-budding assay in the presence of GTP, indicating that Glo3 Arf GAP function is necessary for COPI vesicle formation (Lewis *et al*, 2004).

Overexpression of Glo3, but not Gcs1, is able to suppress the temperature sensitivity of allele specific *S. cerevisiae* Arf1 mutants. C-terminal domain swapping of Glo3 and Gcs1 generating Gcs1-A-Glo3 and Glo3-A-Gcs1 suggested different roles for the C-terminal domains. Sequence comparison revealed two repeats of an ISSXXXFG sequence motif in Glo3 as well as in the homologous human and mouse ArfGAP3 proteins. Substitution of conserved isoleucine, serine, phenylalanine and glycine residues with alanine residues in both motifs abolished the ability to suppress temperature sensitivity, suggesting this motif is essential for Glo3 function (Yahara *et al*, 2006).

Mammalian Arf GAP, ArfGAP3

A human cDNA clone homologous to rat ArfGAP1 was determined to encode a 516 amino acid protein with putative protein kinase C phosphorylation sites, and an N-terminal $CX_2CX_{16}CX_2C$ zinc finger motif similar to ArfGAP1, Gcs1, and Glo3 (Zhang *et al*, 2000). This novel human Arf GAP was named ArfGAP3, is predominantly localized in the perinuclear region, and displays Arf GAP activity on Arf1 *in vitro* (Liu *et al*, 2001).

***S. cerevisiae* Arf GAP, Age2**

Screening for a high copy suppressor in *S. cerevisiae* of an Arf1 temperature sensitive mutant identified several suppressors of Arf temperature sensitivity (SATs). Besides Gcs1 and Glo3, another suppressor (Sat2) was identified. Although a *gcs1Δ* strain is viable, a *gcs1Δsat2Δ* strain is not viable suggesting an overlapping function (Zhang *et al*, 1998). The cloned *SAT2* gene encodes a 298 amino acid protein with an N-terminal zinc finger motif, was shown to possess Arf GAP activity *in vitro*, and renamed *AGE2* for Arf GAP effector. A *gcs1-3age2* double mutant strain is not viable at 37°C, is impaired in transport of highly glycosylated invertase from the Golgi to the plasma membrane, accumulates Golgi membrane, impairs endocytosis and transport to the vacuole, has a defect in CPY maturation, and missorts CPY to the plasma membrane. Additionally, the *gcs1-3age2* double mutant strain shows a defect in

alkaline phosphatase (ALP) maturation. ALP is a type II vacuolar membrane protein that is transported to the vacuole by a different pathway than CPY (Poon *et al*, 2001). These results indicate that Gcs1 and Age2 act together in transport from the *trans*-Golgi network.

Here we describe the use of the fission yeast *Schizosaccharomyces pombe* as a model system in a genetic approach to study the function of a putative ortholog of the HIV-1 Rev cellular cofactor hRIP. We generate null and temperature sensitive mutants and analyze possible roles for an hRIP ortholog in nucleocytoplasmic transport and intracellular trafficking. Our results contribute to the use of fission yeast as a model system for the study of intracellular membrane trafficking and suggest the possibility of a link between nuclear RNA export and vesicular trafficking.

Figure 1-1. General features of the HIV-1 replication cycle. The mature virion interacts with the cell surface receptors through gp120 triggering fusion between the viral and cellular membranes. The viral core is uncoated enabling the viral RNA genome to be reverse-transcribed, transported into the nucleus, and integrated into the cellular DNA. Viral RNA is transcribed and exported to the cytoplasm by Rev. The Env polyprotein is translated in the ER and transported to the cell surface. The Gag and Gag-Pol polyproteins are translated in the cytoplasm and the virion core particle is assembled at the plasma membrane. The particle buds from the cell surface and upon release, the protease cleaves the Gag and Gag-Pol polyproteins to create a mature virion.

Figure 1-2. Arf GTPase cycle. Arf in the GDP bound form is inactive. The exchange of GDP for GTP by an Arf GEF produces the active GTP bound form of Arf, which is able to associate with membranes. An Arf Gap stimulates GTP hydrolysis, returning Arf back to an inactive GDP bound form, which is released from the membrane to the cytosol.

Figure 1-3. Classification and domain structures of Arf GAP families. Arf GAPs are grouped based in their domains. Alternate names are in parentheses. Accession numbers and species are listed: h = human; r = rat; m = mouse. Arf GAP = Arf GAP zinc finger domain; A = ankyrin repeat; SHD = spa-homology

domain; PBS2 = paxillin-binding sequence; BAR – Bin, amphiphysin and Rvs167 and Rvs161; PH = pleckstrin homology domain; SH3 = src homology 3 domain; SAM = sterile α motif; Rho GAP = Rho GAP domain; GLD = GTP-binding protein-like domain.

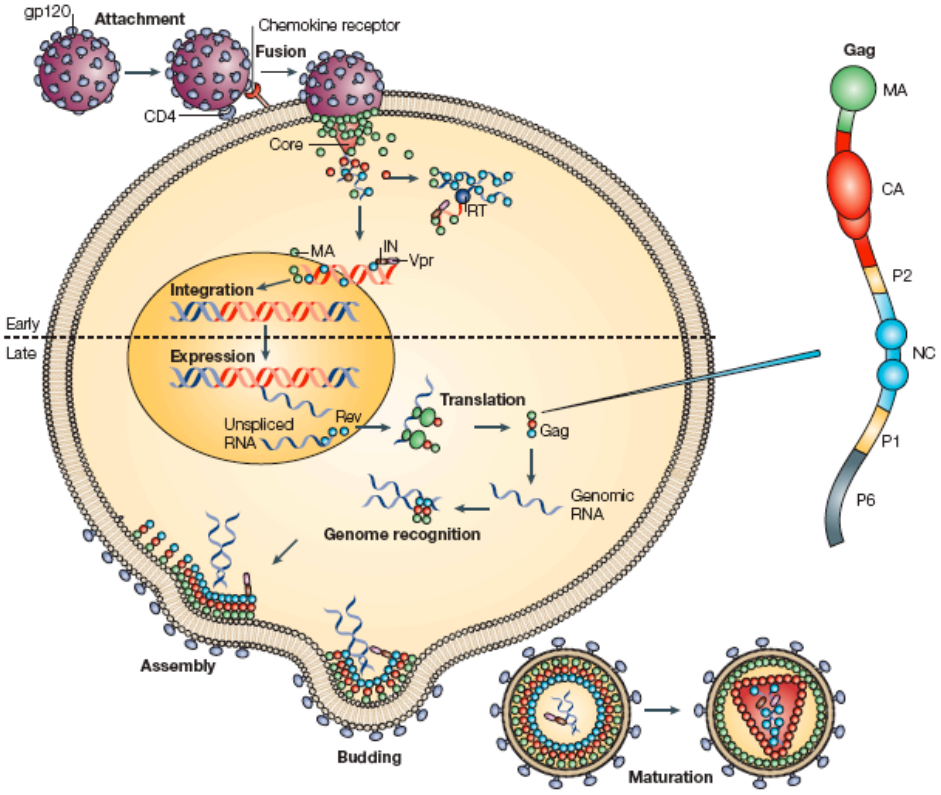

D'Souza and Summers *Nat Rev Microbiol* **3**: 643-655

Figure 1-1

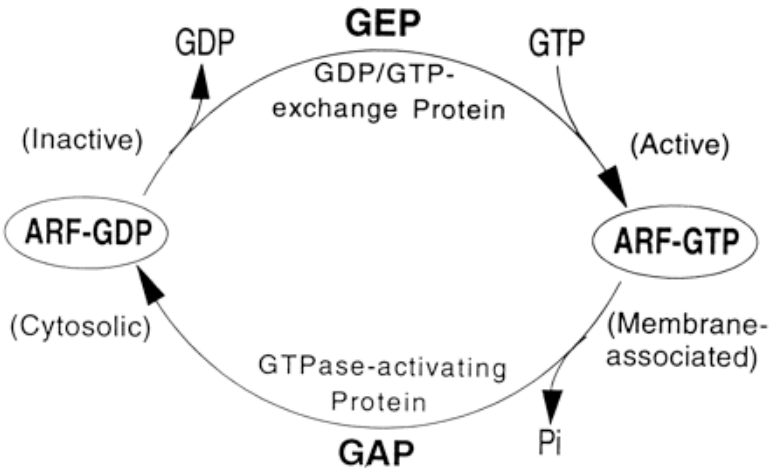

Moss and Vaughan *J Biol Chem* **273**: 21431-21434

Figure 1-2

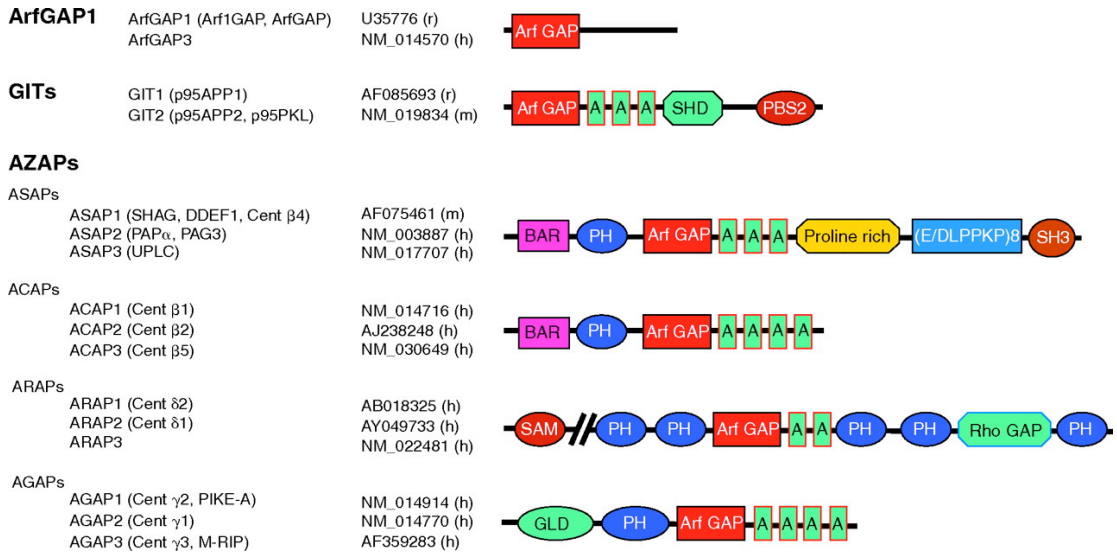

Nie and Randazzo *J Cell Sci* **11**9:1203-1211

Figure 1-3

CHAPTER II

Schizosaccharomyces pombe contains a putative hRIP ortholog essential for viability

INTRODUCTION

A yeast two-hybrid screen to identify HIV-1 Rev nuclear export signal (NES)-interacting cellular co-factors identified the human Rev Interacting Protein (hRIP; Fritz *et al*, 1995; Bogerd *et al*, 1995). The isolated hRIP cDNA encodes a 562 amino acid protein containing an N-terminal zinc finger with homology to Gcs1 and Sps18, a central serine-threonine rich region, C-terminal FG repeats characteristic of nucleoporins (Fritz *et al*, 1995), and C-terminal NPF repeat motif which interacts with EH domains (Salcini *et al*, 1997). A correlation was found between the ability of hRIP to bind to previously described Rev-activation domain mutants (Malim *et al*, 1991) and Rev function (Fritz *et al*, 1995; Bogerd *et al*, 1995), suggesting a possible role for hRIP in nucleocytoplasmic transport. hRIP was also shown by yeast two-hybrid analysis to interact with the NES of human protein kinase inhibitor α (PKI). The PKI NES is able to functionally substitute for the Rev NES, suggesting that PKI and HIV-1 Rev use a common cellular nucleocytoplasmic export pathway (Fridell *et al*, 1996).

Database searches for putative orthologs of hRIP identified a possible ortholog within the *Schizosaccharomyces pombe* genome. *S. pombe* is a

unicellular eukaryote that exists as a haploid organism, allowing for easy genetic manipulation and the generation of mutants as in budding yeast (Moreno *et al*, 1991). Many fission yeast genes contain introns (Wood *et al*, 2002) and fission yeast have been shown to properly splice mammalian introns, suggesting conservation of cellular processes between fission yeast and mammals (Kaufer *et al*, 1985). In addition to the study of mammalian splicing, fission yeast have also been utilized to study nuclear protein export and RNA export using identified *S. pombe* orthologs of key cellular factors implicated in these processes. For example, a genetic screen of a collection of *S. pombe* conditional mutants for defects in nucleocytoplasmic transport of poly(A)$^+$ RNA identified ribonucleic acid export (*rae1*$^+$), which accumulates poly(A)$^+$ RNA in the nucleus (Brown *et al*, 1995). Moreover, studies using a GST-NES$_{Rev}$-GST fusion protein demonstrated nuclear accumulation in a chromosomal region maintenance (*crm1*) mutant *S. pombe* strain, indicating Crm1 plays a role in export of NES-dependent protein export (Kudo *et al*, 1998). These studies suggest that nuclear protein export as well as mRNA export function similarly in fission yeast and mammalian cells, thus establishing *S. pombe* as a good model system for studying these pathways. An additional advantage is that *S. pombe* has fewer predicted genes than *S. cerevisiae* and has no apparent genome duplication event, therefore reducing the possibility of functional redundancy (Wood *et al*, 2002), which complicates functional analysis. Utilizing *S. pombe* as a model system, we have identified a

putative hRIP ortholog. In addition, we have characterized this protein by generating null and temperature sensitive mutant strains, and determined their growth characteristics.

RESULTS

Identification of an *S. pombe* ORF encoding a putative homolog of hRIP

As part of a search to identify a putative homolog of hRIP, we employed a *fasta* alignment algorithm (Pearson and Lipman, 1988) using the amino acid sequence of the hRIP zinc finger, and identified several zinc finger-containing proteins from multiple species (Figure 2-1A). One protein identified is encoded by an open reading frame (ORF; SPAC22E12.17c) on Chromosome 1 of *Schizosaccharomyces pombe* in the Sanger Center genome database. Alignment of this entire ORF with its predicted splice sites against hRIP revealed 51% similarity along the entire length of the genes, suggesting this protein could be a putative hRIP ortholog. To examine whether the ORF is an hRIP ortholog, the cDNA and genomic DNA were cloned from *S. pombe* RNA and chromosomal DNA by RT-PCR and PCR, respectively. Comparison of the cDNA sequence with genomic DNA sequence revealed the presence of two introns. Moreover, the cDNA sequence predicts a 483 amino acid protein with a predicted molecular weight of 53 kDa and similar putative domains to hRIP: an N-terminal zinc finger,

a serine-threonine rich region and some C-terminal FG pairs. Figure 2-1B shows a comparison of the putative structural domains.

Generation of a deletion (null) strain

To examine the null phenotype in fission yeast, a deletion construct was generated in which the SPAC22E12.17c genomic sequence was disrupted with the *ura4*$^{+}$ gene (Figure 2-2A). A linearized DNA fragment encoding genomic DNA (-13 to +1597) disrupted with the *ura4*$^{+}$ gene was transformed into an *ade6-210/ade6-216 leu1-32/leu1-32 ura4-D18/ura4-D18 h*$^{+}$*/h*$^{-}$ diploid strain generated by the mating of wild-type haploid strains YDM105 and YDM108. Fifteen *ura4*$^{+}$ positive transformants (heterozygous diploid strain MZY214) were selected on Edinburgh minimal medium (EMM) supplemented with leucine, and 8 random single colonies were induced to sporulate on malt extract (ME) with leucine. Tetrad analysis of the *ura4*$^{+}$ diploid transformants revealed a 2^{+}:2^{-} segregation ratio for viability in >90% of asci dissected (Figure 2-2B), indicating that the ORF is an essential gene. Chromosomal DNA was isolated from three different MZY214 strains and homologous recombination was confirmed by PCR analysis. All three heterozygous diploid strains tested show bands of the expected 1.2Kb size for oligonucleotide pair F1/R1 (Figure 2-2C, Lanes 1-3) and also show bands of the expected 1Kb size for the oligonucleotide pair F2/R2 (Figure 2-2C, Lanes 7-9). No PCR products were amplified in a wild-type haploid strain (YDM105)

using either oligonucleotide pair (Figure 2-2C, Lanes 4 & 10). These results confirm that the ORF has been disrupted and replaced by the *ura4*$^{+}$ deletion construct.

To confirm that the ORF is essential for viability, the cDNA was cloned into no message in thiamine (*nmt1*) inducible expression plasmids. *Nmt1* is involved in thiamine biosynthesis and is regulated by the level of available thiamine in the cell. Therefore, addition of thiamine to the media represses *nmt1*$^{+}$ expression (Maundrell, 1990). The inducible plasmids, pREP41-HA and pREP81, carry the *S. cerevisiae LEU2* gene as an auxotrophic marker and the inducible plasmids, pREP42 and pREP82, carry the *S. pombe ura4*$^{+}$ gene as an auxotropic marker (Basi *et al*, 1993; Maundrell, 1993). The ORF cDNA was cloned into vectors pREP81 and pREP41-HA generating plasmids pMZA496 and pMZA497, respectively. pMZA496 and pMZA497 were first transformed into the heterozygous diploid strain, MZY214, and then the transformants were selected on Edinburgh minimal medium (EMM) with no supplements, followed by random sporulation analysis. The resulting haploid deletion strains expressing either pREP81-ORF or pREP41-HA-ORF were selected on EMM supplemented with adenine plates. Haploid deletion strains expressing pREP81-ORF or pREP41-HA-ORF (Strains MZY215 & MZY216, respectively) were tested for the ability to grow in EMM with adenine in the absence or presence 15μM thiamine. Both MZY215 and MZY216 grow in the absence of thiamine. As expected, MZY215,

which expresses the ORF from the weakest *nmt* promoter, is not viable on EMM plates with adenine and 15μM thiamine (Figure 2-2D). In contrast, MZY216, which expresses the ORF from the medium strength *nmt* promoter, is slightly retarded for growth on EMM plates with adenine and 15μM thiamine. Additionally, growth curves were performed to analyze the proliferation and viability of cells in the presence of thiamine. Cells were grown to mid-log phase in media lacking thiamine, then pelleted and resuspended in media containing 15μM thiamine. MZY215 shows decreased cell proliferation and viability compared to MZY216 and a wild-type haploid strain, YDM105 (Figure 2-3A-C). To establish loss of HA-ORF expression in the strain MZY216, Western blot analysis was performed on cell lysates using a monoclonal antibody to the HA-tag. There is a significant reduction in HA-ORF expression by 22 hours post-thiamine repression (Figure 2-3D, 22 and 36 hours), confirming reduced expression of HA-ORF in the presence of 15μM thiamine.

Generation of Temperature Sensitive Mutants

We next used the gap repair strategy to generate temperature sensitive (*ts*) mutants (Kostrub *et al*, 1998). The strain MZY215 has no available selectable markers, therefore it was mated with a *his*$^-$ *h*$^-$ haploid strain (YDM258; *his3-D1 ade6-216 leu1-32 ura4-D18 h*$^-$*)*, which allowed for the isolation of a *his*$^-$ deletion strain expressing plasmid pMZA496 (Strain MZY473). To generate the

genomic DNA template for PCR mutagenesis and gap repair, the full-length genomic ORF sequence (-484 to +2403) was cloned into the fission yeast plasmid pBG1 containing the *S. pombe his3*$^{+}$ gene as a selectable marker (Burke and Gould, 1994), generating plasmid pMZA498. For PCR mutagenesis, the ratio of available deoxynucleotides was altered to limit dATP, and Mn^{2+} was added as a sub-optimal cation in the reaction to increase misincorporaton of dNTP and to reduce the fidelity of the DNA polymerase. The plasmid, pMZA498, was digested with SacI, to delete most of the genomic DNA but leave 5' and 3' overhangs of at least 250 nucleotides sharing DNA sequence with the mutagenesis PCR products. The linearized pMZA498 plasmid was separated from the SacI insert by gel electrophoresis and co-transformed with the heterogeneous mutant PCR population into the strain MZY473. The yeast will "repair" the gap in the plasmid by homologous recombination using the PCR product. The transformations were plated onto EMM with adenine, leucine, and 15μM thiamine at 25°C to repress expression of pMZA496 forcing the yeast to rely on a repaired plasmid for growth. Of the resulting colonies, 800 were patched onto fresh EMM with adenine, leucine, and 15μM thiamine plates, grown at 25°C, replica plated, and tested for temperature sensitivity at 36°C in the presence of thiamine. Thirty-three colonies were found to be temperature sensitive in the presence of thiamine and the plasmids were isolated from four colonies with the tightest *ts* phenotypes. Automated DNA sequencing analysis

revealed multiple nucleotide changes that result in several amino acid changes in each mutant. Each mutant was named to reflect the patched plate number and letter, and the colony number. One mutant, *1A1,* contains mutations in the central serine/threonine rich region and the C-terminal FG repeat region. The second mutant, *4A3,* has mutations immediately following the zinc finger and in the C terminal FG repeat region. The third mutant, *4A1*, contains mutations in all three of these domains. The fourth mutant, *5A2*, contains mutations in all three domains as well as an additional 34 amino acids due to a mutation in the stop codon. Figure 2-4 includes the amino acid sequences of all four *ts* mutant alleles compared to the wild-type allele. Based on the reproducibility of the tightest *ts* phenotypes, *1A1* and *4A3* were further characterized in functional assays.

Generation of deletion strains with *ts* covers

To generate deletion strains with plasmids expressing wild-type, *1A1*, or *4A3* alleles, we first cloned the wild-type and isolated *ts* mutants into pIRT2 (Hindley *et al*, 1987), a cloning vector with a *S. cerevisiae LEU2* gene, generating plasmids pMZA505, pMZA506, and pMZA507, respectively. The plasmids were transformed into the heterozygous diploid strain MZY214, selected on EMM plates, and random sporulation analysis was performed. The deletion strains expressing pMZA505, pMZA506, and pMZA507 (strains MZY504, MZY505, and MZY507, respectively) are able to grow at 25°C but not at the restrictive

temperature of 36°C, confirming their temperature sensitivity.

Strains MZY504, MZY505, and MZY507 have no available selectable markers for use in functional assays. To regain selectable markers, the alleles were integrated back into the genome using 5-fluoroorotic acid (5-FOA). 5-FOA prevents the growth of *ura4*$^{+}$ cells thus selecting for integration of the allele into the genome by homologous recombination, releasing the *ura4*$^{+}$ marker (Boeke *et al*, 1987). MZY504, MZY505, and MZY507 were grown overnight in nonselective conditions and then plated onto nonselective plates containing 5-FOA to isolate single cells having undergone homologous recombination.

The gene-converted haploid strains, MZY509 (wild-type), MZY510 (*1A1* allele), and MZY511 (*4A3* allele), were further confirmed by auxotrophic selection and temperature sensitivity. The gene-converted haploid strains are unable to grow on EMM plates containing adenine, adenine and uracil, or adenine and leucine, therefore confirming loss of both the *ura4*$^{+}$ disruption cassette and the pIRT2 cover plasmid with the *LEU2* gene. The *ts* allele gene-converted strains are viable at 25°C but not viable at 36°C confirming that the *ts* allele is necessary for cell viability at 25°C (Figure 2-5A).

Prior to use in functional assays, the growth kinetics of the gene-converted strains needed to be determined. Therefore, MZY509, MZY510, and MZY511 were grown to mid-log phase at 25°C, then shifted and grown at 30°C and 36°C. The results demonstrate that the MZY509 proliferates with wild-type growth

kinetics at both 30°C (Figure 2-5B) and 36°C (Figure 2-5C). MZY510 and MZY511 proliferate at minimal levels at 30°C (Figure 2-5B), but do not proliferate at 36°C (Figure 2-5C).

Is hRIP able to functionally complement the deletion mutant?

Because the lethality of the *ORFΔ*::*ura4*$^{+}$ allele can be rescued by plasmid expression of the ORF cDNA and because many mammalian proteins have been shown to functionally complement *S. pombe* mutants (Zhao and Lieberman 1995), we tested whether hRIP could functionally complement the *ORFΔ*::*ura4*$^{+}$ allele. First, hRIP was cloned into the pREP41-HA expression plasmid, generating plasmid pMZB563, which was then transformed into the heterozygous diploid strain, MZY214. The resulting haploid deletion strains expressing pMZB563 were non-viable. To evaluate whether this was due to an inability of hRIP to functionally replace the ORF or to a lack of hRIP expression, the plasmid pMZB563 was transformed into the wild-type haploid strain YDM105, hRIP expression induced by growth in EMM lacking thiamine, and denatured protein extract generated at various time points. Western blot analysis using an antibody to the HA-epitope tag revealed very little expression of full-length HA-hRIP protein at 36 hours post-thiamine release with a significant visible truncation product (Figure 2-6).

Using an alternative strategy to test whether hRIP can functionally replace the ORF, the HA-ORF expression plasmid, pMZA497, or HA-hRIP expression plasmid, pMZB563, were transformed into the gene-converted strains and assayed for the ability to functionally compensate for the loss of the ORF at the restrictive temperature of 36°C. The results demonstrate that the *ts* strains expressing HA-ORF are able to grow at both the permissive temperature of 25°C and the restrictive temperature of 36°C, confirming that the restoration of the ORF episomally rescues the *ts* phenotype (Figure 2-7, Row 3 compared with Rows 1 & 2). Experience by others in the laboratory has determined that removing the first four amino acids of hRIP increases expression levels in mammalian cells, therefore hRIP starting at amino acid four was cloned into pREP41-HA, generating plasmid pMZB564. There are some notable amino acid differences between hRIP and the ORF. hRIP contains four C-terminal NPF motifs that interact with EH domains in Eps15 (Salcini *et al*, 1997). However, the *S. pombe* ORF does not contain any NPF motifs. To test whether the presence of the NPF motifs could inhibit the ability of hRIP to functionally replace the ORF, a C-terminal truncation mutant lacking the four NPF motifs, hRIP-ΔNPF, was cloned into the pREP41-HA expression plasmid, generating plasmid pMZB565. To determine whether the hRIP zinc finger catalytic domain alone could be expressed and functionally replace the ORF, site-directed mutagenesis of the tryptophan at amino acid 93 was changed to a stop codon by site-directed

mutagenesis, generating plasmid pMZB566. These strains expressing hRIP constructs are viable at 25°C but are not viable at 36°C (Figure 2-7 Rows 4-6). Western blot analysis was negative for expression of all of the hRIP proteins. Thus, the ability of hRIP to functionally compensate for loss of the ORF has yet to be determined.

The ORF has a punctate cytoplasmic localization.

A first approach to establish a cellular function for the ORF was to analyze its subcellular localization by indirect immunofluorescence. A deletion strain expressing HA-ORF, MZY216, was grown to log phase in EMM medium with adenine in the absence of thiamine. Indirect immunofluorescence was performed using a α-HA antibody to detect the HA-tagged protein. We observed that HA-ORF has a punctate cytoplasmic localization (Figure 2-8A). To confirm whether this localization is similar to endogenous protein, indirect immunofluorescence was performed on a wild-type haploid strain (MZY259) using a peptide antibody generated against amino acids 431 to 444 of the ORF (Ab1120). The endogenous protein also has a punctate cytoplasmic localization (Figure 2-8B), suggesting that HA-ORF has the same localization as the endogenous protein.

Due to the presence of a putative Arf GAP catalytic domain as well as the demonstration that the ORF is essential, this ORF has been named *agv1*$^{+}$, for Arf GAP essential for viability, and will be hereafter referred to by this name.

DISCUSSION

We have determined that the putative hRIP ortholog, *agv1*$^{+}$, is an essential gene in fission yeast. Tetrad analysis of an *agv1* heterozygous diploid strain results in a 2^{+}:2^{-} segregation ratio, indicating that *agv1*$^{+}$ is essential. Additionally, a haploid *agv1Δ* strain containing a thiamine repressible *agv1*$^{+}$ expression construct is able to proliferate in the absence of thiamine and is inhibited in the presence of thiamine, confirming that the *agv1*$^{+}$ gene product is essential for viability.

The DNA sequence of the four isolated *agv1*^{ts} mutants revealed multiple nucleotide changes resulting in more than one amino acid change in each mutant. However, the *ts* mutants generated are useful for studying loss of Agv1 function at restrictive temperature in functional assays. Cloning of the rest of the *ts* mutants could reveal mutants with less amino acid changes and characterization of these new mutants could reveal milder temperature sensitivity phenotypes, thereby providing possible intermediate mutants for functional analysis.

Mammalian proteins have been able to functionally complement a number of *S. pombe* genes, suggesting conserved functions and pathway (Zhao and Lieberman, 1995). Attempts to determine whether hRIP can functionally complement loss of Agv1 have failed because of the inability to express full-length hRIP in *S. pombe*. Analysis of the hRIP amino acid sequence revealed

several stretches in the serine/threonine rich region where a serine codon used infrequently in *S. pombe* is used consecutively for three out of four codons in a row (http://www.kazusa.or.jp/codon/), possibly causing a pause in translation long enough for the ribosome to fall off and for translation to terminate. Generation of an hRIP construct that can be expressed at full-length at normal levels will be necessary to conclusively determine whether hRIP can functionally compensate for the loss of Agv1.

hRIP and Agv1 contain N-terminal zinc fingers similar to Gcs1 (Fritz *et al*, 1995 and this study). In *S. cerevisiae*, Gcs1 has been shown to have overlapping Arf GAP function with Glo3 in Golgi to ER retrograde transport (Poon *et al*, 1999) and with Age2 in post-Golgi transport (Poon *et al*, 2001). *S. pombe* does not appear to have the same functional redundancy. The genome of *S. pombe* has now been fully sequenced (Wood *et al*, 2002) and there are four genes, in addition to *agv1*$^{+}$, encoding proteins with similar zinc fingers. Somewhat surprisingly, none of these proteins maintain overlapping function for the essential function of Agv1. This lack of functional redundancy suggests that *S. pombe* is a good model system for studying a putative hRIP ortholog.

Figure 2-1. A fission yeast ORF and hRIP contain a similar zinc finger.

(A) FASTA alignment of the zinc finger of hRIP and other zinc finger containing proteins.

CEAL >gil1435195 (U51013) centaurin alpha [Rattus norvegicus];
PTIN >gnlIPIDld1020948 (D89940) phosphatidylinositol-3,4,5-triphosphate binding protein [Bos taurus];
ITKP >gil1947086 (U88368) inositol(1,3,4,5)tetrakisphosphate receptor [Sus scrofa];
ARFG >gil1130494 (U35776) ADP-ribosylation factor 1-directed GTPase activating protein [Rattus norvegicus];
GCS1 >gil408803 (L24125) zinc finger protein [Saccharomyces cerevisiae];
ARF1 >gil2286211 (AF011427) putative ARF1 GTPase activating protein [Drosophila melanogaster];
SPX18 >gil172687 (M90351) SPX18 [Saccharomyces cerevisiae];
GN1 hu >gnlIPIDld1005605 (D26069) KIAA0041 [Homo sapiens];
KIAA7 >gil2209291 (U81031) KIAA0167 [Homo sapiens];
BRCAa >gil1931654 (U95973) BRCA1-associated RING domain protein isolog [Arabidopsis thaliana];
GN1 ce >gnlIPIDle288403 (Accession number Z75711, z75711.gb_in) K02B12.7 [Caenorhabditis elegans];
CAEL >gil746450 (U23486) similar to S. cerevisiae zinc finger protein GCS1 [Caenorhabditis elegans];
GL03 >gil603361 (U18916) Glo3p [Saccharomyces cerevisiae];
Schpo Candidate >gil1220292 (Z70043) unknown [Schizosaccharomyces pombe];
YIE4 > >gil600004 (Z46861) unknown [Saccharomyces cerevisiae].

* = conserved amino acids; Blue amino acid = conserved cysteines; Red amino acid = invariant arginine.

(B) Schematic diagram of putative structural domains. Both hRIP and the fission yeast ORF contain N-terminal zinc finger domains (Zn), central serine and threonine rich regions (S/T), and C-terminal FG repeats (FG).

Figure 2-2. The *S. pombe* ORF is essential for viability.

(A) Schematic diagram of *ura4*$^+$ deletion construct used to disrupt the ORF in *S. pombe*. The EcoRI/PvuII internal fragment of the ORF was replaced with the *S. pombe ura4*$^+$ gene. Arrows indicate the position of oligonucleotide pairs used in PCR analysis. AGD = Arf GAP Domain.

(B) Tetrad analysis of heterozygous diploid strains, which have one disrupted allele and one wild-type allele, resulting in two viable and two non-viable spores per tetrad. Columns A-E represent five separate asci from a single strain.

(C) The disruption of the allele is confirmed by PCR analysis. PCR analysis was performed on chromosomal DNA from 3 different colonies of the heterozygous diploid MZY214 using two different oligonucleotide pairs. Each oligonucleotide pair contained one oligonucleotide complementary to flanking genomic DNA and the other complementary to sequences in the *ura4*$^+$ marker. Lanes 1-6 are PCR products for oligonucleotide pair F1/R2. Lanes 7-12 are PCR products for oligonucleotide pair F2/R2. Lanes 1-3 and 7-9 contain PCR products from three different MZY214 colonies. Lanes 4 and 10 contain PCR products from a wild-type haploid strain (YDM105). Lanes 5 and 11 contain PCR products from reactions lacking DNA template. Lane 6 and 12 are blank. Lane 13 contains 1Kb marker (New England Biolabs).

(D) Growth of a deletion strain expressing pREP81-ORF (MZY215) and a wild-type strains (YDM105) on Edinburgh minimal medium (EMM) plates with appropriate supplements in the absence (-) and presence (+) of 15μM thiamine.

Figure 2-3. Thiamine represses expression of the ORF.

(A) Growth curve of wild-type and deletion strains in the presence of thiamine. Wild-type haploid YDM105 and deletion strains expressing pREP81-ORF (MZY215) or pREP41-HA-ORF (MZY216) were grown to mid-log phase (OD_{595nm} = 0.5/ml) at 30°C in EMM with adenine, uracil, and leucine and then shifted to EMM with adenine, uracil, leucine, and 15μM thiamine at 30°C. The optical density (OD_{595nm}/ml) of each culture was determined by spectrophotometry at 4, 8, 12, 24, and 48 hours.

(B) Viability of wild-type and deletion strains in the presence of 15μM thiamine. Aliquots from time points in (A) were treated with Trypan Blue and the viability (% live cells/ml) was determined by counting the number of viable cells visualized on a hemocytometer through a light microscope.

(C) Cell proliferation of wild-type and deletion strains in the presence of 15μM thiamine. Aliquots from time points in (A) were counted (number of cells per ml) on a hemocytometer.

(D) Expression of HA-ORF is repressed in the presence of thiamine. Strain MZY216 was grown to mid-log phase (OD_{595nm} = 0.5/ml) at 30°C in EMM with

adenine and then shifted to EMM with adenine and 15μM thiamine at 30°C. Denatured protein lysates were generated from aliquots at 0, 4, 8, 22, and 36 hours post-thiamine addition, 10μg of each total lysate was resolved on a 10% SDS polyacrylamide gel and HA-ORF protein expression was assayed by Western Blot using an antibody to the HA epitope (1:250; 12CA5; Roche). The HA-ORF-His_6 labeled lane contains 1μg of partially purified protein used as a positive control for the HA antibody. The lane labeled YDM105 contains 10μg of denatured protein lysate from a wild-type haploid strain.

Figure 2-4. Sequence of temperature sensitive mutants. The ORF amino acid sequence is aligned with the amino acid sequences of the *1A1*, *4A3*, *4A1*, and *5A2 ts* alleles. Red = amino acids changes.

Figure 2-5. Characterization of temperature sensitive mutants.

(A) Growth of gene-converted strains expressing wild-type or *ts* alleles on minimal media plates at 25°C and 36°C. MZY509, MZY510, and MZY511 were grown on EMM plates with adenine, uracil, and leucine, then replica-plated to two new EMM plates with adenine, uracil, and leucine and grown at 25°C or 36°C for 48 hours.

(B) Growth of strains expressing wild-type or *ts* alleles in minimal media at 30°C. The gene-converted strains were grown to mid-log phase (OD_{595nm} =

0.5/ml) in EMM with adenine, uracil, and leucine at 25°C then shifted to EMM with adenine, uracil, and leucine pre-warmed to 30°C. The optical density (OD_{595nm}/ml) of each culture was determined by spectrophotometry at 0, 1, 2, 3, 4, 5, 8, 12, 24, 36, and 38 hours.

(C) Growth of strains expressing wild-type or *ts* alleles in minimal media at 36°C. The gene-converted strains were grown to mid-log phase (OD_{595nm} = 0.5/ml) in EMM with adenine, uracil, and leucine at 25°C then shifted to EMM with adenine, uracil, and leucine pre-warmed to 36°C. The optical density (OD_{595nm}/ml) of each culture was determined by spectrophotometry at 0, 4, 8, 12, 24, 36, 42, and 72 hours.

Figure 2-6. Detection of hRIP expression in *S. pombe* by Western blot analysis. A wild-type haploid strain expressing pREP41-HA-hRIP was grown to mid-log phase (OD_{595nm} = 0.5/ml) in EMM with adenine and 15μM thiamine then shifted to EMM with adenine. Denature protein lysates were generated from aliquots at 0, 24, 36, and 48 hours post-thiamine release, and 10μg of each total lysate was resolved on a 10% SDS polyacrylamide gel, and protein expression assayed by Western Blot using an antibody to the HA epitope (1:250; 12CA5; Roche). The arrow indicates full-length HA-hRIP, which runs around 73kDa.

Figure 2-7. The ORF genetically complements the *ts* mutants at 36°C. Gene-converted strains expressing *nmt1*-promoter driven ORF or hRIP constructs were grown on EMM plates with appropriate supplements then replica plated to two new EMM plates with appropriate supplements and grown at 25°C or 36°C for 48 hours. Row 1 is mock transformed gene-converted strains; Row 2 is the gene-converted strains transformed with pREP41-HA empty vector; Row 3 is transformed with pREP41-HA-ORF; Row 4 is transformed with pREP41-HA-hRIP (+4); Row 5 is transformed with pREP41-HA-hRIPΔNPF; Row 6 is transformed with pREP41-HA-hRIPW93*.

Figure 2-8. The ORF has a punctate cytoplasmic localization in *S. pombe*.

(A) The strain MZY216 was grown to mid-log phase (OD_{595nm} = 0.5/ml) at 30°C in EMM supplemented with adenine, and fixed with 4% paraformaldehyde. The localization of HA-ORF was detected by indirect immunofluorescence using a monoclonal HA antibody (1:250; 12CA5; Roche).

(B) The wild-type haploid strain MZY259 was grown to mid-log phase (OD_{595nm} = 0.5/ml) in EMM supplemented with adenine, uracil, leucine, and histidine. The localization of the endogenous protein was detected by indirect immunofluorescence using a peptide polyclonal antibody to the ORF, Ab1120 (1:200; AnaSpec).

A

```
                                 *  *  *    *       *    *  *    *          ***                ***
hRIP 1 MAASAKRKQEEKHLKMLRDMTGLPRNRKCFDCDQR-GPTYVNMTVGSFVCTSCSGSLRGLNP----PHRVKSISMTTFTQQEIEFLQKHGNEVCKQIWLGLFDDR
CEAL 7                RALLELLTRPGNSRCADCGAP-DPDWASYTLGVFICLSCSGIHRNIPQ----VSKVKSVRLDAWDETQVEFMTSHGNEAAR
PTIN 7                KAVLELLQRPGNARCADCGAP-DPDWASYTLGVFICLSCSGIHRNIPH----VSKVKSVRLDTWEDVQVEFMASRGNAIAR
ITKP 16                        PGNAHCADCGAP-DPDWASYTLGVFICLSCSGIHRNIPQ----VSKVKSVRLDTWEEPQVEFMASRGNSAARAVF
ARFG  8               KVLKEVRAQDENNVCFECGAF-NPQWVSVTYGIWICLECSGRHRGL---------VRSVTMDKWKDIELEKMKAGGN
Gcs1 12               RRLLQLQKIGANKKCMDCGAP-NPQWATPKFGAFICLECAGIHRGL---------VRSITMDQFKPEELLRMEKGGNE
ARF1  8               RVLQELKPQDENSKCFECGTH-NPQWVSVTYGIWICLECSGKHRSL---------VRSVTMDKWKDIELEKMKAGGNRNARE
Sps18 25                    NNNCFECKSV-NPQFVSCSFGIFICVNCANLLRGM---------VKSITMDNFEEKDVRRVEKSGN
GN1hu 262                 IPGNASCCDCGLA-DPRWASINLGITLCIECSGIHRSLK--------VRSLTLDTWEPELLKLMCELGNDVINRVYEANVEKM
KIAA7 584                   NSICVDCGAP NPTWASLNLGALICIECSGIHRNL--------RVRSLDLDDWPRELTLVLTAIGNDTANRVW
BRCAa 229               LRGLPGNNACAECNAP-EPDWASLNLGVLLCIQCSGVHRNL--------RSLSLDVKVWEPTILDLFRNLGNVYCNSLWEGL
GN1ce 8               RVLKELRPCDDNNFCFECEAN-NPQWVSVSYGIWICLECSGIHRSLGVHLSF---VRSVTMDKWKDIELAKMKAGGNRKFAEFLQSQPDYKE
CAEL 16                 MRKMRALPPNKLCFDCGAR-NPTWCTVTYGVFLCIDCSAVHRNLGVHLTF---VRSTNLDTNWTWLQLRAMQLGGNGNANQFFKAHGCN
Glo3 17               QVFQKLGSNMENRVCFDCGNK-NPTWTSVPFGVMLCIQCSAVHRNMGVHITF---VKSSTLDKWTINNLRRFKLGGNHKARDFFLKNNGKQL
Schpo Candidate 5     KLLTSLRSQRDNKVCFDCGAK-NPTWSSTTFGIYLCLDCSAAHRNMGVHISFVRFLRSTVLDSWTYAQLRVMRVGGNENARNYFKRHGGVSL
YIE4 1       MSTSVPVKKALSALLRDPGNSHCADCKAQLHPRWASWSLGVFICIKCAGIHRSLGTHISK---VKSVDLDTWKEEHLVKLIQFKNNLRANSYYEATLADE
```

B

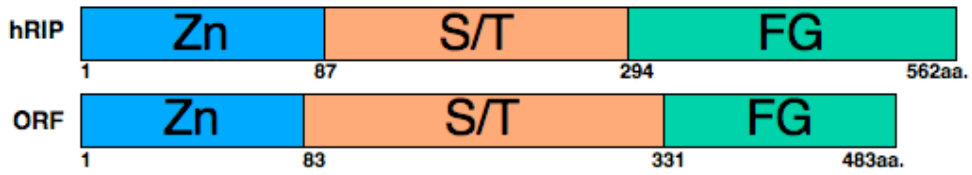

Figure 2-1

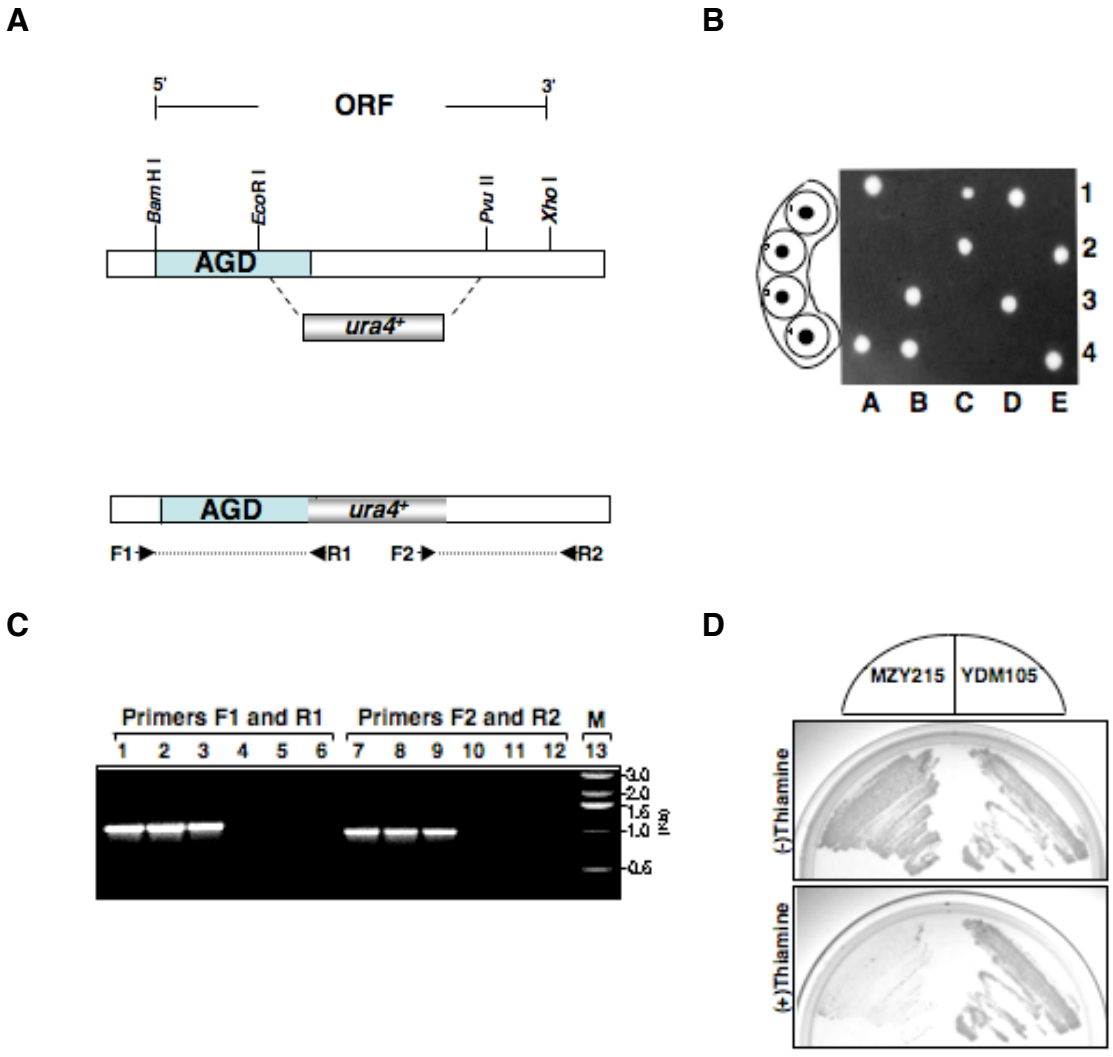
A
5'
ORF
3'
Bam H I
EcoR I
Pvu II
Xho I
AGD
ura4+
AGD
ura4+
F1
R1
F2
R2
B
1
2
3
4
A B C D E
C
Primers F1 and R1
Primers F2 and R2
M
1 2 3 4 5 6 7 8 9 10 11 12 13
3.0
2.0
1.5
1.0
0.5
kb
D
MZY215
YDM105
(-)Thiamine
(+)Thiamine

Figure 2-2

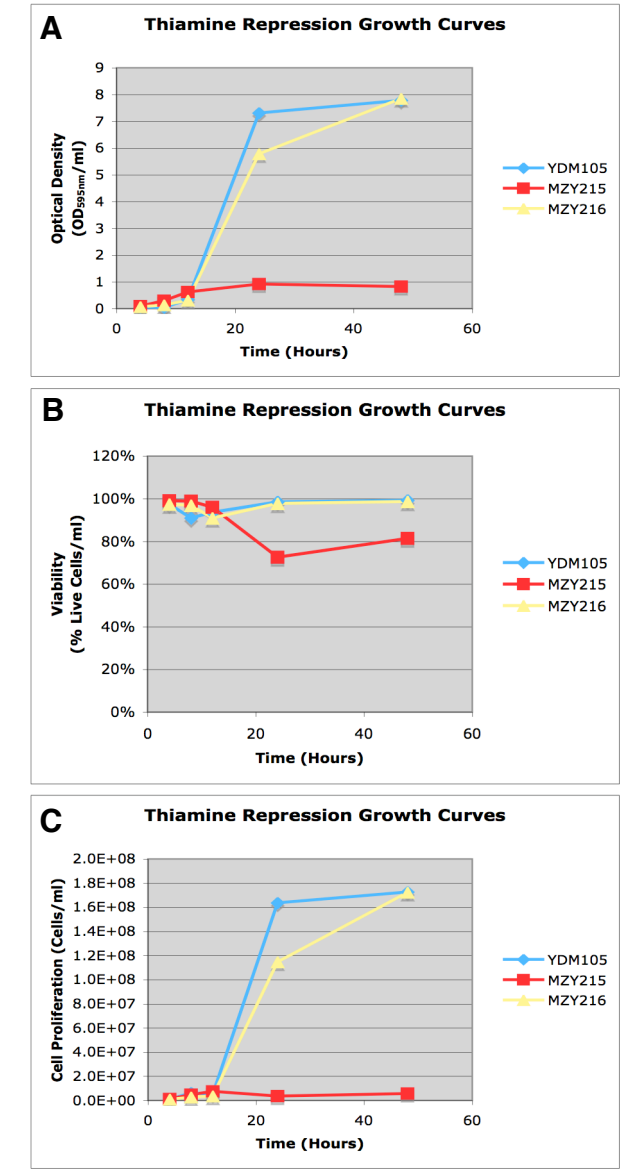
A
Thiamine Repression Growth Curves
Optical Density (OD595nm/ml)
Time (Hours)
YDM105
MZY215
MZY216
B
Thiamine Repression Growth Curves
Viability (% Live Cells/ml)
Time (Hours)
YDM105
MZY215
MZY216
C
Thiamine Repression Growth Curves
Cell Proliferation (Cells/ml)
Time (Hours)
YDM105
MZY215
MZY216
D
HA - ORF - HIS6
YDM105
MZY216
0
4
8
22
36
Time (Hours)
70kDa
1° α - HA (1:250)
2° α - mouse HRP (1:5000)

Figure 2-3

```
ORF          MTATKEESQKLLTSLRSQRDNKVCFDCGAKNPTWSSTTFGIYLCLDCSAAHRNMGVHISF
ORF-1A1      MTATKEESQKLLTSLRSQRDNKVCFDCGAKNPTWSSTTFGIYLCLDCSAAHRNMGVHISF
ORF-4A3      MTATKEESQKLLTSLRSQRDNKVCFDCGAKNPTWSSTTFGIYLCLDCSAAHRNMGVHISF
ORF-4A1      MTATKEESQKLLTSLRSQRDNKVCFDCGAKNPTWSSTTFGIYLCLDCSAAHRNMGVHISF
ORF-5A2      MTATKEESQRLLTSLRSQRDNKVCFDCGAKNPTWSSTTFDIYLCLDCSAAHRSMGVHISF

ORF          VRFLRSTVLDSWTYAQLRVMRVGGNENARNYFKRHGGVSLLNSKDCRLKYSSKTAKQYLE
ORF-1A1      VRFLRSTVLDSWTYAQLRVMRVGGNENARNYFKRHGGVTLLNSKDCRLKYPSKTAKQYPV
ORF-4A3      VRFLRSTVLDSWTYAQLRVMRVGDNENARNYFKRHGGVSLLNSKDCRLKYSSKTAKQYLE
ORF-4A1      VRFLRSTVLDSWTYAQLRVMRVGGDENARNYFKRHGGVSLLNSKDCRLKYSSKTAKQYLE
ORF-5A2      VRFLRSTVLDSWTYAQLRVMRVGGNANARNYFKRHGGVSLLNSKDCRLKYSSKTAKQYLE

ORF          KLKSLAVEDEANYPDILDMDFLSNTHEGSSAADTTNEDDDFFSAWDKASVKKSDDNLDDK
ORF-1A1      KLKSLAVEDEANYPDILDMDFLSNTHEGSSAADTTNEDDDFSSAWDKASVKKSDDNLDDK
ORF-4A3      KLKSLAVEDEANYPDILDMDFLSNTHEGSSAADTTNEDDDFFSAWDKASVKKSDDNLDDK
ORF-4A1      KLKSLAVEDEANYPDILDMDFLSNTHEGSSAADTTNEDDDFFSAWDEASVKKSDDNLDDK
ORF-5A2      KLKSLAVEDEANYPDILDMDFLSNTHEGSSAADTTNEDDDFFSAWDRASVKKSDDNLDGK

ORF          TDLASTSSSVVVESGEKDEPVVVTEEKTMVSPPSRPDSTSTTKSKTSSISSARARPIRAS
ORF-1A1      TDLASTSSSVVVESGEKDEPVVVTEEKTMVSPPSRPDSTSTTKSKTSSISSARARPIRAS
ORF-4A3      TDLASTSSSVVVESGEKDEPVVVTEEKTMVSPPSRPDSTSTTKSKTSSISSARARPIRAS
ORF-4A1      TDLASTSSSVVVESGEKDEPVVVTEEKTMVSPPSRPDSTSTTKSKTSSISSARARPIRAS
ORF-5A2      TDLASTSSSVVVESGEKDEPVVVTEEKTMVSPPSRPDSTSTTKSKTSSISSARARPIRAS

ORF          SRPTASKLGASRPQKLGIKKANADIDFDEFEKAVLSSESAPTKKPAAVASKESTVDTLVD
ORF-1A1      SRPTASKLGASRPQKLGIKKANADIDFDEFEKAVLSPESAPTKKPAAVASKESTVDTLVD
ORF-4A3      SRPTASKLGASRPQKLGIKKANADIDFDEFEKAVLSSESAPTKKPAAVASKESTVDTLVD
ORF-4A1      PRPTASKLGASRPQKLGTKKANADIDFDEFEKAVLSSESAPTKKPAAVASKESTVDTLVD
ORF-5A2      SRPTACKLGASRPQKLGIKKANADIDFDEFEKAVLSSESAPTKKPAAVASKESTVDTLVD

ORF          NGVEEVKESTSTTVQGKPVKPVLKSAASAKSTKSDDSNLNANFARLGFGQFAAASNARAK
ORF-1A1      NGVEEVKESTSTTVRGKPVKPVLKSAASAKSTKSDDSNLNANFARLGFGQFAAASNARAK
ORF-4A3      NGVEEVKESTSTTVQGKPVKPVLKSAASAKSTKSDDPNLNANFARLGFGQFAAACNARAK
ORF-4A1      NGVEEIKESTSTTVQGKPVKPVLKSAASAKSTKSGDSNLNANFARLGFGQFAAASNARAK
ORF-5A2      NGVEEVKESTSTTVQGKPVKPVLKSAASAKSTKSDDSNLNANFARLGFGQFAAASNARAK

ORF          AAAKARELKKNEVNAPTYARDHFASQKSISSDQYFGRGSFDPEAAAEAQERLSSFRDATA
ORF-1A1      AAAKARELKKNEVNAPTYARDHFASQKSISSDQYFGRGSFDPEAAAEAQERLSSFRDATA
ORF-4A3      AAAKARELKENEVNAPTYARDHFASQKSISPDQYFGRGSFDPEAAVEAQERLSSFRDATA
ORF-4A1      AAAKARELKKNEVNAPTYARDHFASQKSISSDQYFGRGSFDPEAAAEAQERLSSFRDATA
ORF-5A2      AAAKARELKKNEVNAPTYARDHFASQKSIPSDQYFGRGSFDPEAAAEAQERLSSFRDATA

ORF          ISSKSYFGEEEDENEEGESSHRPDSAYLRDIAETATEDIEAIKVAIHQGAEKLSDFIQKV
ORF-1A1      ISSKSYFGEEEDENEEGESSHRPDSAYLRDIAGTATEDIEAIKVAIHQGAEKLSDFIQKV
ORF-4A3      ISSKSYFGEEEDENEGGESSHRPDSAYLRDIAETATGDIEAIKVAIHQGAEKLSDFIQKV
ORF-4A1      ISSKSYFGEEEDENEEGESSHRPDSAYLRDIAETATEGIEAIKVAIHQGAEKLSDFIQKV
ORF-5A2      ISSKSYFGEEEGENEEGESSHRPDSAYLRDVAETATEDIEAMKVAIHQGAEELSDFIQKV

ORF          GARYNF-----------------------------------
ORF-1A1      GARYNF-----------------------------------
ORF-4A3      GARYNL-----------------------------------
ORF-4A1      GARYNF-----------------------------------
ORF-5A2      GARYNFYFIRPTLAQVARTCASVPVSVPHLLKFTSTTKTN
```

Figure 2-4

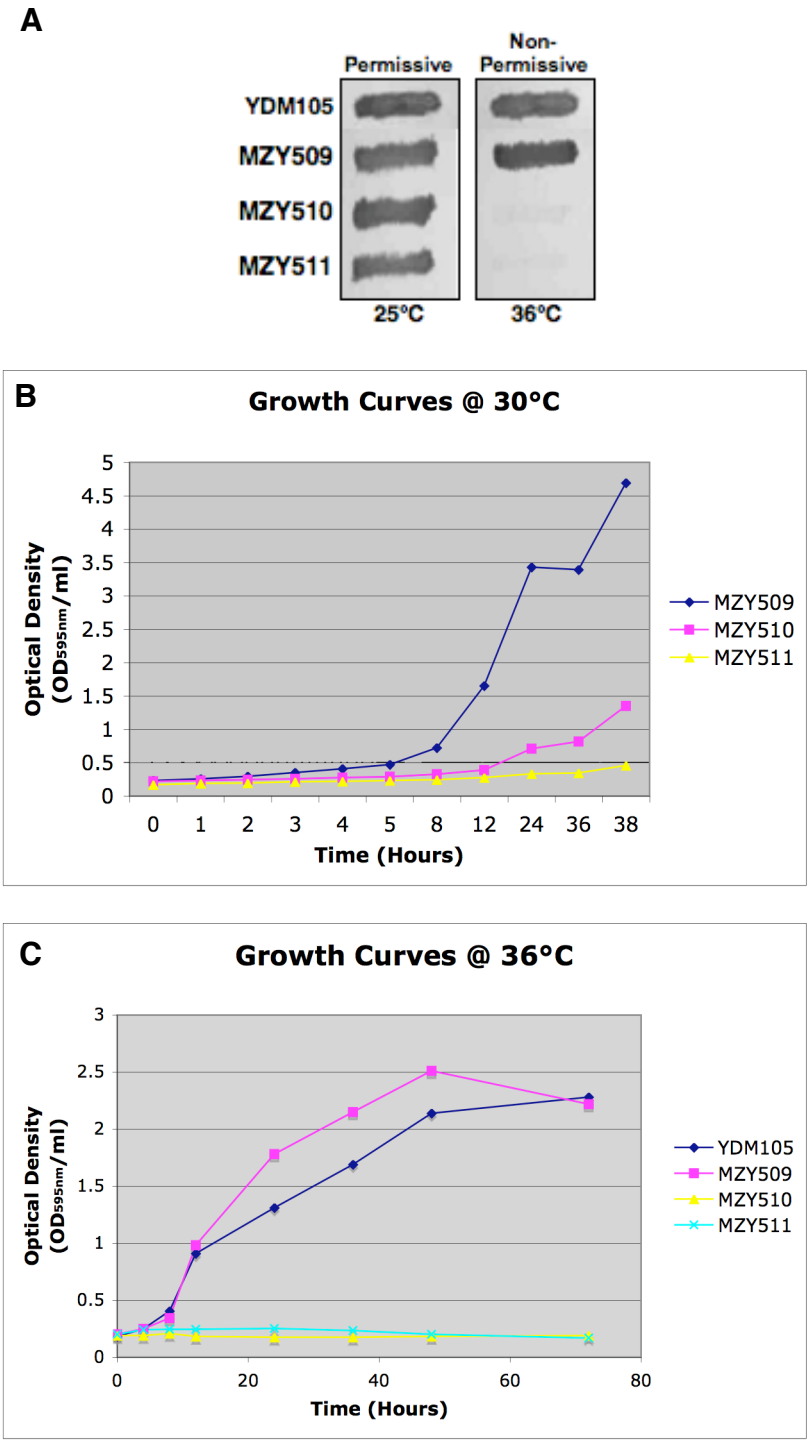
A
Permissive
Non-Permissive
YDM105
MZY509
MZY510
MZY511
25°C
36°C
B
Growth Curves @ 30°C
Optical Density (OD595nm/ml)
Time (Hours)
MZY509
MZY510
MZY511
C
Growth Curves @ 36°C
Optical Density (OD595nm/ml)
Time (Hours)
YDM105
MZY509
MZY510
MZY511

Figure 2-5

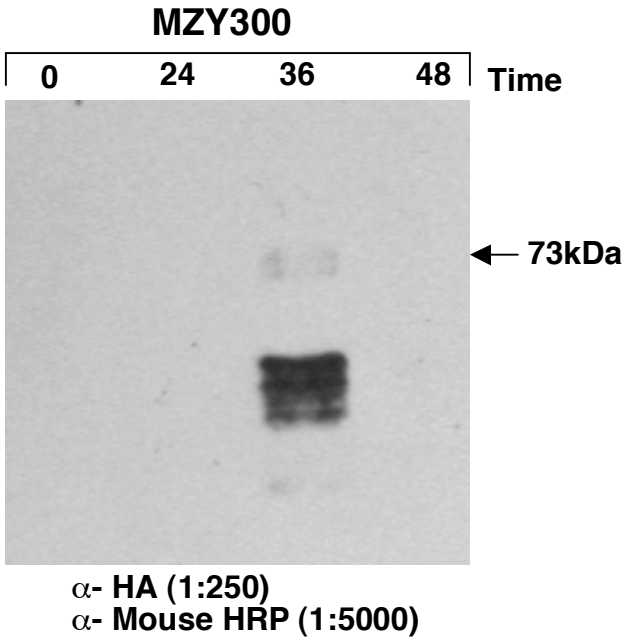

Figure 2-6

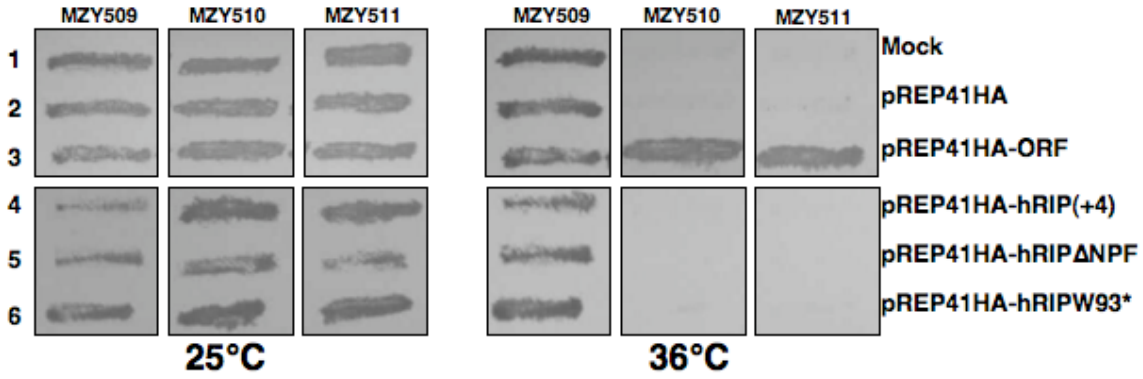
MZY509
MZY510
MZY511
MZY509
MZY510
MZY511
1
2
3
4
5
6
Mock
pREP41HA
pREP41HA-ORF
pREP41HA-hRIP(+4)
pREP41HA-hRIPΔNPF
pREP41HA-hRIPW93*
25°C
36°C

Figure 2-7

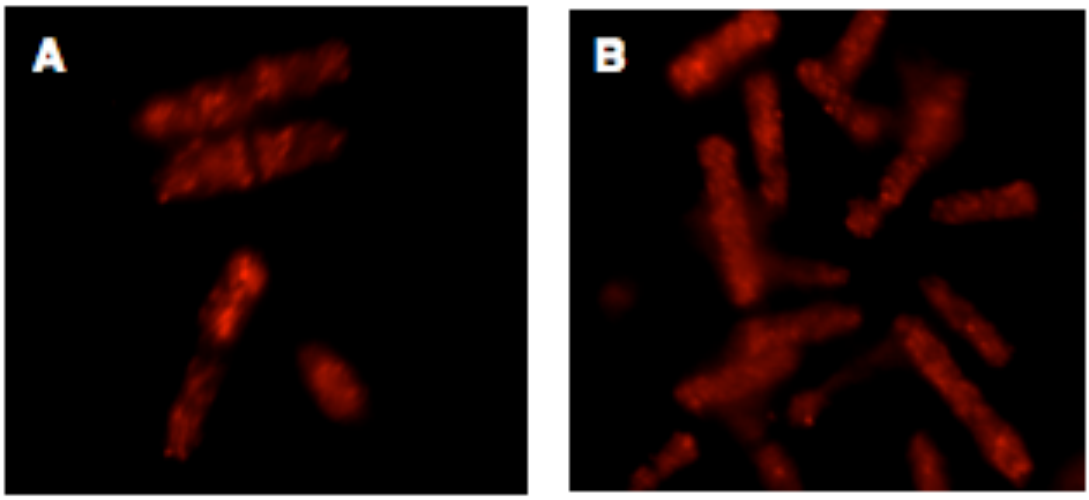

Figure 2-8

CHAPTER III

Agv1 is an Arf GTPase activating protein

INTRODUCTION

Due to the correlation of hRIP binding to HIV-1 Rev with Rev function in nuclear export of partially spliced and unspliced HIV-1 viral RNA; we had reason to suspect a role for Agv1 in nucleocytoplasmic transport. However, results from multiple nucleocytoplasmic transport assays indicate that Agv1 does not play a role in poly $(A)^+$ RNA nuclear export, in leucine-rich NES-dependent nuclear export, or in nuclear localization signal (NLS)-dependent nuclear import (See Supplemental Section).

Both hRIP and Agv1 contain an N-terminal zinc finger similar to Gcs1 and Sps18 (Fritz *et al*, 1995; This Study). Gcs1 has been demonstrated to be a GTPase activating protein (GAP) for adenosine diphosphate (ADP)- ribosylation factor 1 (Arf1; Poon *et al*, 1996), suggesting a possible role for hRIP and Agv1 in intracellular trafficking. Gcs1 and two other *S. cerevisiae* proteins, Glo3 and Age2, and mammalian ArfGAP1 and ArfGAP3 proteins belong to the ArfGAP1 family of Arf GAPs. Mutational analysis of ArfGAP1 by N-terminal truncation and substitution of conserved cysteine residues in the N-terminal zinc finger with alanine residues results in loss of GAP activity, indicating that the zinc finger is the 'catalytic' domain (Cukierman *et al*, 1995). Further studies mutating an

invariant arginine residue in the zinc finger domain to a lysine residue results in a loss of Arf GAP activity in *in vitro* GAP assays (Mandiyan *et al*, 1999; Randazzo *et al*, 2000; Yanagisawa *et al,* 2002; Lewis *et al*, 2004), confirming the zinc finger domain is essential for Arf GAP catalytic activity.

Morphological studies of *S. cerevisiae* Arf GAP mutant strains indicate that loss of Arf GAP function results in disruption of intracellular membranes. Specifically, a double mutant strain *glo3Δgcs1-28* grown at 37°C, accumulates highly elaborated ER membranes (Poon *et al*, 1999). However, single mutant *gcs1Δ* or *glo3Δ* strains do not accumulate intracellular membranous structures (Blader *et al*, 1999; Poon *et al*, 2001; Lewis *et al*, 2004). Additionally, a single mutant *age2Δ* strain does not accumulate membrane or display any morphological phenotypes. However, a *gcs1-3age2* double mutant strain accumulates Golgi membrane at 37°C (Poon *et al*, 2001).

S. cerevisiae Arf GAP mutant strains also display defects in the processing of carboxypeptidase Y (CPY). CPY is a yeast vacuolar protease that is often used to study trafficking through the secretory pathway to the vacuole by following post-translational modifications, which change the molecular weight of CPY during the maturation process. The differences in molecular weight can be detected as differences in electrophoretic mobility on denaturing gels and are indicative of compartmental location. Newly synthesized *S. cerevisiae* CPY is translocated to the ER, the signal peptide is removed, and core glycosylation

occurs to form a 67kDa P1 form of CPY. After transport to the Golgi, oligosaccharide modification generates a 69kDa P2 form of CPY. Pro-CPY is then targeted to the vacuole where the N-terminal pro segment is cleaved by vacuolar hydrolases to form the 61kDa mature (mCPY) form (reviewed in Jung *et al*, 1999). Single mutant *glo3Δ* and *gcs1Δ* strains each display a transient accumulation of the ER P1 form of CPY, however, the double mutant strain, *glo3Δgcs1-28*, displays a complete block in CPY processing, accumulating the ER P1 form (Poon *et al*, 1999), indicating a disruption in ER-Golgi transport. A single mutant *age2Δ* strain displays normal processing and transport of CPY to the vacuole, however, the *gcs1-3age2* double mutant strain accumulates and secretes the P2 Golgi form of CPY (Poon *et al*, 2001), consistent with a defect in trafficking from the Golgi to the vacuole.

The following section presents findings from comprehensive phenotypic analyses of two *ts* mutant strains, *agv1-1A1* and *agv1-4A3*. Specifically, intracellular localization of fission yeast Arf1, organelle intracellular membrane distribution, endocytosis, and processing and transport of Cpy1 were examined in the absence of Agv1 activity. Genetic complementation studies with these *ts* strains were performed using previously characterized *S. cerevisiae* or mammalian Arf GAPs. Collectively, these data demonstrate that Agv1 is an Arf GAP, which is functionally indispensable in fission yeast.

RESULTS

S. pombe Arf1 localization is unaltered in *agv1^{ts}* strains

The N-terminal zinc finger domain of *S. pombe* Agv1 is homologous to the catalytic domain found in Arf GAPs, which hydrolyze GTP bound to Arf1. Therefore, we examined whether the loss of Agv1 function might effect the subcellular localization of Arf1 at the restrictive temperature of 36°C. A wild-type strain, YDM259, and the gene-converted strains *agv1^{+}* (MZY509), *agv1-1A1* (MZY510), and *agv1-4A3* (MZY511) were grown to mid-log phase at 25°C, shifted to 36°C and incubated further for 3 hours at the restrictive temperature. The intracellular localization of Arf1 was analyzed in each strain by indirect immunofluorescence using a α-human Arf1 rabbit polyclonal antibody (Langille *et al*, 1999). *S. pombe* Arf1 displays a punctate localization within the cytoplasm and accumulates at the septum of dividing cells in each strain at 25°C (Figure 3-1, Panels A-D). Following three hours at restrictive temperature, Arf1 continues to have a punctate cytoplasmic distribution with a concentration at the septum of dividing cells of all strains (Figure 3-1, Panels E-H), suggesting that loss of Agv1 does not affect the localization of Arf1.

Organelle distribution is altered in *agv1^{ts}* stains.

Next, we systematically tested whether loss of Agv1 actually disrupted specific pathways involved in vesicular membrane trafficking. Because Arf GAPs

have been implicated in the early secretory pathway, we examined whether Agv1 is functionally involved in this process. To address this possibility, we used an established reporter protein-based assay. The localization of an *nmt*-promoter driven GFP-13g6 reporter construct (Brazer *et al*, 2000) was determined at restrictive temperature by fluorescence microscopy. 13g6 (encoded by gene spac13g6.03) is a multi-spanning membrane protein that localizes to the endoplasmic reticulum (ER; Brazer *et al*, 2000), and the complete sequence of the *S. pombe* genome predicts 13g6 to be a glycosylphosphatidylinositol (GPI) anchor biosynthesis protein (Wood *et al*, 2002). The gene-converted strains, *agv1*$^{+}$, *agv1-1A1*, and *agv1-4A3* were transformed with the plasmid pREP1-GFP-13g6 (Brazer *et al*, 2000) generating strains MZY512, MZY513, and MZY514 that express a GFP-tagged 13g6 protein. The resultant strains were grown in EMM supplemented with adenine and uracil, but lacking thiamine, to induce expression of GFP-13g6. To validate this assay, a fission yeast secretion-associated and *ras*-superfamily-related (*sar1*) temperature sensitive strain was used as a positive control. The fission yeast *sar1*$^{+}$ gene is essential and a *sar1 ts* strain accumulates ER membrane, as well as the core-glycosylated ER form of acid phosphatase, indicating a block in protein transport and in secretion from the ER (Matynia *et al*, 2001). Using this approach, the intracellular distribution of GFP-13g6 was analyzed at 25°C and following two or four hours at 36°C. At permissive temperature, GFP-13g6 is localized at the nuclear envelope; the

protein is also detected at the plasma membrane with occasional reticular structures connecting the nuclear envelope to the cell periphery in each strain (Figure 3-2, Panels A-D). Following two hours at restrictive temperature, GFP-13g6 is localized at the nuclear envelope, plasma membrane, and reticular structures in the *agv1*$^{+}$ strain (Figure 3-2, Panel F). Similarly, in the *sar1*^{ts} strain (MZY600), GFP-13g6 is localized to the nuclear envelope, plasma membrane, as well as an increasing number of reticular structures (Figure 3-2, Panel E). By contrast, GFP-13g6 is localized in discrete spots within the cytoplasm of 50% of the *agv1*^{ts} cells (Figure 3-2, Panels G & H). Following four hours at restrictive temperature, the intracellular localization of GFP-13g6 remains unchanged in wild-type or *sar1*^{ts} strains (Figure 3-2, Panels I & J). Most importantly, GFP-13g6 aggregates in discrete patches in the cytoplasm of >95% the *agv1*^{ts} cells (Figure 3-2, Panels K & L), suggesting that loss of Agv1 activity disrupts ER - Golgi transport.

To further delineate the role of Agv1 in ER - Golgi transport, we analyzed the intracellular localization in wild-type or *agv1*^{ts} strains using a GFP-gma12 reporter protein previously shown to localize to Golgi membrane (Brazer *et al*, 2000). Galactomannan, alpha 1,2 (Gma12) is an *S. pombe* α-1,2 galactosyltransferase (Chappell *et al*, 1994). The gene-converted strains, *agv1*$^{+}$, *agv1-1A1*, and *agv1-4A3*, were transformed with the plasmid pREP1-GFP-gma12 (Brazer *et al*, 2000), generating strains MZY515, MZY516, and MZY517.

The resulting strains were grown in EMM supplemented with adenine and uracil but lacking thiamine to induce expression of the GFP-gma12 fusion protein. The intracellular localization of GFP-gma12 was analyzed at 25°C and following two or four hours at 36°C. At permissive temperature, we found that GFP-gma12 was localized in patches of various size and number in the cytoplasm in all strains (Figure 3-3 Panels A-D). Following two hours at restrictive temperature, GFP-gma12 was localized to patches in the cytoplasm in the *agv1*$^{+}$ strain (Figure 3-3, Panel F). By contrast, the intracellular localization of GFP-gma12 was altered in the *agv1*^{ts} strains. GFP-gma12 was localized to more diffuse patches in the cytoplasm about 50% of the *agv1*^{ts} cells (Figure 3-3, Panels G & H) and in the *sar1*^{ts} strain (MZY601; Figure 3-3, Panel E). Following four hours at restrictive temperature, GFP-gma12 remained localized as patches within the cytoplasm of wild-type cells (Figure 3-3, Panel J). However, the protein was significantly more diffuse and present in diffuse patches throughout the cytoplasm of >90% the *agv1*^{ts} and *sar1*^{ts} cells under these conditions (Figure 3-3, Panels I, K, & L). Moreover, GFP-gma12 localizes to the nuclear envelope and the plasma membrane in about 30% of *agv1-4A3* cells following 4 hours at restrictive temperature (Figure 3-3, Panel K & M). The change in GFP-gma12 localization observed further indicates a disruption in ER - Golgi transport.

To determine whether the diffuse localization of GFP-gma12 results from the loss of Golgi organelle integrity or from protein degradation, aliquots from the

0, 2, and 4-hour time points at 36°C corresponding to the previous experiment for strains MZY515 and MZY517 were collected, denatured protein extracted, and the lysates resolved on a 10% SDS polyacrylamide gel. The expression of GFP-gma12 was detectable by Western blot analysis using a α-GFP monoclonal antibody, however, a GFP truncation product was detected in both strains. The level of expression of the GFP truncation product is higher in the MZY517 temperature sensitive stain than the wild-type MZY515 strain (Figure 3-4, compare lanes 5-7 with lanes 2-4), however, the level of expression of the truncation product decreases at restrictive temperature (Figure 3-4, compare lanes 6 & 7 with lane 5), indicating that the increased diffuse GFP-gma12 localization pattern is not due to an increase in truncated GFP, and suggesting that the diffuse localization pattern may result from loss of Golgi organelle integrity. Taken together, these data suggest a disruption in ER-Golgi trafficking at restrictive temperature.

Endocytosis is unaffected in *agv1^{ts}* strains

Next we tested whether Agv1 plays a role in the endocytic pathway, using a standard fluorescent microscopy based assay that monitors the uptake of the vital stain N-(3-triethylammoniumpropyl)-4-(ρ-diethylaminophenyl-hexatrienyl) pyridium dibromide (FM4-64). FM4-64 has been used to follow endocytosis and trafficking to the vacuole in budding and fission yeast (Vida and Emr, 1995;

Brazer *et al*, 2000). To study endocytosis and trafficking to the vacuole, the strains YDM259, *agv1-1A1*, and *agv1-4A3* were grown at 25°C to mid-log phase, incubated in media containing FM4-64 for 15 minutes at 25°C, washed to remove free FM4-64, incubated in media lacking FM4-64 for 0, 15, 45, or 60 minutes at 36°C, and visualized immediately. At zero or 15 minutes, FM4-46 localizes to the endocytic vesicles in all strains (Figure 3-5, Panels A-F). After 45 minutes, FM4-64 begins to localize to the vacuolar membranes as well as the endocytic vesicles in the wild-type strain (Figure 3-5, Panel G). However, the dye remains localized in endocytic vesicles of the *agv1^{ts}* strains (Figure 3-5, Panels H & I). After 60 minutes, FM4-64 localizes to vacuolar membrane in < 50% of the wild-type cells (Figure 3-5, Panel J), but remains in endocytic vesicles of the *agv1^{ts}* strains (Figure 3-5, Panels K & L), suggesting that Agv1 does not play a direct role in endocytosis, but might play a role in transport to the vacuole.

Intracellular membrane accumulates in *agv1^{ts}* strains.

Similar to previous studies of *S. cerevisiae* Arf GAPs, we analyzed the morphology of strains YDM259, *agv1^{+}*, *agv1-1A1*, and *agv1-4A3* at permissive or restrictive temperature using transmission electron microscopy (TEM). The TEM micrographs in Figure 3-6 reveal that the *agv1^{ts}* strains have a similar morphology to both the wild-type strain and the *agv1^{+}* strain at permissive temperature (Figure 3-6, Panels A-D). Following 3 hours at restrictive

temperature, the *agv1*$^{+}$ cells are indistinguishable from the wild-type haploid cells (Figure 3-6, compare panels E & F). In contrast, *agv1-1A1* and *agv1-4A3* cells at restrictive temperature show a striking accumulation of intracellular membranes within the cytoplasm and adjacent to the plasma membrane (Figure 3-6, Panels G & H). Taken together, our results indicate that loss of Agv1 results in a disruption in membrane trafficking within the ER and the Golgi membranes.

Cpy1p processing is blocked in *agv1*^{ts} strains

As an alternative approach to assess the role of Agv1 in ER - Golgi transport as well as a possible role in transport to the vacuole, the processing and maturation of carboxypeptidase Y (Cpy1) was examined by pulse-chase radiolabeling analysis. *S. pombe* Cpy1 is initially synthesized as an 110kDa pro-precursor form that is converted to a 32kDa mature heterodimer via a 51kDa intermediate form (Tabuchi *et al*, 1997). To maintain cell viability, the *agv1*$^{+}$, *agv1-1A1*, and *agv1-4A3* strains were pulse-labeled with radio-labeled methionine and cysteine for 15 minutes at a semi-permissive temperature of 30°C, then chased with excess unlabeled methionine and cysteine at 30°C. Isotopically radio-labeled Cpy1 present in cells was immunoprecipitated using a rabbit polyclonal antibody to Cpy1 and the immunoprecipitates resolved by SDS polyacrylamide gel electrophoresis followed by visualization using autoradiography. In the wild-type gene-converted strain, *agv1*$^{+}$, the pro-Cpy1

and mature Cpy1 bands are both detected after a 15-minute pulse (Figure 3-7A). By 30 minutes, pro-Cpy1 has been processed to the mature form. In the *agv1*^{ts} strains, the pro-Cpy1 is the predominant detectable band following a 15-minute pulse. After a 30-minute chase, we observe a significant accumulation of the pro-Cpy1 form in the *agv1-1A1* and *agv1-4A3* strains, with some of the pro-Cpy1 processed to the mature form. These results are consistent with previous studies of *S. cerevisiae* Arf GAPs and suggest that loss of Agv1 results in a disruption of processing of Cpy1 prior to transport to the vacuole.

It is important to note that the compartmental localizations of the various forms of Cpy1 have not been definitively demonstrated in *S. pombe*. The pro-Cpy1 form is predicted to be the same size in both the ER and the Golgi (Tabuchi *et al*, 1997), and thus, this method is limited in its ability to determine whether the block in *S. pombe* Cpy1 occurs in ER to Golgi trafficking, intra-Golgi trafficking, or in trafficking from the TGN to the vacuole. As a supplementary approach, we tested whether Cpy1 was secreted in the absence of Agv1 using colony immunoblotting. Strains *agv1*$^{+}$, *agv1-1A1*, and *agv1-4A3* were grown to mid-log phase at 25°C, overlaid with nitrocellulose, shifted to the semi-permissive temperature of 30°C overnight and colony immunoblot analysis performed with a rabbit polyclonal *S. pombe* Cpy1 antibody. To control for the specificity of the assay, a *S. pombe* vacuolar protein sorting 34 (*vps34*) deletion strain was analyzed in parallel. Deletion of Vps34 expression in *S. pombe*, results in a loss

of phosphatidylinositol 3-kinase activity, a temperature sensitive phenotype, a disruption of Cpy1 delivery to the vacuole, and missorting of Cpy1 to the plasma membrane with subsequent secretion (Stack *et al*, 1995; Takegawa *et al*, 1995; Tabuchi *et al*, 1997). At the semi-permissive temperature, Cpy1 is missorted to the plasma membrane and secreted from cells in the *vps34Δ* strain (Figure 3-7B). By contrast, we observe no discernible effect on delivery of Cpy1 to vacuole in the wild-type haploid strain, YDM258, *agv1*$^{+}$, *agv1-1A1*, or *agv1-4A3* strains, as judged by the lack of secreted Cpy1. These results indicate that Cpy1 is not transported to the membrane in the absence of Agv1 function, and suggests that Agv1 plays a role before exit from the Golgi apparatus.

Genetic complementation analysis in *agv1*^{ts} strains

Genetic complementation studies have been used extensively to identify Arf GAPs in yeast. To demonstrate whether Agv1 is an Arf GAP, we performed genetic complementation assays using previously characterized *S. cerevisiae* or mammalian Arf GAPs. *Nmt*-promoter driven GAP-specific expression constructs were transformed into the *agv1*$^{+}$, *agv1-1A1*, and *agv1-4A3* strains. The resultant colonies were patched on EMM plates with appropriate supplements, replica plated to two fresh plates, and grown in parallel at 25°C or 36°C for 48 hours. All *agv1*$^{+}$-derived strains are viable at permissive (25°C) and restrictive (36°C) temperatures (Figure 3-8). Mock transformed *agv1*^{ts} strains are viable at 25°C

but not at 36°C, confirming the temperature sensitivity of the gene-converted strains (Figure 3-8, row 1). The *agv1*^{ts} strains transformed with pREP41-HA-*agv1*$^{+}$, but not the empty vector pREP41-HA, are viable at 36°C, confirming that Agv1 activity is essential to rescue the *ts* phenotype (Figure 3-8, compare row 3 with row 2). Strikingly, *agv1*^{ts} strains expressing Gcs1-EGFP, Age2-EGFP, or ArfGAP1-EGFP, are not viable at 36°C, indicating that these Arf GAPs are unable to functionally substitute for Agv1 at restrictive temperature (Figure 3-8, rows 5-7). However, the *agv1*^{ts} strains expressing Glo3-EGFP, but not the pREP41-EGFPC empty vector, are viable at 36°C (Figure 3-8, compare row 9 with row 8), indicating that *S. cerevisiae* Glo3 is able to functionally replace the loss of Agv1 activity.

Previous studies have shown that mutation of an invariant arginine residue in the zinc finger of Arf GAP domains ablates Arf GAP activity *in vitro* (Randazzo *et al*, 2000; Mandiyan *et al*, 1999; Lewis *et al,* 2004; and Yanagisawa *et al,* 2001). To determine whether Agv1 possesses an Arf GAP activity that is essential for viability, the *agv1* gene-converted strains were transformed with a plasmid that expresses a catalytically inactive form of Glo3 or Agv1. We found that *agv1*^{ts} strains expressing either HA-Agv1-R52K or Glo3-R59K-EGFP mutants are viable at 25°C; however the cells were not viable at 36°C (Figure 3-8, rows 10 and 11). Based on these results, we conclude that an Arf GAP catalytic activity is essential for cell viability in the absence of Agv1 function.

It has been previously reported that in budding yeast, expression of pairs of Arf GAPs with overlapping functions are required for normal cell growth (Poon *et al*, 1999; Poon *et al*, 2001). We tested whether co-expression of overlapping pairs of *S. cerevisiae* Arf GAPs affected viability to the absence of Agv1 activity. We first confirmed the growth characteristics of individual Arf GAPs using different plasmid backbones. Similar to our previous findings, the *agv1^{ts}* strains expressing Glo3-EGFP, but not Glo3-R59K-EGFP or Gcs1-EGFP were viable at 36°C (Figure 3-8, rows 12-14). We next co-transformed known pairs of *S. cerevisiae* Arf GAP constructs into the gene-converted *agv1* strains. The *agv1^{ts}* strains that co-expressed Glo3-EGFP and Gcs1-EGFP, or Glo3-EGFP and Age2-EGFP were viable at 36°C (Figure 3-8, rows 15-17). By contrast, *agv1^{ts}* strains that co-expressed Gcs1-EGFP and Age2-EGFP were not viable at 36°C (Figure 3-8, row 18). These data suggest that the catalytic Arf GAP activity of Glo3 is sufficient to confer viability in the absence of Agv1 function.

The previous studies examine the ability of each *agv1^{ts}* strain to grow on plates at the restrictive temperature of 36°C. To extend this analysis, we monitored the growth kinetics for each of the previous strains in liquid culture at 36°C. All strains were grown to saturation in EMM with appropriate supplements at 25°C, and then diluted to an OD_{595nm} of 0.2/ml in EMM with appropriate supplements pre-warmed to 36°C. The optical density of each strain was determined by spectrophotometry following 0, 4, 8, 12, 24, 36, 48, and 72 hours

at 36°C. To compare the growth curves of each strain, the natural logarithm of the measured optical density for each strain during log phase growth (8-36 hours) was calculated and plotted for kinetic analysis. The slope of each line was then determined by linear regression and the slopes compared to the wild-type haploid strain, YDM105, by analysis of variance. Table 3-1 contains the average slope of each strain based on three growth curves at 36°C.

We found that the *agv1*$^{+}$ gene-converted strain or *agv1* strains expressing HA-Agv1 or Agv1-EGFP, but not *agv1*^{ts} strains expressing catalytically inactive HA-Agv1-R52K or Agv1-R52K-GFP grew with kinetics similar to that of a wild-type haploid stain (YDM105), consistent with a requirement for a functional Agv1 Arf GAP domain. The *agv1* strains expressing Glo3-EGFP but not the *agv1*^{ts} strains expressing the catalytically inactive Glo3-R59K-EGFP grew with near wild-type kinetics at 36°C. *Agv1*^{ts} strains expressing Gcs1-EGFP, ArfGAP1-EGFP, or Age2-EGFP were not viable at 36°C. These data are consistent with the results obtained with these strains grown on plates. To determine whether the co-expression of known *S. cerevisiae* Arf GAPs affect growth kinetics, the gene-converted strains were co-transformed with *GLO3* and *GCS1*, *GLO3* and *AGE2*, or *GCS1* and *AGE2* expression constructs. The *agv1*^{ts} strains expressing Glo3-EGFP and Gcs1-EGFP, or Glo3-EGFP and Age2-EGFP grew with wild-type kinetics. As expected, the *agv1*^{ts} strains, expressing Gcs1-EGFP and Age2-EGFP were not viable at 36°C. Expression of all of the constructs was confirmed

by GFP fluorescence, indirect immunofluorescence, and/or Western blot analysis. Collectively, our genetic complementation data indicate that the Arf GAP activity of Glo3 is able to confer viability to the *agv1^{ts}* strains at the restrictive temperature in the absence of Agv1 function.

Co-localization of coat components

S. cerevisiae Glo3 has been shown by yeast two-hybrid to interact with the β'-COP and γ-COP subunits of the COPI coat (Eugster *et al*, 2000) and by immunoprecipitation to interact with γCOP (Lewis *et al*, 2004). We considered performing immune-based co-localization studies to determine whether Agv1 could interact with known coat proteins. Prior to initiating such studies, we tested a panel of commercial antibodies directed against mammalian COPI coat proteins, rat β-COP, mouse γ-COP, human ε-COP, and to adaptor protein (AP) complexes, mouse α-Adaptin (AP-2), and mouse γ1-Adaptin (AP-1) for their ability to detect putative orthologs in *S. pombe*. MZY216, the haploid *agv1Δ* strain expressing the plasmid pREP41-HA-*agv1^{+}*, was grown to mid-log phase in EMM supplemented with adenine at 30°C, and cells were fixed and processed for visualization by indirect immunofluorescence microscopy. We were unable to detect expression of γ-COP, β-COP, or ε-COP fission yeast putative orthologs in these cells using antibodies directed against these proteins (Data not shown). By contrast, we were able to reproducibly detect signals using antibodies directed

against γ1-Adaptin and α-Adaptin (Figure 3-9, Panels B & F). In subsequent experiments, we determined that neither protein co-localizes with Agv1 *in vivo* (Figure 3-9, Panels D & H). These findings suggest that at steady state, Agv1 is not associated with clathrin-coated vesicles involved in endocytosis (AP-2) or trafficking from the TGN to recycling endosomes (AP-1).

As an alternative approach, mammalian Cos7 cells were transfected with either pHM6-*agv1*$^{+}$ or pHM6-*agv1-R52K* mammalian expression constructs and their intracellular distribution was analyzed using indirect immunofluorescence microscopy. Consistent with previous reports, α-Adaptin was cytoplasmically localized predominantly on vesicular structures in the absence or presence of wild-type or catalytically inactive Agv1 in cells expressing wild-type *S. pombe* Agv1 (Figure 3-10, Panel B & F). Similar localization results were observed for γ1-Adaptin (Figure 3-10, Panel J & N). Neither HA-Agv1-His_6 nor HA-Agv1-R52K-His_6 co-localize with α-Adaptin or γ1-Adaptin (Figure 3-10, Panels D, H, L, & P), further supporting the notion that Agv1 does not associate with clathrin coated vesicles in endocytosis or in trafficking from the TGN to recycling endosomes at steady state. Additional localization studies of COPI coat components, indicate that the punctate cytoplasmic localization of β-COP or γ-COP is unaffected in the presence of wild-type or catalytically inactive Agv1 (Figure 3-11, Panels B, F, J, & N). However, we found that HA-Agv1-His_6 or HA-Agv1-R52K-His_6 appear to localize near γ-COP (Figure 3-11, Panels L & P) in

transfected cells, thus raising the possibility that Agv1 can associate with components of the COPI coat.

DISCUSSION

The localization of Arf1 does not appear to be altered in the *agv1*^{ts} strains at restrictive temperature. This result is not unexpected given that Glo3 and Gcs1 interact specifically with constitutively active Arf1-Q71L and not with wild-type Arf1 in yeast two-hybrid experiments (Eugster *et al*, 2000). However, our fluorescence microscopy-based studies of ER-membrane and Golgi-membrane GFP fusion proteins do indicate a disruption of transport between the ER and the Golgi at 36°C. The localization of GFP-13g6 after 2 hours at restrictive temperature suggests a possible defect in anterograde transport from the ER to the Golgi. This might seem contradictory given than the Sar1 GTPase, not an Arf GTPase, mediates anterograde transport. However, it has been shown in mammalian cells that trafficking from the ER to the Golgi involves sequential steps for COPII and COPI coats. Vesicular-tubular clusters (VTC) leaving the ER rapidly lose COPII coats and acquire COPI coats *in vitro* (Aridor *et al*, 1995). COPI vesicles form adjacent to COPII sites *in vivo* and move toward the Golgi (Stephens *et al*, 2000). The COPI coat on anterograde VTCs is thought to function in the sorting of cargo, thus, could tightly coupling anterograde and retrograde trafficking pathways. Because of this coupling of the pathways, loss

of Golgi to ER retrograde transport results in a depletion of cellular factors necessary for anterograde transport (reviewed in Duden, 2003). It is unclear whether fission yeast have any pre-Golgi intermediates. However, if early steps in the secretory pathway are highly conserved, it is possible that COPI coats might be involved in anterograde transport in fission yeast. Loss of Agv1 could result in the inability to hydrolyze GTP and the inability to interact with cargo resulting in a block in anterograde transport as well as retrograde transport. In such a case, any ER membrane protein could become concentrated at post-ER/pre-Golgi intermediates consistent with the GFP-13g6 localization in discrete patches in the cytoplasm. It has been previously shown by fluorescence photobleaching recovery that YFP-tagged β-1,4-galactosyltransferase (YFP-GalT), localizes to the ER after disassembly of the Golgi by Brefeldin A (BFA) treatment (Ward *et al*, 2001). GFP-gma12 has also been shown to localize to the ER in wild-type cells treated with BFA (Brazer *et al*, 2000). The tight coupling of retrograde and anterograde transport would suggest a loss of Golgi membrane as well as an accumulation of ER membrane. The GFP-gma12 localization data is consistent with an eventual breakdown of the Golgi and a recycling of membrane back to the ER.

FM4-64 is a well-established dye for studying endocytosis and vacuolar delivery in fission yeast. Our studies following FM4-64 internalization found no discernible defect in endocytosis. However, it appears that delivery of FM4-64 to

vacuoles is inefficient in the wild-type cells tested and is not delivered to vacuoles in the *agv1^{ts}* strains tested. Thus we are unable to eliminate a possible defect in vacuolar transport in the *agv1^{ts}* strains.

The morphology of the *agv1^{ts}* strains at restrictive temperature by electron microscopy reveals a striking accumulation of intracellular membrane. It has been shown repeatedly that this phenomenon is not observed in *gcs1Δ strain* or *glo3Δ* strains (Blader *et al*, 1999; Poon *et al*, 2001; Lewis *et al*, 2004). Deletion of the *S. cerevisiae* Glo3-Gcs1 Arf GAP pair is required to produce ER membrane accumulation (Poon *et al*, 1999). In light of our previous findings, we conclude that loss of Agv1 function disrupts membrane transport between the ER and the Golgi, which is manifested by the accumulation of intracellular membranes.

The role of *S. cerevisiae* Arf GAPs in CPY transport has been previously studied using pulse-chase immunoprecipitation. A *glo3Δ* strain exhibits a transient accumulation of the P1, ER-glycosylated form of CPY with complete processing to the mature form by one hour. The double mutant, *glo3Δgcs1-28*, exhibits a complete block of CPY processing as judged by the accumulation of the P1 form (Poon *et al*, 1999). A complete block in processing of the *S. pombe* pro-Cpy1 form in *agv1^{ts}* mutants is not surprising, given that the retrograde and anterograde transport pathways are though to be tightly coupled. It is also consistent with previous data indicating that ER to Golgi transport of CPY is defective in a *sec21-1* mutant, and that antibodies to β-COP inhibit ER to Golgi

transport of VSV-G (Hosobuchi *et al*, 1992; Pepperkok *et al*, 1993). This data, coupled with the fact that fission yeast Cpy1 is not missorted to the plasma membrane at semi-permissive temperature provides evidence that Agv1 is involved in the ER-Golgi shuttle rather than in post-Golgi transport.

Our genetic complementation data show that the Arf GAP activity of Glo3 can compensate for the loss of Agv1 function. As previously reported for other Arf GAPs (Lewis *et al*, 2004), the catalytically dead mutant, Agv1-R52K, fails to confer viability in the absence of Agv1 function at restrictive temperature. Similar results were obtained using a Glo3 mutant with the equivalent mutation. During the course of this work, a difference in growth kinetics was observed between cells expressing the pREP41 plasmid containing the *S. cerevisiae LEU2* gene and those expressing the pREP42 plasmid containing the *S. pombe ura4*$^{+}$ gene. However, it has been previously reported that the *S. cerevisiae LEU2* gene is not expressed efficiently in fission yeast (reviewed in Zhao and Lieberman 1995). Thus, it is likely that in the *agv1*^{ts} strains, the levels of Arf GAP expression achieved using one construct might vary considerably from those levels achieved using the other expression construct. Similarly, differences in the Arf GAP activity among the *agv1*^{ts} strains could have direct effects on the rate of cell growth and proliferation.

Figure 3-1. *S. pombe* Arf1 remains localized at the septum in dividing cells at restrictive temperature. The wild-type strain YDM259 and the gene-converted strains *agv1*$^{+}$, *agv1-1A1*, and *agv1-4A3* were grown to mid-log phase (OD_{595nm} = 0.5/ml) at 25°C in EMM supplemented with adenine, uracil, and leucine and shifted to EMM supplemented with adenine, uracil, and leucine pre-warmed to 36°C. Cells were fixed in 4% paraformaldehyde following 0 and 3 hours at 36°C. The localization of Arf1 was detected by indirect immunofluorescence using a rabbit polyclonal antibody to human Arf1 (1:250; Langille *et al*, 1999). The antibody for Arf1 was detected with an Alexa Fluor® 594 goat anti-rabbit secondary antibody.

(A-D) Localization of endogenous Arf1 in YDM259 (A), *agv1*$^{+}$ (B), *agv1-1A1* (C), and *agv1-4A3* (D) strains at 25°C.

(E-H) Localization of endogenous Arf1 in YDM259 (A), *agv1*$^{+}$ (B), *agv1-1A1* (C), and *agv1-4A3* (D) strains following 3 hours at 36°C.

Figure 3-2. GFP-13g6 localizes to discrete spots within the cytoplasmic in *agv1*^{ts} strains at restrictive temperature. *agv1*$^{+}$, *agv1-1A1*, *agv1-4A3* , and *sar1*^{ts} were grown in EMM with appropriate supplements to mid-log phase (OD_{595nm} = 0.5/ml) at 25°C and shifted to EMM with appropriate supplements pre-warmed to 36°C. Cells were fixed in ice-cold methanol following 0, 2, and 4 hours at 36°C. The localization of GFP-13g6 was detected using fluorescence microscopy.

(A-D) Localization of GFP-13g6 in the strains *sar1^{ts}* (A), *agv1^{+}* (B), *agv1-1A1* (C), and *agv1-4A3* (D) at 25°C.

(E-H) Localization of GFP-13g6 in the strains *sar1^{ts}* (E), *agv1^{+}* (F), *agv1-1A1* (G), and *agv1-4A3* (H), following 2 hours at 36°C.

(I-L) Localization of GFP-13g6 in the strains *sar1^{ts}* (I), *agv1^{+}* (J), *agv1-1A1* (K), and *agv1-4A3* (L), following 4 hours at 36°C.

Figure 3-3. GFP-gma12 localization becomes more diffuse in the *agv1^{ts}* strains at restrictive temperature. *agv1^{+}*, *agv1-1A1*, *agv1-4A3*, and *sar1^{ts}* were grown in EMM with appropriate supplements to mid-log phase (OD_{595nm} = 0.5/ml) at 25°C and shifted to EMM with appropriate supplements pre-warmed to 36°C, and an aliquot fixed in ice-cold methanol following 0, 2, and 4 hours at 36°C. The localization of GFP-gma12 was detected using fluorescence microscopy.

(A-D) Localization of GFP-gma12 in the strains *sar1^{ts}* (A), *agv1^{+}* (B), *agv1-1A1* (C), and *agv1-4A3* (D), at 25°C.

(E-H) Localization of GFP-gma12 in the strains *sar1^{ts}* (E), *agv1^{+}* (F), *agv1-1A1* (G), and *agv1-4A3* (H), following 2 hours at 36°C.

(I-L) Localization of GFP-gma12 in the strains *sar1^{ts}* (I), *agv1^{+}* (J), *agv1-1A1* (K), and *agv1-4A3* (L), following 4 hours at 36°C.

(M) Localization of GFP-gma12 in the *agv1-4A3* strain following 4 hours at 36°C minus DAPI.

Figure 3-4. GFP-gma12 degradation does not increase at restrictive temperature. GFP-gma12 expression was determined by Western Blot analysis of denatured protein lysates from strains *agv1⁺* and *agv1-4A3* at 0, 2, and 4 hours at 36°C. Lane 1 contains 10μg of cell lysate from Cos7 cells that were transfected with pEGFP. The remaining lanes each contain 20μg of total denatured protein lysate from the *agv1⁺* strain expressing GFP-gma12 after 0 (Lane 2), 2 (Lane 3), and 4 (Lane 4) hours at 36°C and from the *agv1-4A3* strain expressing GFP-gma12 after 0 (Lane 5), 2 (Lane 6), and 4 (Lane 7) hours at 36°C. GFP-gma12 was detected with a monoclonal antibody to GFP (1:200).

Figure 3-5. Endocytosis is unaffected in the agv1^{ts} strains at restrictive temperature. YDM259, *agv-1A1*, and *agv1-4A3* were grown in EMM with appropriate supplements to mid-log phase (OD_{595nm} = 0.5/ml) at 25°C, incubated in EMM with appropriate supplements and 50μM FM4-64 for 15 minutes at 25°C, washed in EMM with appropriate supplements to remove free FM4-64, and shifted to EMM with appropriate supplements pre-warmed to 36°C. Cells were collected and FM4-64 internalization visualized by fluorescence microscopy following 0, 15, 45, and 60 minutes at 36°C. White arrows indicate vacuoles.
(A-C) FM4-64 staining in strains YDM259 (A), *agv1-1A1* (B), and *agv1-4A3* (C), following 0 minutes at 36°C.

(D-F) FM4-64 staining in strains YDM259 (D) *agv1-1A1* (E), and *agv1-4A3* (F), following 15 minutes at 36°C.

(G-I) FM4-64 staining in strains YDM259 (G), *agv1-1A1* (H), and agv1-4A3 (I), following 45 minutes at 36°C.

(J-L) FM4-64 staining in strains YDM259 (J), *agv1-1A1* (K), and *agv1-4A3* (L) ,following 60 minutes at 36°C.

Figure 3-6. Intracellular membranes accumulate in *agv1^{ts}* strains at restrictive temperature. YDM259, *agv1^{+}*, *agv1-1A1*, and *agv1-4A3* were grown in EMM with appropriate supplements to mid-log phase (OD_{595nm} = 0.5/ml) at 25°C and shifted to EMM with appropriate supplements pre-warmed to 36°C. Cells were fixed in 2.5% gluteraldehyde following 0 and 3 hours at 36°C. The ultrastructural morphology of each strain was visualized by transmission electron microscopy.

(A-D) Ultrastructural morphology of strains YDM259 (A), *agv1^{+}* (B), *agv1-1A1* (C), and *agv1-4A3* (D) at 25°C.

(E-H) Ultrastructural morphology of strains YDM259 (E), *agv1^{+}* (F), *agv1-1A1* (G), and *agv1-4A3* (H) after 3 hours at 36°C. Lower panels represent a higher magnification corresponding to the red arrows in (G) and (H).

Figure 3-7. Processing of *S. pombe* Cpy1 to the mature form is blocked in the *agv1^{ts}* strains at restrictive temperature.

(A) Strains *agv1^{+}*, *agv1-1A1*, and *agv1-4A3* were grown to mid-log phase (OD_{595nm} = 0.5/ml) in yeast nitrogen base (YNB) supplemented with adenine, uracil, and leucine at 25°C, shifted to 30°C for 30 minutes, pulse-labeled with Trans ^{35}S-label for 15 minutes, and chased with excess unlabeled methionine and cysteine for 0, 10, or 30 minutes at 30°C. *S. pombe* Cpy1 was immunoprecipitated with a rabbit polyclonal antibody to Cpy1, resolved on a 10% SDS polyacrylamide gel, and detected by autoradiography. B = beads only.

(B) Colony immunoblotting analysis of *S. pombe* Cpy1 secretion. Cells were grown on a nitrocellulose filter overlaid on an EMM plate with appropriate supplements overnight at 30°C, and the filter processed for immunoblotting using rabbit polyclonal antibody against Cpy1 (1:500). YDM259 was used as a negative control. *Vps34Δ* cells were used as a positive control for Cpy1 missorting.

Figure 3-8. *S. cerevisiae* Glo3 genetically complements the *agv1^{ts}* strains at restrictive temperature.

(A) Gene-converted strains expressing *nmt41 or nmt42*-promoter driven ARF GAP constructs were grown on EMM plates with appropriate supplements at 25°C then replica plated to two new EMM plates with appropriate supplements

and grown at 25°C or 36°C for 48 hours. Row 1 is mock transformed gene-converted strains; Row 2 is the gene-converted strains transformed with the empty vector pREP41-HA; Row 3 is transformed with pREP41-HA-*agv1*$^{+}$; Row 4 is transformed with the empty vector pREP42-EGFPC; Row 5 is transformed with pREP42-*GCS1*-EGFP; Row 6 is transformed with pREP42-*AGE2*-EGFP; Row 7 is transformed with pREP42-RnArfGAP1-EGFP; Row 8 is transformed with the empty vector pREP41-EGFPC; Row 9 is transformed with pREP41-*GLO3*-EGFP; Row 10 is transformed with pREP41-*glo3-R59K*-EGFP; Row 11 is transformed with pREP41-HA-*agv1*$^{+}$-R52K; Row 12 is transformed with pREP42-*GLO3*-EGFP; Row 13 is transformed with pREP42-*glo3-R59K*-EGFP; Row 14 is transformed with pREP41-*GCS1*-EGFP; Row 15 is transformed with pREP41-*GLO3*-EGFP and pREP42-*GCS1*-EGFP; Row 16 is transformed with pREP41-*GLO3*-EGFP and pREP42-*AGE2*-EGFP; Row 17 is transformed with pREP41-*GCS1*-EGFP and pREP42-*GLO3*-EGFP; and Row 18 is transformed with pREP41-*GCS1*-EGFP and pREP42-*AGE2*-EGFP.

Table 3-1. Slopes corresponding to growth kinetic studies. Slopes are representative of three separate growth curve experiments. Slopes in red are statistically different from the YDM105 wild-type slope ($p < 0.0001$).

Figure 3-9: α-Adaptin and γ1-Adaptin do not co-localize with Agv1 in *S. pombe*. The strain MZY216 was grown to mid-log phase (OD_{595nm} = 0.5/ml) at 30°C in EMM supplemented with adenine and fixed in 4% paraformaldehyde. The localization of α-Adaptin and γ1-Adaptin were detected by indirect immunofluorescence using antibodies to mouse α-Adaptin (1:100; Santa Cruz) and to mouse γ1-Adaptin (1:100; Santa Cruz). The localization of Agv1 was detected by indirect immunofluorescence microscopy using a monoclonal HA antibody (1:250; 12CA5). The nuclei were visualized using DAPI (A & E). The antibodies for α-Adaptin and γ1-Adaptin were detected with Alexa Fluor® 488 goat anti-rabbit secondary antibody (B & F). The antibody for HA was detected with Alexa Fluor® 594 goat anti-mouse (1:500; Molecular Probes; C & G). Merges are shown in panels D & H.

Figure 3-10. α-Adaptin and γ1-Adaptin do not co-localize with Agv1 in mammalian cells. Cos7 cells were transfected with pHM6-*agv1*$^{+}$ (Panels A-D and I-L) or pHM6-*agv1-R52K* (Panels E-H and M-P) using ESCORT IV transfection reagent and fixed in ice-cold methanol 48 hours post transfection. The localization of α-Adaptin and γ1-Adaptin were detected by indirect immunofluorescence using antibodies to mouse α-Adaptin (1:100; Santa Cruz) and to mouse γ1-Adaptin (1:100; Santa Cruz). The localization of Agv1 was detected by indirect immunofluorescence microscopy using a monoclonal HA

antibody (1:500; 12CA5). The nuclei were visualized using DAPI (A, E, I, & M). The antibodies for α-Adaptin and γ1-Adaptin were detected with Alexa Fluor® 488 goat anti-rabbit secondary antibody (1:1500; Molecular Probes; B, F, J, and N). The antibody for HA was detected with Alexa Fluor® 594 goat anti-mouse secondary antibody (1:1500; Molecular Probes; C, G, K, O). Merges are shown in panels D, H, L, and P.

Figure 3-11. γ-COP partially co-localizes with Agv1 in mammalian cells. Cos7 cells were transfected with pHM6-*agv1*$^{+}$ (Panels A-D and I-L) or pHM6-*agv1-R52K* (Panels E-H and M-P) using ESCORT IV transfection reagent and fixed in ice-cold methanol 48 hours post transfection. The localization of β-COP and γ-COP were detected by indirect immunofluorescence using antibodies to rat β-COP (1:100; Santa Cruz) and to mouse γ-COP (1:100; Santa Cruz). The localization of Agv1 was detected by indirect immunofluorescence microscopy using a monoclonal HA antibody (1:500; 12CA5). The nuclei were visualized using DAPI (A, E, I, & M). The antibodies for β-COP and γ-COP were detected with Alexa Fluor® 488 donkey anti-goat (1:1500; Molecular Probes; B, F, J, and N). The antibody for HA was detected with Alexa Fluor® 594 goat anti-mouse (1:1500; Molecular Probes; C, G, K, O). Merges are shown in panels D, H, L, and P.

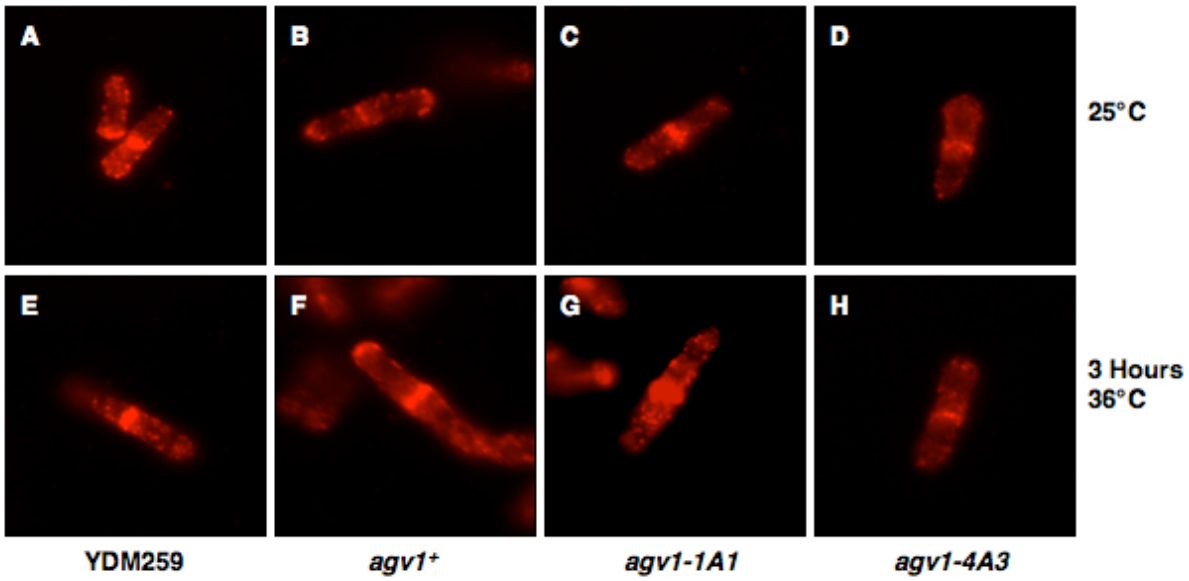

Figure 3-1

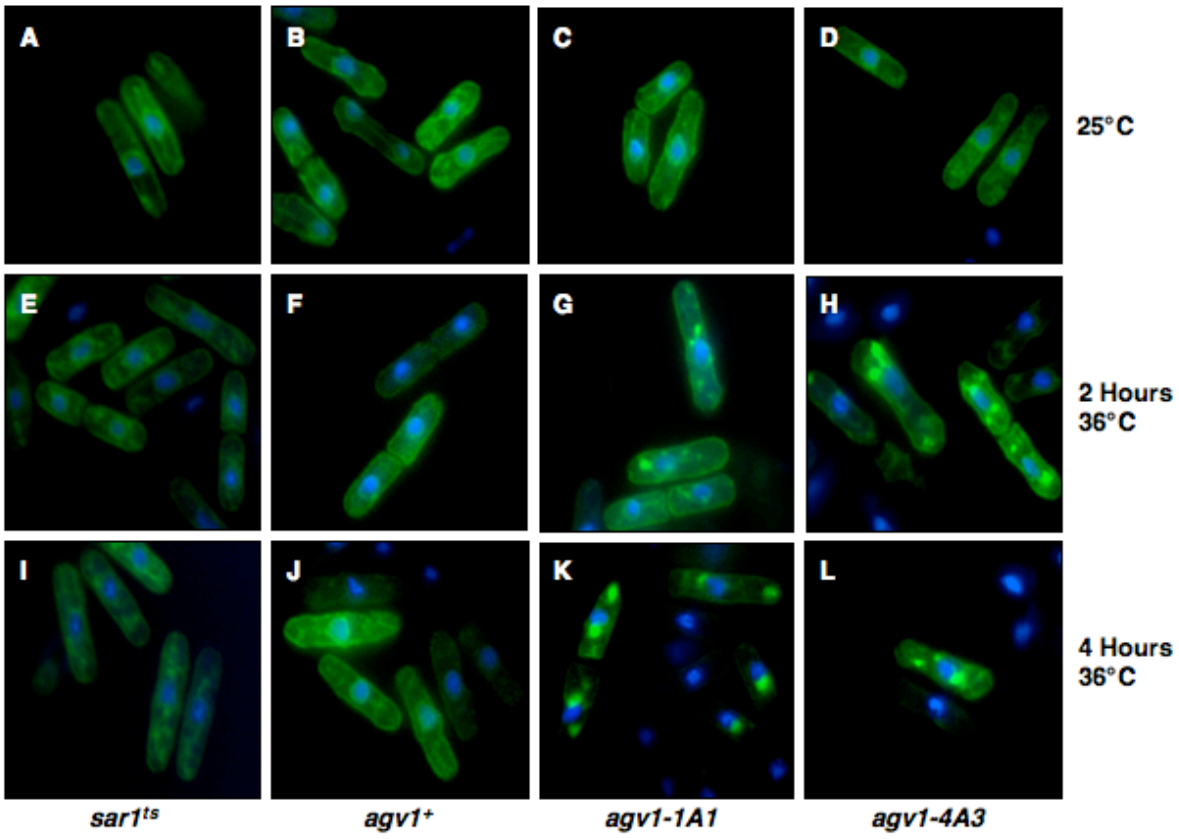
A
B
C
D
25°C
E
F
G
H
2 Hours
36°C
I
J
K
L
4 Hours
36°C
sar1ts
agv1+
agv1-1A1
agv1-4A3

Figure 3-2

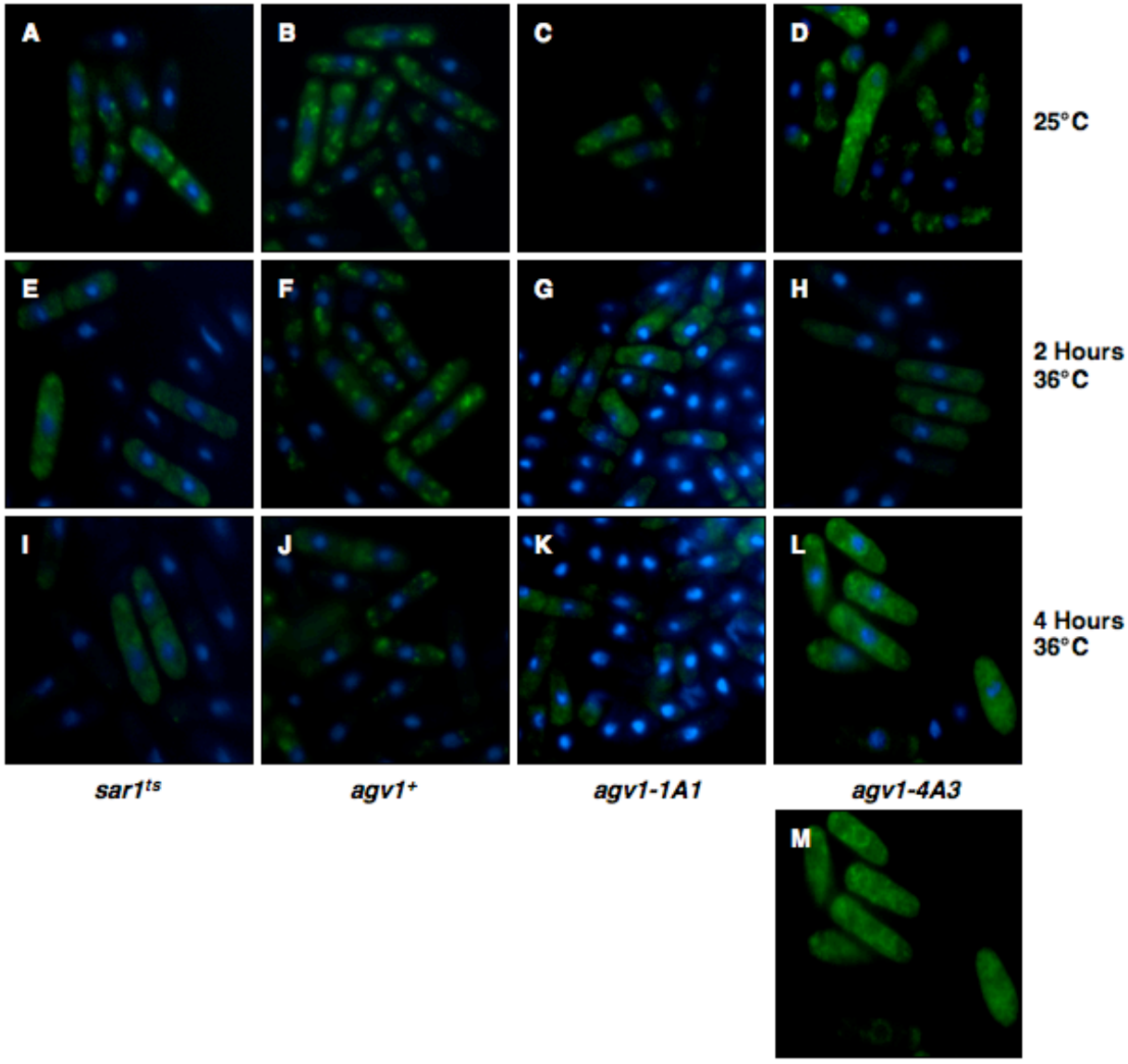
A
B
C
D
25°C
E
F
G
H
2 Hours
36°C
I
J
K
L
4 Hours
36°C
sar1ts
agv1+
agv1-1A1
agv1-4A3
M

Figure 3-3

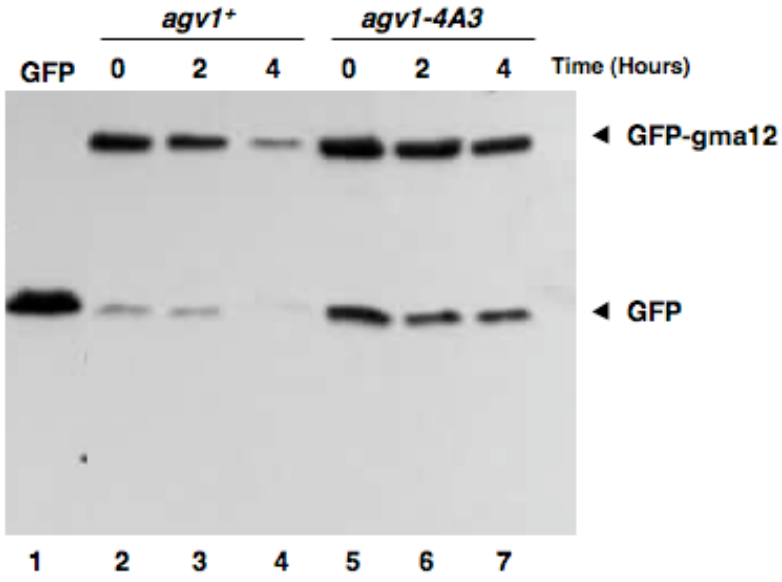
agv1+
agv1-4A3
GFP
0
2
4
0
2
4
Time (Hours)
GFP-gma12
GFP
1
2
3
4
5
6
7
1° α-GFP 1:200
2° α-Mouse HRP 1:5000

Figure 3-4

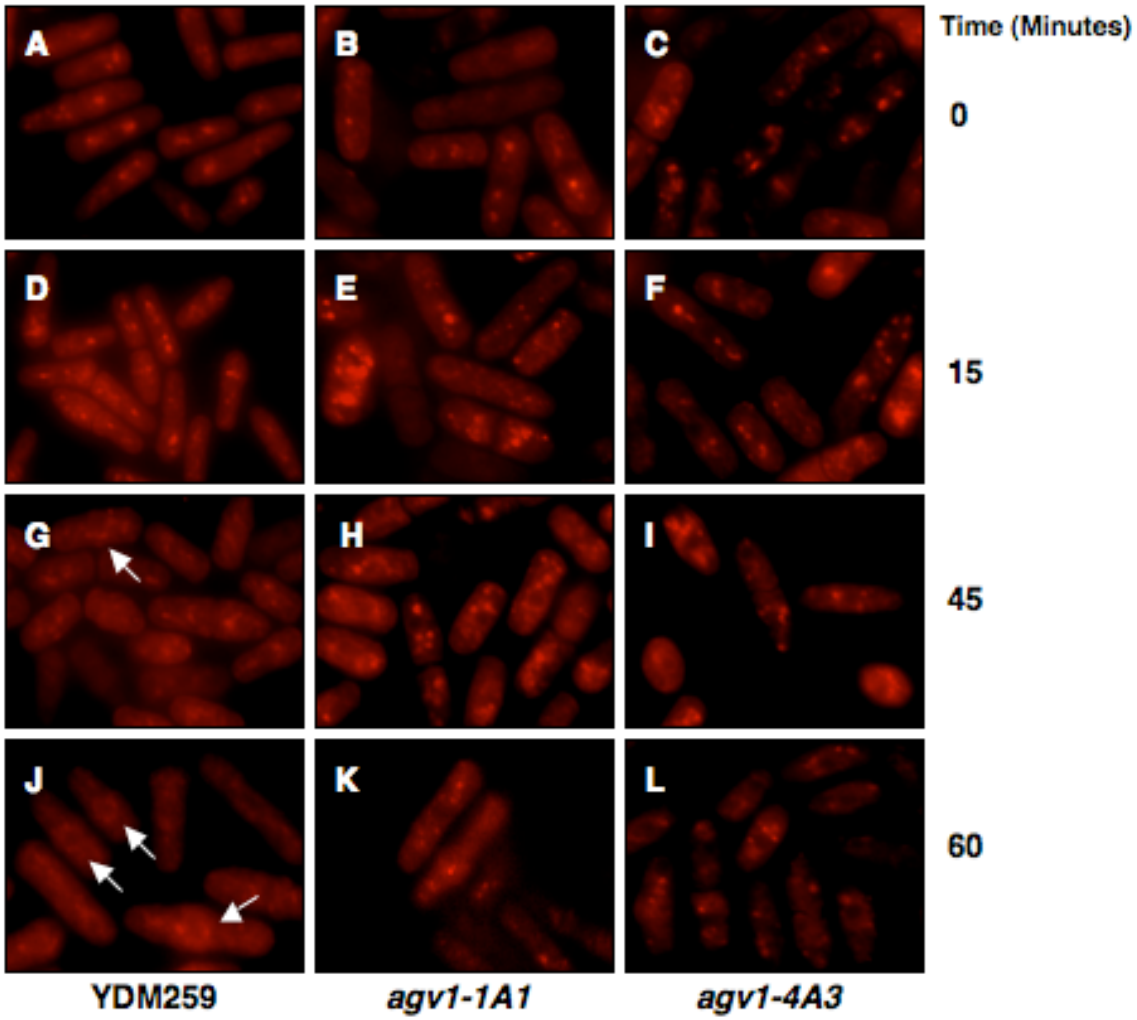
A
B
C
D
E
F
G
H
I
J
K
L
Time (Minutes)
0
15
45
60
YDM259
agv1-1A1
agv1-4A3

Figure 3-5

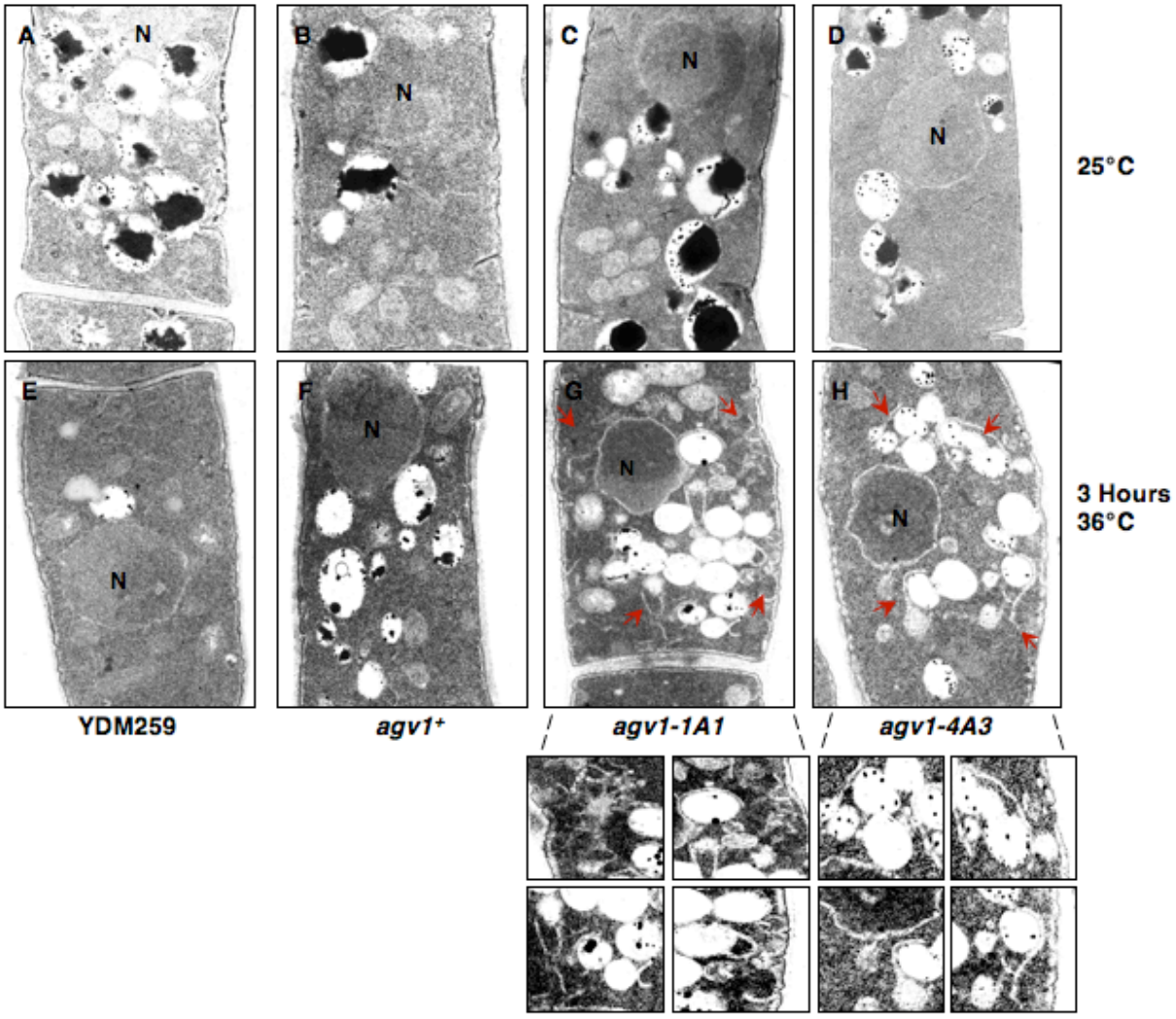
A
N
B
N
C
N
D
N
25°C
E
N
F
N
G
N
H
N
3 Hours
36°C
YDM259
agv1+
agv1-1A1
agv1-4A3

Figure 3-6

A

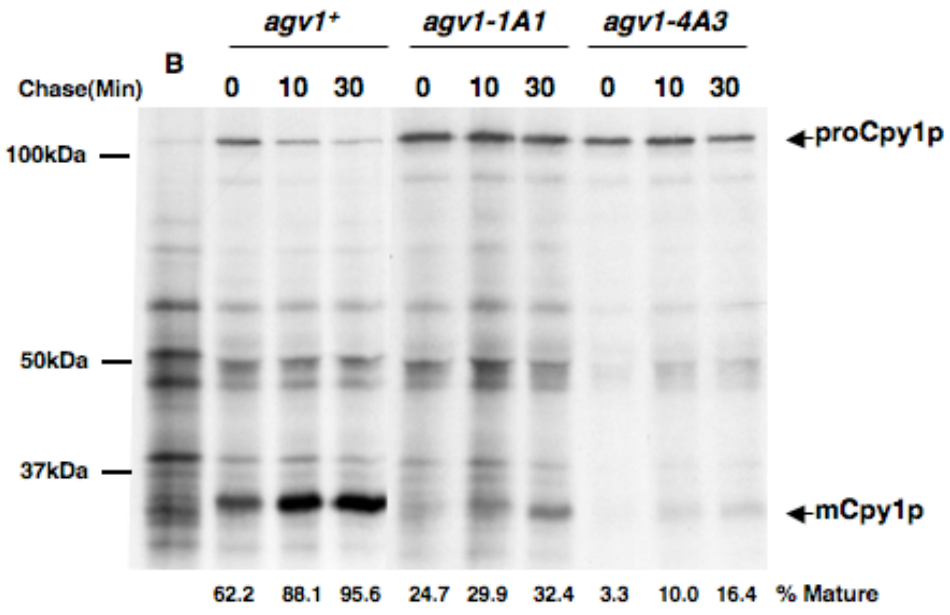
agv1+
agv1-1A1
agv1-4A3
B
Chase(Min)
0 10 30 0 10 30 0 10 30
100kDa
50kDa
37kDa
proCpy1p
mCpy1p
62.2 88.1 95.6 24.7 29.9 32.4 3.3 10.0 16.4 % Mature

B

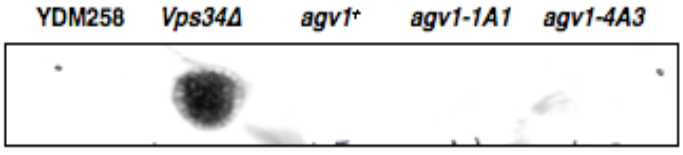
YDM258
Vps34Δ
agv1+
agv1-1A1
agv1-4A3

Figure 3-7

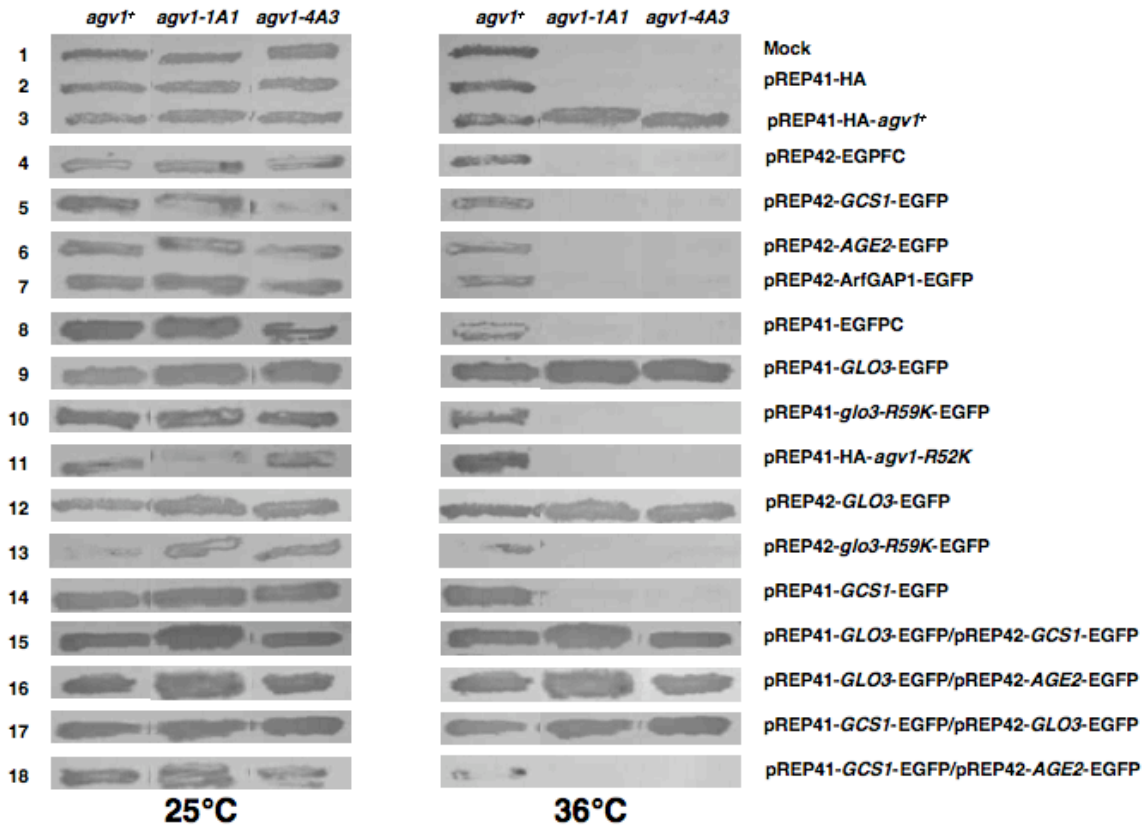
agv1+
agv1-1A1
agv1-4A3
agv1+
agv1-1A1
agv1-4A3
1
2
3
4
5
6
7
8
9
10
11
12
13
14
15
16
17
18
Mock
pREP41-HA
pREP41-HA-agv1+
pREP42-EGPFC
pREP42-GCS1-EGFP
pREP42-AGE2-EGFP
pREP42-ArfGAP1-EGFP
pREP41-EGFPC
pREP41-GLO3-EGFP
pREP41-glo3-R59K-EGFP
pREP41-HA-agv1-R52K
pREP42-GLO3-EGFP
pREP42-glo3-R59K-EGFP
pREP41-GCS1-EGFP
pREP41-GLO3-EGFP/pREP42-GCS1-EGFP
pREP41-GLO3-EGFP/pREP42-AGE2-EGFP
pREP41-GCS1-EGFP/pREP42-GLO3-EGFP
pREP41-GCS1-EGFP/pREP42-AGE2-EGFP
25°C
36°C

Figure 3-8

TABLE 3-1: Slopes for Growth Kinetic Studies

Plasmid Backbone	Arf GAP	*agv1*$^{+}$	*agv1-1A1*	*agv1-4A3*
	MOCK	0.060	-0.004	-0.002
pREP41	HA-Agv1	0.057	0.070	0.072
pREP41	HA-Agv1-R52K	0.053	0.007	0.004
pREP41	Glo3-EGFP	0.060	0.062	0.054
pREP41	Glo3-R59K-EGFP	0.069	-0.004	-0.005
pREP41	Gcs1-EGFP	0.056	-0.002	-0.006
pREP42	Agv1-EGFP	0.047	0.069	0.078
pREP42	Agv1-R52K-EGFP	0.056	0.013	0.002
pREP42	Glo3-EGFP	0.030	0.070	0.025
pREP42	Glo3-R59K-EGFP	0.035	-0.004	-0.005
pREP42	Gcs1-EGFP	0.068	0.001	-0.003
pREP42	Age2-EGFP	0.040	0.000	0.000
pREP42	ArfGAP1-EGFP	0.052	0.000	0.001
pREP41/pREP42	Glo3-EGFP/Gcs1-EGFP	0.071	0.081	0.012
pREP41/pREP42	Gcs1-EGFP/Glo3-EGFP	0.063	0.065	0.025
pREP41/pREP42	Glo3-EGFP/Age2-EGFP	0.069	0.086	0.056
pREP41/pREP42	Gcs1-EGFP/Age2-EGFP	0.065	-0.001	-0.002
Wild-type Haploid Strain YDM105		0.065		

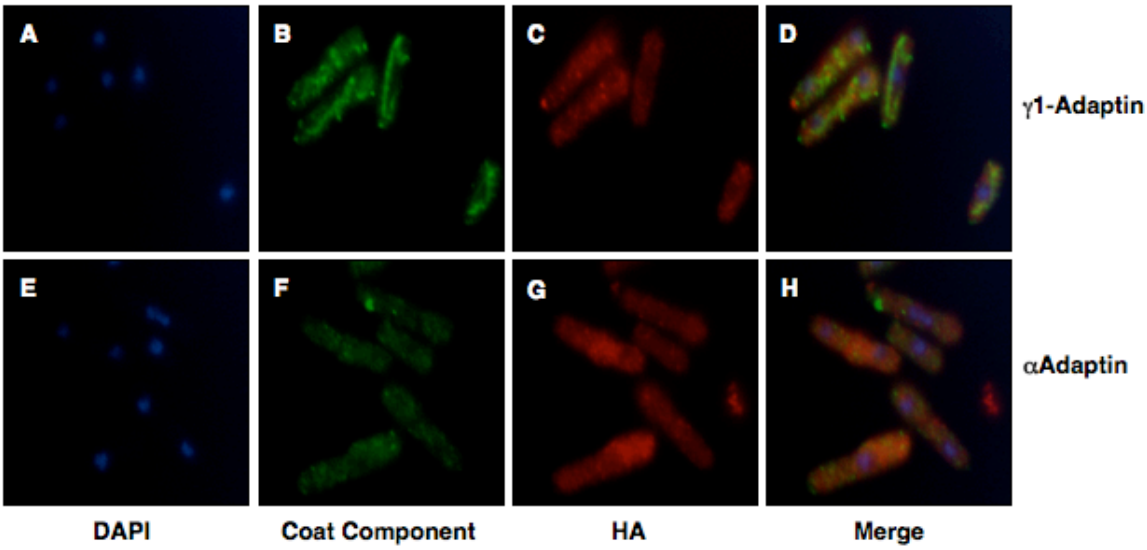

Figure 3-9

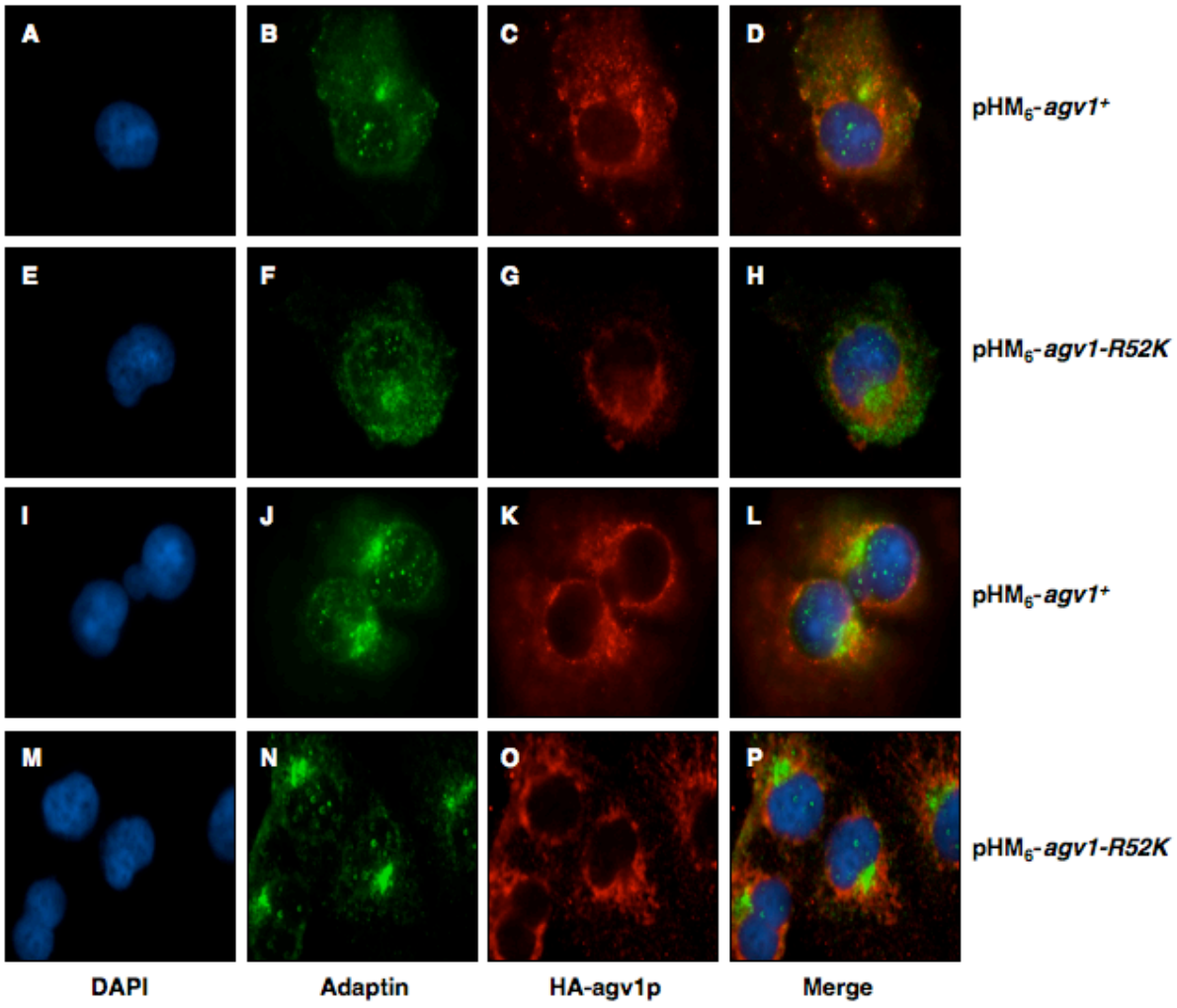
A
B
C
D
pHM6-agv1+
E
F
G
H
pHM6-agv1-R52K
I
J
K
L
pHM6-agv1+
M
N
O
P
pHM6-agv1-R52K
DAPI
Adaptin
HA-agv1p
Merge

Figure 3-10

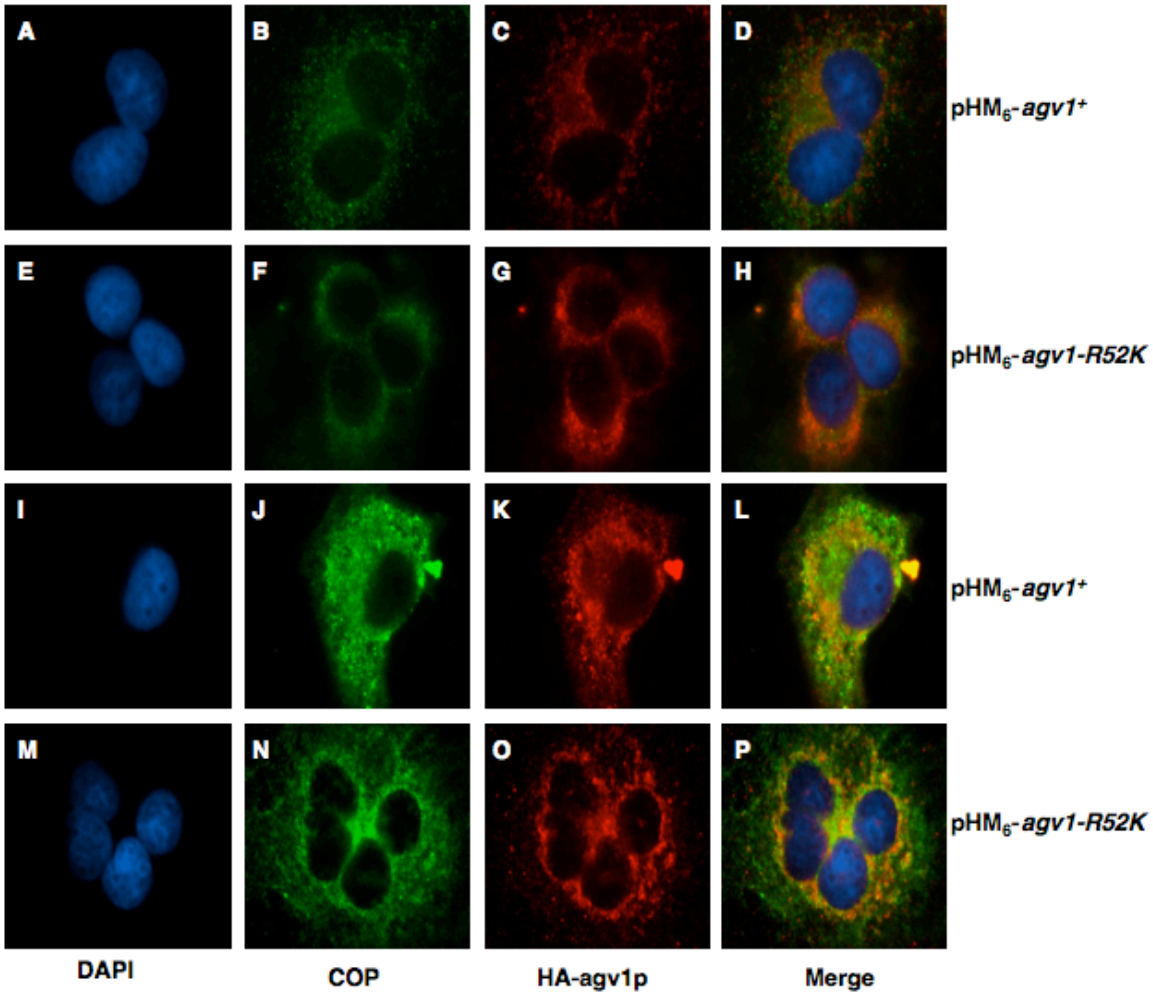
A
B
C
D
pHM6-agv1+
E
F
G
H
pHM6-agv1-R52K
I
J
K
L
pHM6-agv1+
M
N
O
P
pHM6-agv1-R52K
DAPI
COP
HA-agv1p
Merge

Figure 3-11

CHAPTER IV

SUMMARY

To develop a genetic approach for studying the function of hRIP, we sought to identify a putative ortholog in a genetically tractable model organism, *Schizosaccharomyces pombe*. Following cloning of a candidate gene, we generated null and temperature sensitive (*ts*) mutants and used them to perform a comprehensive phenotypic analysis. Genetic complementation studies also were analyzed using known yeast and mammalian Arf GAPs. These collective approaches were able to demonstrate that the candidate gene is an Arf GAP, which is essential for viability, *agv1*$^{+}$.

Phylogenetic analysis

The N-terminal zinc finger amino acid sequence of hRIP was initially used as a query in database searches for putative orthologs in species ranging from yeast to mammals. The absence of an hRIP ortholog in budding yeast prompted us to examine the genome of another genetically tractable organism, *S. pombe*. Five proteins containing the C-X_2-C-$X_{16\text{-}17}$-C-X_2-C zinc finger domain can be predicted from the *S. pombe* genome. Two of the predicted proteins contain an internal zinc finger, while the other two have an N-terminal zinc finger. Because it is most similar overall to hRIP coding sequence, ORF SPAC22E12.17c (*agv1*$^{+}$)

was selected for further investigation. It is important to note that although there are other fission yeast proteins that contain a zinc finger, their activities are not sufficient to confer viability to the *agv1Δ* or *agv1^{ts}* strains. Based on these observations, we conclude these proteins do not have overlapping function with Agv1. In contrast, the four *S. cerevisiae* proteins containing an N-terminal C-X_2-C-X_{16-17}-C-X_2-C zinc finger domain have overlapping functions in that they are able to cover or partially cover for each other in deletion mutants (Poon *et al*, 1999; Poon *et al*, 2001; Zhang *et al*, 2003). Although hRIP and Agv1 share sequence homology, there is a great deal of evolutionary time and distance between human and fission yeast. Therefore, it is not surprising that distantly related genes are unable to functionally substitute for each other. Moreover, in the absence of complementation data, classification as an ortholog necessitates use of bioinformatics and analyses with other members of a given protein family.

To gain insight into the possible phylogenetic relationship between Arf GAPs, we analyzed fourteen divergent zinc finger domain containing proteins using PROfile Multiple Alignment with predicted Local Structure (PROMALS; Pei and Grishin, 2007). At present, PROMALS is widely considered the most effective alignment algorithm for studying highly divergent protein families. This strategy employs the alignment of multiple protein sequences using secondary structure prediction, and primary amino acid sequences. PROMALS identified 299 related Arf GAPs and the generated alignment strongly suggests that Agv1 is

a pre-metazoan ancestral paralog for the ArfGAP1 and ArfGAP3 subfamilies. Based on these analyses, there is probably an extinct ancient Arf GAP, which gave rise to the three putative N-terminal zinc finger-containing *S. pombe* Arf GAPs. However, Agv1 appears to be the most likely candidate for the ancestral paralog, which gave rise to a duplication or divergence for these particular families of ARF GAPs (Figure 4-1). We propose that, at some point, prior to the divergence of the budding yeasts and ancestral single cell fission organisms, Agv1 underwent a duplication event, which led to the formation of two paralog families. One paralog family gave rise to Glo3 in *S. cerevisiae* and ArfGAP3 in humans and still closely resembles Agv1. The other paralog family underwent a later duplication event that formed two additional paralog families: one gave rise to Gcs1 in *S. cerevisiae* and ArfGAP1 in human; the other gave rise to Age2 in *S. cerevisiae* and centaurin-α1 in human. Interestingly, hRIP appears to have developed at some point further along the ArfGAP1 pathway - its current arrangement of domains first evident in sperm-producing eukaryotes. Complementary analyses of primary amino acid sequences and secondary structure provide compelling evidence that Agv1 is an ancestor of the ArfGAP families involved in vesicular transport. Moreover, the PROMALS alignments suggest hRIP most likely descended from one of the two additional Agv1 paralog families.

Agv1 structural domains: Implications for function(s)

Comprehensive analyses of the putative structural domains of Agv1 suggest a possible role in trafficking within the cytoplasm. The N-terminus contains a C-X_2-C-X_{16-17}-C-X_2-C zinc finger, which is essential for GAP activity in many Arf GAPs including mammalian proteins ArfGAP1, ASAP1, and PAPβ (Cukierman, *et al*, 1995; Randazzo *et al*, 2000; Mandiyan *et al*, 1999) as well as *S. cerevisiae* proteins Gcs1, Glo3, and Age2 (Poon *et al*, 1996; Lewis *et al*, 2004; Poon *et al*, 2001). ArfGAP3 is another member of the ArfGAP1 family of Arf GAPs, which exhibits Arf GAP activity and contains this zinc finger motif (Liu *et al*, 2001). A catalytically inactive form of Agv1, in which the invariant arginine residue is mutated to a lysine residue, fails to restore viability in the absence of Agv1, further supporting that the Arf GAP activity of Agv1 is essential for viability.

Analysis of mammalian ArfGAP1 truncation mutants reveals that the highly hydrophobic serine-threonine rich central region of this protein is essential for sensitivity to membrane curvature (Bigay *et al*, 2005). Gcs1, the proposed *S. cerevisiae* homolog of ArfGAP1 has also been shown to be sensitive to membrane curvature. This central region is conserved in both ArfGAP1 and Gcs1 and forms two amphipathic helices. These motifs have been named ArfGAP1 lipid packing sensors (ALPS1 and ALPS2). Mutations of the most conserved hydrophobic residues in the ALPS motifs reduce sensitivity to

membrane curvature in both *in vitro* Arf GAP assays and flotation assays using liposomes of defined sizes (Bigay *et al*, 2005; Mesmin *et al*, 2007). The amphipathic helices generated by the ALPS motifs have polar faces rich in serine and threonine residues rather than the positively charged residues normally found in most amphipathic helices, preventing electrostatic interactions and generating an amphipathic helix that senses rather than promotes membrane curvature. Replacing the serine and threonine residues with charged lysine residues reduces sensitivity to membrane curvature as measured by *in vitro* Arf GAP assays, flotation assays and binding assays using liposomes of defined sizes (Drin *et al*, 2007).

S. pombe Agv1 also contains a central region rich in serine and threonine residues. Many of these residues are present within helical regions; however, they do not appear to constitute an ALPS similar to those described for the budding yeast Arf GAP Gcs1 or the mammalian Arf GAP, ArfGAP1. Instead, these residues appear to form three α-helices, generating a Bin/Amphiphysin/Rvs (BAR) domain. BAR domains have been shown to be present in proteins involved in membrane remodeling, T-tubule formation, recycling of synaptic vesicles, and have been associated with sensing and/or inducing membrane curvature (Peter *et al*, 2004). A BAR domain forms a bundle of three α-helices, which homo- or heterodimerize with other BAR domains. This structure generates a crescent-shaped structure capable of binding negatively

charged membranes electrostatically via an interaction mediated by its positively charged concave surface. A BAR domain is often preceded by an amphipathic helix and termed an N-BAR domain. Two dimerized N-BAR domains would generate a structure with terminal amphipathic helices that could insert into the lipid membrane, displace phospholipids, and induce membrane curvature (Peter *et al*, 2004). Given that the rate of GTP hydrolysis by ArfGAP1 has been shown to increase with an increase in membrane curvature (Bigay *et al*, 2003), and that the BAR domain is predicted to bind more tightly to curved membranes than to flat membranes (Peter *et al*, 2004), the presence of a BAR domain could regulate the timing of GTP hydrolysis by Agv1 during vesicle formation.

Recently, a well-conserved repeated ISSXXXFG sequence has been reported to be necessary for *S. cerevisiae* Glo3 function *in vivo* (Yahara *et al*, 2006). This putative motif is also conserved in mammalian ArfGAP3. Agv1 contains a similar motif in its C-terminal non-catalytic domain; interestingly, the *agv1-4A3* mutant strain contains a serine to a proline mutation in this motif. It has been previously suggested that this motif could function in mediating interactions between the Arf GAP and the COPI coat or cargo proteins. In support of this notion, *S. cerevisiae* Glo3 has previously been shown to interact with SNAREs as well as COPI coat components (Eugster *et al*, 2000; Lewis *et al*, 2004; and Watson *et al*, 2004). The interaction of the SNAREs, Bet1, Sec22, or Bos1 with Arf1 and the COPI coat is Glo3 dependent (Rein *et al*, 2002).

However, the precise function of this repeat sequence remains to be demonstrated. Our preliminary experiments suggest the possibility that Agv1 may have the ability to localize with COPI coat proteins.

Anterograde and retrograde transport in the ER - Golgi shuttle

Previous genetic screens in *S. cerevisiae* have identified factors involved in ER retrieval using the normally secreted α-factor receptor, Ste2, fused to the dilysine motif from a subunit of the N-oligosaccharyl transferase complex, WBP1 (Ste2-WBP1). The presence of a dilysine motif brings the resultant fusion protein to the ER, thereby abolishing the ability of cells expressing the protein to mate. Interestingly, a *glo3* mutant strain mislocalizes Ste2-WBP1 to the plasma membrane (PM), hence is competent for mating (Dogic *et al*, 1999). Based on this observation, it has been suggested that Glo3 plays a role in retrograde transport.

Our intracellular localization analysis of ER- and Golgi-membrane resident GFP fusion proteins in the *agv1*^{ts} strains indicate loss of Agv1 results in a disruption of transport between the ER and the Golgi at 36°C. The diffuse localization of GFP-gma12 after four hours at 36°C is consistent with a loss of ER-retrieval resulting in a lack of factors essential for anterograde transport. Most likely, the subsequent block in anterograde transport results in a depletion of factors required to maintain Golgi integrity. In contrast, the punctate

cytoplasmic localization of GFP-13g6 after two hours at 36°C suggests a possible defect in anterograde transport from the ER to the Golgi. Ultrastructural analysis using electron microscopy shows striking accumulation of intracellular membranes within the cytoplasm in the *agv1*^{ts} strains at restrictive temperature. However, these findings provide limited insight as to whether Agv1 plays a role in retrograde transport, or both retrograde transport and anterograde transport. Lastly, pulse-chase immunoprecipitation analysis of Cpy1 in *agv1*^{ts} strains results in an accumulation rather than a delay in processing of pro-Cpy1, consistent with a block within the ER or Golgi. It is worth noting, this assays newly synthesized Cpy1 at a semi-permissive temperature (30°C), which might offer an advantage for monitoring a potential defect in anterograde transport.

Newly synthesized membrane proteins, soluble lysosomal/vacuolar proteins, and secreted proteins are transported along the secretory pathway using vesicular trafficking steps conserved among all species. An N-terminal signal sequence directs these proteins to the ER rather than to the cytoplasm for translation. Properly folded proteins are able to exit the ER and are taken up into coat protein complex II (COPII) vesicles, which require the GTPase Sar1, the GAP Sec23/24 complex, and the coat component Sec13/31 complex. The COPII vesicles travel to the ER-Golgi intermediate compartment (ERGIC). Whether the ERGIC is a pre-existing compartment or formed by the fusion of the COPII vesicles is still unclear. Nevertheless, the ERGIC contains both COPII and COPI

components and therefore is the first sorting step in the secretory pathway. Retrograde cargo retrieval from the ERGIC back to the ER is mediated by COPI vesicles. It is still up for debate whether anterograde transport from the ERGIC to the *cis*-Golgi is COPI-dependent or COPI-independent (reviewed in Béthune et al, 2006). However, trafficking from the ER to the Golgi has been shown to involve sequential steps for COPII and COPI coats by the use of stage specific *in vitro* transport assays. Vesicular-tubular clusters (VTC) leaving the ER rapidly lose COPII coats and acquire COPI coats *in vitro* (Aridor *et al*, 1995). Other studies in living cells confirm that VTC structures moving toward the Golgi rapidly acquire COPI proteins (Stephens *et al*, 2000). The COPI coat on the anterograde moving VTCs are thought to function in cargo sorting, suggesting that the anterograde and retrograde transport pathways are tightly linked. Due to the tight coupling of the two pathways, loss of Golgi to ER retrograde transport results in a lack of factors necessary for anterograde transport (reviewed in Duden, 2003). COPI vesicles are also believed to mediate further anterograde transport within the Golgi apparatus (reviewed in Béthune *et al*, 2006; Gaynor *et al*, 1998).

Cargo sorting, membrane curvature, and the role of Arf GAPs in COPI vesicle generation

COPI vesicle biogenesis is initiated by the activation of GDP-bound Arf1 by a guanine nucleotide exchange factor (GEF), which stimulates the binding of GTP causing a conformational change leading to the exposure of an N-terminal myristoylation signal and an amphipathic helix, which associate with the membrane. The remaining steps in the generation of COPI vesicles are regulated by the uptake and sorting of cargo, the interaction of cargo with Arf GAPs and coat components, as well as lipid composition and membrane curvature. In addition to *S. cerevisiae* Glo3 having been previously shown to interact with v-SNAREs and COPI coat components (Eugster *et al*, 2000; Lewis *et al*, 2004; Watson *et al*, 2004), the recruitment of mammalian ArfGAP1 to membrane by the ER retention-defective complementation group 2 (ERD2) receptor (Aoe *et al*, 1997) is believed to play a role in the regulation of Arf1 activation (Aoe *et al*, 1999). Studies also suggest that Arf GAP activation, and thus vesicle formation, is mediated by lipid composition and membrane curvature. The rate of GTP hydrolysis stimulated by mammalian ArfGAP1 increases with a decrease in the size of a lipid polar head group and an increase in the number of monounsaturated acyl chains suggesting that lipid packing plays a role in Arf GAP activity (Figure 4-2A; Antonny *et al*, 1997; reviewed in Nie and Randazzo, 2006). Furthermore, the rate of ArfGAP1 stimulated GTP hydrolysis

increases when liposomes decrease in radii from large radii (150nm) to typical coated vesicle size (<50nm), suggesting ArfGAP1 is sensitive to membrane curvature (Figure 4-2B; Bigay *et al*, 2003; reviewed in Nie and Randazzo, 2006).

Current models for COPI vesicle formation take into account the role of cargo and membrane composition and curvature in the stimulation of GTP hydrolysis. In the 'control by curvature' model (Figure 4-3A; Nie and Randazzo, 2006), the coatomer and Arf GAP are recruited to the membrane at the same time. The Arf GAP binds to Arf1 and COPI, forming a complex, which collects cargo and aggregates together to polymerize the vesicular coat and begin bending the membrane. When the membrane reaches the correct curvature, the Arf GAP is activated, hydrolyzing GTP. The inactivated GDP-bound Arf1 dissociates from the tip of the budding vesicle. The negative membrane curvature around the neck of the budding vesicle keeps the Arf GAP from hydrolyzing GTP prematurely (Bigay *et al*, 2003; Nie and Randazzo, 2006). In the 'proofreading' model (Figure 4-3B), Arf1 is activated, an active Arf GAP and COPI coat are recruited and bind to the membrane with a low affinity, cargo associates with the COPI coat proteins displacing Arf1-GTP from the COPI coat proteins. The Arf-GTP binds to Arf GAP causing the irreversible hydrolysis of GTP. Arf is inactivated and the GDP-bound Arf dissociates from the membrane and is recycled. The coat then polymerizes, the vesicle buds, and is released (Nie and Randazzo, 2006).

The control by curvature and proofreading models are both plausible for vesicle formation by BAR domains containing Arf GAPs. The amphipathic helix at the N-terminus of an N-BAR domain induces membrane curvature (Peter *et al*, 2004), which would allow for an Arf GAP to already be in the active form before the induction of membrane curvature as seen in the proofreading model. However, the ALPS motifs in mammalian ArfGAP1 and *S. cerevisiae* Gcs1 are able to sense, but are not predicted to induce, membrane curvature (Drin *et al*, 2007). If the curvature of the membrane and the packing of the lipids effects GTP hydrolysis stimulated by ArfGAP1, then ArfGAP1 cannot be in an active form until the membrane reaches the correct curvature to generate gaps in the lipid head groups. This would argue for the control by curvature model, and suggests the possibility that different Arf GAPs might form vesicles by different mechanisms. Modifying the control by curvature model to reflect an earlier role for cargo in the recruitment of an inactive Arf GAP to the membrane would satisfy the requirement for cargo and positive membrane curvature in Arf GAP activation.

Viral RNA uses vesicular trafficking pathways for transport within the cytoplasm.

We have recently shown using a dominant negative mutant of hRIP, hRIPΔN360, and using RNA interference that loss of functional hRIP causes

mislocalization of Rev-directed RNA to the perinuclear region indicating that hRIP is a cellular Rev cofactor involved in movement of HIV-1 viral RNA from the nuclear periphery to the cytoplasm (Sanchez-Velar *et al*, 2004). Overexpression of hRIPΔN360 or depletion of hRIP by RNA interference inhibits HIV-1 production and causes accumulation of Rev-directed viral RNAs around the nuclear periphery in mammalian cells (human T cell lines and primary macrophages), confirming that hRIP is required for HIV-1 viral replication (Yu *et al*, 2005).

Studies suggest that viral RNA is transported through the cytoplasm on the way to the plasma membrane for assembly and budding via vesicular trafficking pathways. Tumor susceptibility gene (Tsg101) is a protein involved in the vacuolar protein sorting (Vps) pathway and was identified in a yeast two-hybrid screen for proteins that could bind to the PTAP late domain of the HIV-1 p6 protein. Depletion of Tsg101 by RNA interference results in late stage arrest of HIV-1 budding (Garrus *et al*, 2001).

Additionally, studies indicate that MLV genomic RNA is transported to the PM by endosomal vesicles. A single MLV RNA molecule was visualized in living cells moving in a directed rectilinear fashion over long distances on what appear to be vesicles. The MLV RNA co-localizes predominantly with transferrin-containing recycling endosomes, but also co-localizes with late endosomes and lysosomes in a Gag and Env dependent manner (Basyuk *et al*, 2003). Further studies using MLV RNA reporters with mutations in the packaging signal indicate

that stem-loop A is required for the directed RNA movement on endosomes. A cellular reporter mRNA, LacZ, shows high levels of directed movement and co-localizes with late endosomes, suggesting that in the absence of RNA with packaging signals, Gag and Env can transport cellular RNA on endosomal vesicles (Basyuk et al, 2005).

An additional precedent for cellular RNA traveling on a vesicle was the identification of Pab1, a budding yeast poly A binding protein as an Arf1-Q71L interactor by affinity chromatography (Trautwein *et al*, 2004). Pub1, a poly U binding protein, does not interact with Arf1-Q71L, and Pab1 does not interact with Sar1, indicating the Arf1-Pab1 interaction is specific. Treatment of the reaction with RNase A abolishes the interaction, indicating that the Arf1-Pab1 interaction is RNA dependent. Pab1 sediments with vesicles in an *in vitro* Golgi budding assay, suggesting that Pab1 is associated with COPI vesicles. The co-sedimentation was abolished when the reaction was treated with RNase A, indicating the association is also RNA dependent (Trautwein *et al*, 2004). To further assess the Arf1–RNA interaction, anti-Arf1 immunoprecipitates were subjected to RT-PCR, resulting in all mRNAs tested being present in the anti-Arf1 complex, and suggesting that COPI vesicles could associate with a variety of different mRNAs. Using an GFP-MS2 fusion protein to detect the localization of an MS2-binding domain-containing ASH1 mRNA reporter construct, ASH1 mRNA

was unable to localize to the bud tip in *arf1Δ* cells, indicating that Arf1 is necessary for correct localization of ASH1 mRNA (Trautwein *et al*, 2004).

Summary

At present, it remains to be determined whether hRIP and S. pombe Agv1 may be functional orthologs. Homology is defined as a similarity between structures due to a shared ancestry. Genes are considered homologous when they share a high sequence identity or similarity. Homologous genes are considered orthologs if they are separated by a speciation event and orthology can be established by functionally replacing a mutant copy of one gene with the similar gene from a different species. Based on our collective findings (see supplemental section), we suggest hRIP and Agv1 may share the ability to perform certain process-specific functions. First, we have shown that Agv1 can selectively interact with the Rev NES *in vitro*. Second, the ability of Rev-GFP to shuttle between the nucleus and the cytoplasm is altered in cells depleted of hRIP or in the *agv1*^{ts} strains at 36°C. Third, in the absence of hRIP or Agv1 activity, 5S rRNA is mislocalized and accumulates aberrantly at the nuclear periphery or in tubular structures within the cytoplasm, respectively. Fourth, hRIP has been found to interact with cellular factors involved in multiple vesicular membrane trafficking pathways.

Our results indicate that Arf GAP catalytic activity is necessary to maintain viability in the absence of Agv1 function. Based on sequence comparisons of known yeast Arf GAPs, Agv1 contains a novel repeat motif predicted to mediate protein-protein interactions. Initially described in *S. cerevisiae* Glo3, this motif is also present in members of the ArfGAP3 family (Yahara *et al*, 2006). We predict, therefore, that similar to other members of this subfamily, Agv1 might interact with COPI coat components, SNAREs, and other cargo proteins. It is also worth noting that similar to other Arf GAPs, Agv1 appears to contain a BAR domain, which might function to sense and induce membrane curvature. The presence of an N-BAR domain in Agv1 raises the intriguing possibility that membrane curvature is an important feature of the regulation of its catalytic activity.

To date, the functional dissection of Arf GTPase regulation has been complicated by the multiple biological roles of Arf and by the functional redundancies of Arf effectors. Unlike budding yeast, which has Arf GAP pairs with overlapping function, we have established that Agv1 is an essential Arf GAP in fission yeast. Therefore, Agv1 represents a new and important tool for studying mechanisms for sensing membrane curvature, regulating rates of GTP hydrolysis, and forming COPI coated vesicles. Agv1 is also uniquely suited to be exploited as the simplest Arf GAP available for studying basic fundamental components, which can be systematically identified and characterized without the drawback of the activity of other Arf GAPs. Systematic investigation of the Agv1

domains and characterization of their functions can advance our understanding of the role of Arf GAPs in the ER - Golgi shuttle specifically as well as in vesicular membrane trafficking in general.

Figure 4-1. Evolutionary relationship of the ArfGAP1/3 family. Arf GAP amino acid sequences were aligned using both PROMALS (Pei and Grishin, 2007) and Clustal W (Thompson *et al*, 1994).

(A) The rooted phenogram was generated using the K2 (Kimura 2-parameter) distance model while treating the gaps as missing sequences and is typical of the results produced with sequences aligned by either PROMALS or Clustal W. However, the arm-lengths, which attempt to reflect estimated evolutionary distance/time, vary due to the manner in which each program deals with gaps in sequences. SPAC824.09c and SPAC622.14 are predicted *S. pombe* Arf GAPs, which maintain an N-terminal zinc finger domain in common with an ancient ancestral Arf GAP. AGD8 and UBP20 are *A. thaliana* Arf GAPs, and together with *S. cerevisiae* Glo3 and human ArfGAP3, maintain the N-terminal zinc finger, central serine-threonine rich region/putative BAR domain, and the C-terminal ISSXXXFG "cargo" motif similar to Agv1. *S. cerevisiae* Age2 and human Centaurinα1 maintain an N-terminal zinc finger domain and a portion of the serine-threonine rich region. *S. cerevisiae* Gcs1 and human ArfGAP1 maintain an N-terminal zinc finger domain and a portion of the serine-threonine rich region that forms ALPS motifs. Putative Arf GAPs: hRIP and Rab-R, *D. melanogaster* Drongo, mosquito HRB (mHRB), and vertebrate HRB (vHRB), maintain an N-terminal zinc finger and the central serine-threonine rich region/BAR domain, and have acquired C-terminal NPF motifs.

(B) The PROMALS alignment of these distantly related Arf GAPs suggests Agv1 is the most likely candidate for a pre-metazoan ancestral paralog, which underwent a duplication event, leading to the formation of two paralog families. One paralog family gave rise to Glo3 in *S. cerevisiae* and ArfGAP3 in humans and still closely resembles Agv1. The other paralog family underwent a later duplication event that formed two additional paralog families: one gave rise to Gcs1 in *S. cerevisiae* and ArfGAP1 in human; the other gave rise to Age2 in *S. cerevisiae* and centaurin-α1 in human. Interestingly, hRIP appears to have developed at some point further along the ArfGAP1 pathway - its current arrangement of domains first becoming evident in sperm-producing eukaryotes. The green rectangles represent a α-helix; the yellow arrows represent a β-strand; the blue arrowheads indicate the NPF motifs; the red plus signs inside a circle represent duplication events.

Figure 4-2. ArfGAP1 activation is based on lipid polar head groups and membrane curvature.

(A) Smaller polar head groups pack less tightly than larger polar head groups and allow peripheral membrane proteins, such as an Arf GAP, to access the central hydrophobic portion of the lipid bilayer and become active.

(B) On a tightly packed flat membrane, an ArfGAP in unable to penetrate the lipid bilayer and is therefore inactive. On the convex portion of a budding vesicle,

the lipid packing is looser, allowing an ArfGAP to penetrate the bilayer and consequently become active.

Figure 4-3. Control by curvature and proofreading models for Arf1 function in COPI vesicle formation.

(A) In the control by curvature model, Arf1 is activated by GTP exchange for GDP at the membrane by a GEF (1). The COPI coat components are recruited to the membrane by the activated Arf1-GTP (2a). At the same time, Arf GAP is recruited, binds to the membrane (2b), and is incorporated into the Arf1-GTP-COPI coat complex (3). The COPI coat polymerizes, driving vesicular budding (4). The Arf GAP is activated by the curved surface of the membrane (5) and subsequently hydrolyzes GTP, causing the inactivated Arf to dissociate from the membrane (6). The COPI coat is stably polymerized and remains anchored to the membrane through interactions with cargo and with inactive Arf GAP at the base of the bud. Upon release of the bud, the entire vesicular surface is convex, activating the remaining Arf GAP.

(B) In the proofreading model, Arf is activated through GTP exchange for GDP by GEF (1) and the COPI coat components and an active Arf GAP are recruited to the site of vesicle formation (2). The COPI coat proteins bind to cargo on the membrane displacing Arf-GTP (3a). The active Arf GAP binds to Arf-GTP, hydrolyzes the GTP on Arf and causing Arf-GDP to dissociate from the

membrane (3b). The COPI coat then polymerizes leading to membrane budding of the coated vesicle.

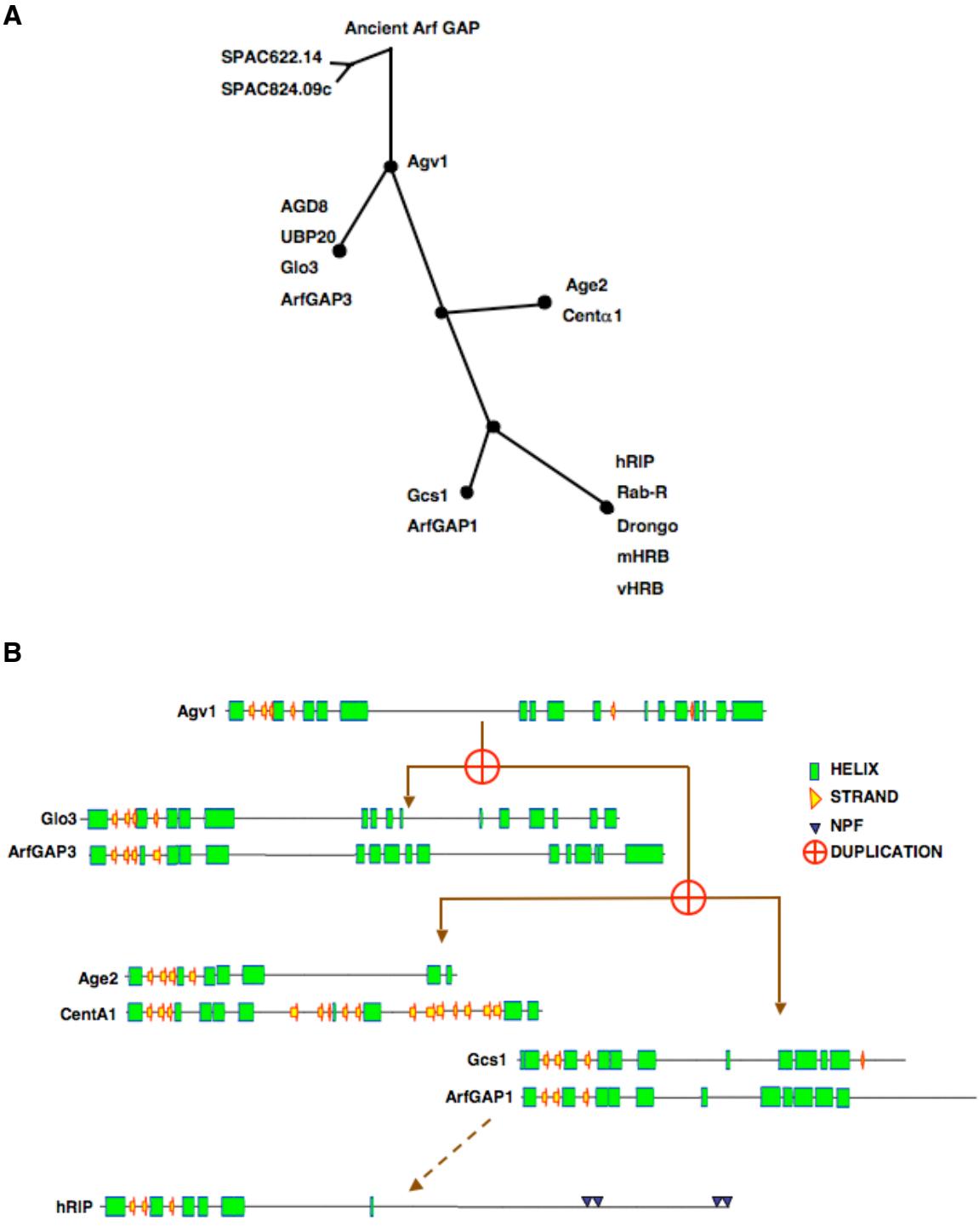
A
Ancient Arf GAP
SPAC622.14
SPAC824.09c
Agv1
AGD8
UBP20
Glo3
ArfGAP3
Age2
Centα1
hRIP
Rab-R
Drongo
mHRB
vHRB
Gcs1
ArfGAP1
B
Agv1
Glo3
ArfGAP3
Age2
CentA1
Gcs1
ArfGAP1
hRIP
HELIX
STRAND
NPF
DUPLICATION

Figure 4-1

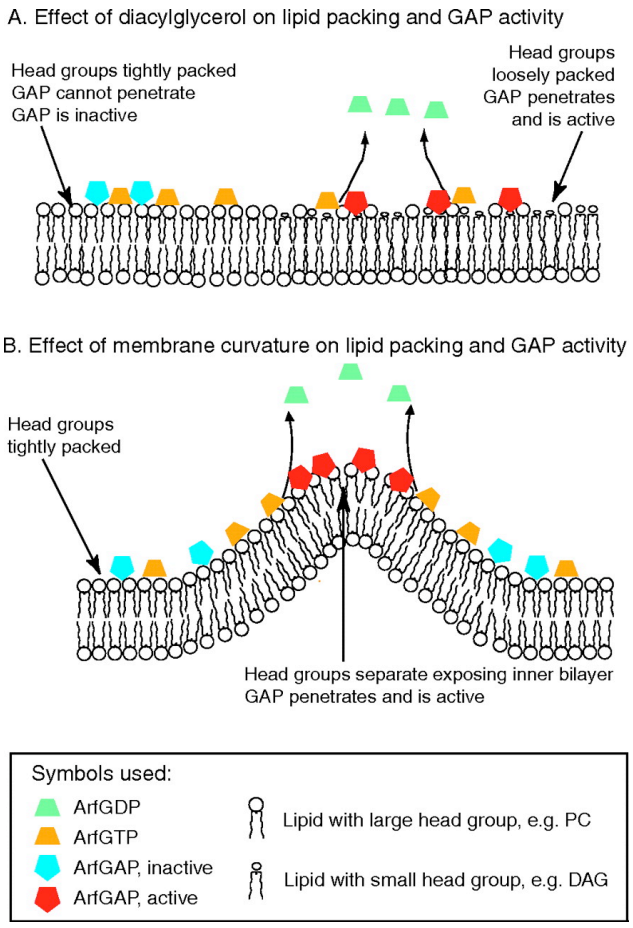

Nie and Randazzo *J Cell Sci* **119**: 1203-1211

Figure 4-2

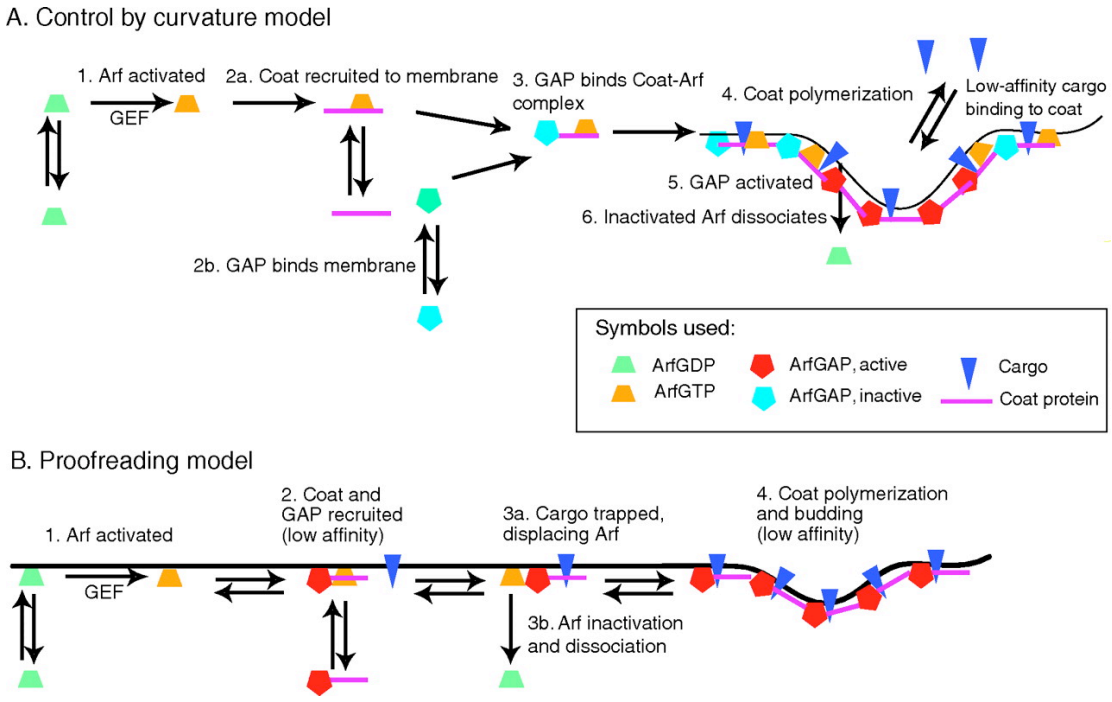

Nie and Randazzo *J Cell Sci* **119**: 1203-1211

Figure 4-3

CHAPTER V

MATERIALS AND METHODS

Plasmids and Yeast Strains

Recombinant DNA plasmids and *S. pombe* strains were constructed using standard techniques described in Sambrook *et al*, 1989 and Moreno *et al*, 1991. The plasmids used in these studies are listed in Table 5-1. The yeast strains used in these studies are listed in Table 5-2.

Cloning of the *agv1*$^+$ cDNA and genomic sequence

Cellular RNA and chromosomal DNA were isolated from a 50 ml culture of wild-type haploid *S. pombe* cells (YDM105; *ade6-210 leu1-32 ura4-D18 h*$^+$ or YDM108; *ade6-216 leu1-32 ura4-D18 h*$^-$) grown to mid-log phase (OD_{595nm} = 0.5/ml), pelleted, most of the media removed, and frozen at -20°C. The pellet was thawed at room temperature (RT), digested with 1μl Enzyme Cocktail [1.8g Driselase and 1.8g β-D-Gluconase, 1.2M sorbitol in 10ml 1X PBS (1mM KH_2PO_4, 10mM Na_2HP0_4, 130mM NaCl, 2.7mM KCl at pH 7.0)] for 15-30 minutes at room temperature (RT), and extracted with 5ml TriReagent (Molecular Research Center). Cell extract was vortexed with 1/5th volume Bromo-Chloro-Propane. The top phase containing total RNA was collected into a sterile RNase-free tube and the RNA was precipitated with 2.5ml (1/2 starting volume) of isopropanol for

15 minutes at room temperature. To collect the DNA, the interface and bottom phase were precipitated with 1/3 volume ethanol, mixed by inversion, incubated on ice for 15 minutes, and collected by centrifugation at 2,000g for 5 minutes at 4°C. The phenol-ethanol supernatant was removed, the DNA pellet washed twice with 0.1M trisodium citrate in 10% ethanol for 30 minutes at RT, then washed with 75% ethanol for 10-20 minutes at RT, and allowed to air-dry for 3-5 minutes at RT. The DNA pellet was stored at -20°C, when needed the DNA was dissolved in 8mM NaOH by slowly pipetting up and down on ice.

Total cellular RNA (5μg) was heated at 75°C for fifteen minutes in the presence of 166pM random DNA hexamers and 10U RNasin (Promega). Following a short incubation at 4°C, 1U Superscript II Reverse Transcriptase (RT; Invitrogen), 5X First Strand Buffer (250mM Tris-HCl pH 8.3, 375mM KCl, 15mM $MgCl_2$), and 200μM each dNTPs were added and the reaction incubated at 42°C for one hour. This cDNA was amplified by PCR with oligonucleotide primers complementary to nucleotides (nts) 5048536-5048508 or 5046927-5046954 of locus SPAC22E12.17c on *S. pombe* 972h$^-$ Chromosome I (Wood, *et al.,* 2002; gi: 63054470/NC_003424.2). Primer sequences are written in the 5' to 3' direction as follows: (SF-1) gat cgc ccc ggg atc gac gga tcc cga aat tgc aaa aat gac tgc tac taa gg, (SR-1) gca tat ccc ggg cca act ctc gag tgc tac ttg agc tta agt tgg acg gat g. The *agv1*$^+$ cDNA was inserted into the BamHI/XhoI restriction sites of

pcDNA3 (Invitrogen), amplified by PCR with oligonucleotides written in the 5' to 3' direction as follows (*agv1*$^{+}$-F) cat cgt cga ctg cta cta agg aag aat ctc aaa aat tg and (*agv1*$^{+}$-R) cta ccc cgg gtt aaa aat tgt atc gag cac caa ctt ttt g, and cloned into the SalI/SmaI restriction sites of pREP41-HA and pREP81 fission yeast expression plasmids (Basi *et al*, 1993) generating thiamine repressible promoter (*nmt1*)-driven plasmids pMZA496 and pMZA497, respectively. The genomic DNA was amplified from chromosomal DNA (1.3*μ*g) by PCR using the SF-1 and SR-1 primers and also cloned into the BamHI/XhoI restriction sites of pcDNA3 (Invitrogen). The genomic sequence was inserted into the BamHI/XhoI restriction sites of pBS-KS (Stratagene) generating plasmid pMZA492. To obtain the full-length genomic sequence (from -484 to +2403) for mutagenesis, chromosomal DNA (1.3μg) was amplified by PCR using oligonucleotide primers complementary to nts 5049008-5048987 or 5046927-5046954 of locus SPAC22E12.17c on *S. pombe* 972h^{-} Chromosome I (Wood, *et al,* 2002; gi: 63054470/NC_003424.2). Primer sequences are written in the 5' to 3' direction as follows: (SF-2) ctc acc cgg gca act tgc tca ctc tac cta a; (SR-2) ctc acc cgg gga agc tgc ata aac atc gtc a. The full-length *agv1*$^{+}$ genomic sequence was inserted into the SmaI restriction site of a derivative of pBG1 (Burke and Gould, 1994) lacking the SacI restriction site in the multiple cloning site, generating plasmid pMZA498. The nucleotide sequence of both strands of both the *agv1*$^{+}$ genomic DNA and cDNA was determined by automated DNA sequence analysis.

Construction of the *agv1* deletion (null) mutant

The *agv1* deletion strain was generated using the one-step gene disruption and replacement strategy described in Grimm *et al*., 1988. The *agv1* knockout cassette was constructed as follows: the BamHI/XhoI fragment of pMZA492 was inserted into compatible restriction sites of pMZA493, a derivative of pSP72 (Promega) lacking EcoRI, EcoRV, and SmaI restriction sites. The resulting plasmid, pMZA494, was digested with EcoRI and PvuII to remove nucleotides 421 through 1281 from the *agv1*$^{+}$ ORF. Following gel purification, the linearized backbone was ligated with an EcoRI/PvuII fragment containing the *ura4*$^{+}$ selectable marker gene. The resulting plasmid, pMZA495, was digested with BglII/XhoI, the *agv1* knockout cassette isolated by gel electrophoresis, and transformed by a standard lithium acetate protocol into a wild-type diploid strain generated by mating haploid strains. YDM105 [*ade6-210 leu1-32 ura4-D18 h*$^{-}$] and YDM108 [*ade6-216 leu1-32 ura4-D18 h*$^{+}$] were mated on malt extract (ME) plates with appropriate supplements by streaking on top of each other with a toothpick and adding 10μl sterile ddH_2O to facilitate mixing. After overnight growth at 30°C, cells were streaked for isolation on Edinburgh minimal medium (EMM) containing uracil and leucine to select for diploids with complemented adenine mutations and grown at 30°C. Single colonies were checked for diploid status generating a temporary diploid strain with the genotype *ade6-210/ade6-*

216 leu1-32/leu1-32 ura4-D18/ura4-D18 h⁻/h⁺ before use in standard lithium acetate transformations.

Homologous recombination of the *ura4⁺* containing *agv1* knockout cassette into the chromosomal DNA, generates a heterozygous diploid (MZY214) with the genotype: *ade6-210/ade6-216 leu1-32/leu1-32 ura4-D18/ura4-D18 (ORF)⁺/(ORF)::ura4 h⁻/h⁺* that grows on EMM with leucine plates. Eight randomly chosen colonies were induced to sporulate on ME with leucine plates at 30°C. After 2 days, asci were transferred to yeast extract with supplements (YES; 0.5% w/v yeast extract, 3.0% w/v glucose, 225mg/L each of adenine, uracil, leucine, histidine, and lysine hydrochloride) plates and placed at 36°C for 2 hours to break down the asci walls. A micromanipulator was used to place the 4 isolated spores of each ascus into a line. The spores were grown at 30°C until colonies formed and ratios of spore segregation were determined.

To confirm integration of the *ura4⁺* knockout cassette into the *agv1⁺* locus, chromosomal DNA was extracted from 10ml cultures of three possible heterozygous diploids strains. The strains were grown to saturation in EMM with leucine at 30°C, collected at 2,500rpm for 5 minutes, washed in 500μl sterile ddH_2O, transferred to a 1.5ml microcentrifuge tube, and resuspended in 0.2ml of breaking buffer (10mM Tris pH 8.0, 1mM EDTA, 100mM NaCl, 1% SDS, 2%

Triton X-100). 0.2ml phenol:chloroform and 0.3g of acid washed glass beads (Sigma, 425-600μm) were added and the tubes vortexed for three minutes. 200μl TE (10mM Tris, pH8.0, 1mM EDTA) buffer was added, the tubes vortexed briefly, the aqueous layer transferred to a new microcentrifuge tube, and the DNA precipitated with three times volume ethanol. The DNA was collected at 14,000rpm for 3 minutes, resuspended in 400μl TE, digested with 0.075mg/ml RNAse A for five minutes at 37°C, precipitated with 0.1M ammonium acetate and three times volume ethanol, resuspended in 100μl TE buffer and transformed in XL-1 Blue (Stratagene) competent bacterial cells. DNA was isolated from bacterial transformants by a standard alkaline lysis protocol (Sambrook *et al*, 1989) and the nucleotide sequence of both strands of the chromosomal DNA was determined by automated DNA sequence analysis.

Disruption of the *agv1*$^+$ chromosomal locus was confirmed by PCR-based analysis using oligonucleotide primers complementary to *agv1*$^+$ sequences flanking the *ura4*$^+$ gene insertion site or to sequences at the 5' and 3' ends of the *ura4*$^+$ gene. Oligonucleotide sequences written in the 5' to 3' direction are as follows: (F1) tag tgt cag aca tta aga aag tat att gga, (R1) taa cac aaa tgc ata cat ata gcc agt ggg, (F2) cat tgg tgt tgg aac aga ata aat tag atg, (R2) ccc gaa ttc gaa gat ggc atg ttt aac ctt g

Plasmid Construction and Site-Directed Mutagenesis

To generate *agv1*$^{+}$ and hRIP expression plasmids, cDNA inserts were generated by PCR amplification using pMZA490 or pBC12-CMV-RAB (Bogerd *et al*, 1995) as a template, and inserted into the SalI/SmaI restriction sites of pREP41-HA and/or pREP81. Oligonucleotide sequences are written in the 5' to 3' direction as follows: (*agv1*$^{+}$-F) cat cgt cga ctg cta cta agg aag aat ctc aaa aat tg, (*agv1*$^{+}$-R) cta ccc cgg gtt aaa aat tgt atc gag cac caa ctt ttt g, (hRIP-F) cat cgt cga ctg cgg cca gcg cga agc gga agc agg, (hRIP+4aa-F) cat cgt cga cta gcg cga agc gga agc agg agg ag, (hRIP-R) cta ccc cgg ggg cta taa gaa agg att ggt tga tga gct tcc, (hRIPΔNPF-R) cag acc cgg gct acg tac gtc caa atg gag cag gca cac.

To generate *agv1*$^{+}$ bacterial expression plasmids for protein purification, inserts were generated by PCR amplification using pMZA496 as a template and inserted into the HindIII restriction site of pHB6 (Roche). Oligonucleotide sequences are written in the 5' to 3' direction as follows: (pHB6-F) cat gaa gct tga ctg cta cta agg aag aat ctc aaa aat tg, (pHB6-R) cta gaa gct tcc aaa att gta tcg agc acc aac ttt ttg. Correct orientation was determined by EcoRI digestion and analysis of restriction fragment sizes.

To generate *agv1*$^{+}$ mammalian expression plasmids for use in Cos7 cell, inserts were generated by PCR amplification using pMZA496 as a template and cloned into the HindIII restriction site of pHM6 (Roche) using oligonucleotides pHB6-F

and pHB6-R. Correct orientation was determined by EcoRI digestion and analysis of restriction fragment sizes.

To generate Arf GAP expression plasmids, inserts were generated by PCR amplification from chromosomal/genomic DNA (Glo3 and RnArfGAP1) or from the plasmids Yep352GLL4 (Age2; Poon *et al*, 2001) or pPP421 (Gcs1; Poon *et al*, 1999) and inserted into the BglII/SmaI (Glo3, ArfGAP1, and Age2) or SalI/BamHI (Gcs1) restriction sites of pREP41-EGFPC and/or pREP42-EGFPC (Craven *et al*, 1998). Oligonucleotide sequences are written 5' to 3' as follows: (Glo3-F) ggc cag atc tcg aca atg agt aac gat gaa gga a, (Glo3-R) cat acc cgg gga ttt tct taa gta gtc cct taa ata act acc, (Gcs1-F) gcc acc cgg gca att tta tcg cgg att gta gac cat gtc aga ttg gaa agt gg, (Gcs1-R) gaa tcc cgg gaa aaa cta tat taa aat tag gat ccg tcc cat ttg tcc tcg tcc, (ArfGAP1-F) cgg ccc ggg tca gat ctt ggc cag ccc aag aac cag aaa agt tct taa gga a, (ArfGAP1-R) tac acc cgg ggc cca gtt ctg gtt gtc cca gcc ctc gtc ggc ggc tgt aga, (Age2-F) cgg cag atc tcg acg tca gtc cca gtc aag aag gca t, (Age2-R) ccg acc cgg gca act cca gac gtt ctt aaa taa ctc g. The nucleotide sequence of both strands of all plasmids were determined by automated DNA sequencing analysis prior to use.

To generate point mutants by site-directed mutagenesis, plasmids pHM6-*agv1*$^{+}$, pREP41-HA-*agv1*$^{+}$, pREP42-*agv1*$^{+}$-EGFP, pREP41-*GLO3*-EGFP, pREP42-

GLO3-EGFP, or pREP41-HA-hRIP(+4aa) were used as template (200ng of each) in PCR reactions with 1X *Pfu* reaction buffer, 250ng forward oligonucleotide, 250ng reverse oligonucleotide, 0.2mM dNTPs, and 1μl *PfuTurbo* DNA polymerase (Stratagene). Cycling parameters were as follows: 1 cycle of 95°C for 30 seconds; 18 cycles of 95°C for 30 seconds, 55°C for 1 minute, 68°C for 2minutes/kb of plasmid length. PCR products were checked on an agarose gel and then DNA was digested by the addition of 2μl DpnI (Stratagene) for ≥2 hours at 37°C to digest the original template DNA. Each reaction was precipitated by the addition of one tenth volume sodium acetate and 3 times volume ethanol at -20°C. Each reaction was resuspended in 5μl sterile ddH_2O and transformed into 50μl of XL-I Blue competent cells (Stratagene). Transformations were plated onto LB/(60μg/ml) ampicillin plates and grown overnight at 37°C. No DNA and No *Pfu* reactions were set up for PCR and DpnI digestion controls, respectively. Six single colonies for each mutant were grown up in 5ml of LB/ampicillin overnight at 37°C. DNA was extracted from each culture and sequenced to determine whether the plasmid contained the mutation. A one-liter plasmid prep was then done for a representative of each mutant. Oligonucleotide sequences are written 5' to 3' as follows: (Agv1[R52K]-F) gca gtg ctg ctc ata aaa ata tgg gtg ttc, (Agv1[R52K]-R) gaa cac cca tat ttt tat gag cag cac tgc, (Glo3[R59K]-F) tgc tct gct gtg cat aaa aac atg ggt gtt cat, (Glo3[R59K]-R) atg aac acc cat gtt ttt atg cac agc aga gca, (Glo3 New Kozak-F) gct ttg tta aat cat atg tcg acc atg agt aac

gat gaa gga gaa a, (Glo3 New Kozak-R) gtt tct cct tca tcg tta ctc atg gtc gac ata tga ttt aac aaa gc, (hRIPW93*-F) gtc tgt aaa cag att tga cta gga tta ttt gat, (hRIPW93*-R) atc aaa taa tcc tag tca aat ctg ttt aca gac. The nucleotide sequence of both strands of every mutant was determined by automated DNA sequencing analysis prior to use.

Lithium Acetate Transformations

Strains were grown to mid-log phase (OD_{595nm} = 0.5/ml) in EMM with appropriate supplements and 10ml collected at 1,400rpm for 5 minutes. The resulting pellet was washed with equal volume of sterile ddH_2O before being resuspended in 1ml of sterile ddH_2O and transferred to a microcentrifuge tube. The cells were collected at 1,400rpm for 5 minutes, resuspended in 1ml of LiOAc/TE Buffer (0.1M Lithium Acetate, 10mM Tris pH8.0, 1mM EDTA), collected again at 1,400rpm for 5 minutes and resuspended in 100μl LiOAc/TE Buffer. Cells were incubated at 25°C for 10 minutes with 2μl of 10mg/ml salmon sperm DNA and 100ng - 10μg of transforming plasmid(s). 260μl of LiOAc/TE/PEG (0.1M Lithium Acetate, 10mM Tris pH8.0, 1mM EDTA, 40% Polyethylene glycol) was added to each transformation and incubated at 25°C or 30°C for 60 minutes. 43μl of sterile DMSO (Electron Microscopy Services) was added and the cells heat shocked at 43°C for 5 minutes before being collected at 4,500rpm for 1 minute. The cells were washed sequentially with 1ml and 0.5ml of sterile ddH_2O and

resuspended in 100-300μl sterile ddH_2O and plated onto EMM plates with appropriate selection and grown at 25°C or 30°C.

Generation and characterization of haploid *agv1Δ* strains expressing cover plasmids

Single colonies of the strain MZY214 transformed with pREP41HA, pREP81, pREP41HA-hRIP, pREP41HA-*agv1⁺*, or pREP81-*agv1⁺* were induced to sporulate on ME plates for 3 days and random sporulation analysis performed. A loopful of cells was placed in 1ml of sterile ddH_2O and ascus walls digested with 5μl Enzyme Cocktail for 2-3 hours at 36°C. Cell pellets were washed once with 1ml of 30% ethanol and three times with 1ml of sterile ddH_2O. Cell pellets were resuspended in 1ml of sterile ddH_2O and plated on EMM with adenine plates at 30°C. Resulting strains contain ORF::*ura4⁺* allele and the pREP plasmid with the *LEU2* gene.

Agv1Δ strains expressing pREP81-*agv1⁺* (MZY215) or pREP41HA-*agv1⁺* (MZY216) were grown to mid-log phase (OD_{595nm} = 0.5/ml) in EMM with adenine. Cells were diluted to an OD_{595nm} of 0.2/ml (Time = 0) in EMM with adenine and 15μM thiamine (Sigma). Cells were grown at 30°C and at 0, 4, 8, 12, 24, 36, and 48 hour time points the OD_{595nm} was measured by spectrophotometry, and the

cell number and percent (%) viability was determined using 0.4% Trypan Blue Stain (GibcoBRL) and a hemacytometer.

Construction of agv1 temperature-sensitive (*agv1^{ts}*) alleles and mutant strains

Agv1 temperature sensitive (*agv1^{ts}*) alleles were obtained using the two-step method described in Kostrub *et al*, 1998. Mutagenic PCR amplification of the *agv1^{+}* full-length genomic sequence was performed as follows: reactions contained 0.1μM SF-2 and SR-2 primers, 2.5U TAQ2000 (Stratagene), 50ng of pMZA498 template DNA, 0.5mM $MnCl_2$, 7mM $MgCl_2$, 0.2mM dATP, and 0.333mM dCTP, dGTP, and dTTP. Reaction conditions were 30 cycles of 95°C (1 minute), 50°C (1 minute) and 73°C (3 minutes). To generate a gapped vector, pMZA498 was digested with SacI and the resulting, linearized pBG1 cloning vector backbone with *agv1^{+}* overlapping ends, purified away from the insert by gel electrophoresis. The heterogeneous mutant *agv1*-derived PCR products and the linearized vector were co-transformed into MZY473 and plated on semi-selective plates containing 15μM thiamine (Sigma). Following incubation at 25°C for several days, transformants were analyzed for auxotrophic complementation, temperature sensitivity and thiamine-dependent growth.

Plasmid DNA was isolated from the chosen mutants (most severe phenotype) as described above for chromosomal DNA and transformed into XL-1 Blue competent *E. coli* cells (Stratagene). DNA was isolated from bacterial transformants using a standard alkaline lysis protocol (Sambrook *et al*, 1989). The nucleotide sequence of both strands of each mutant *agv1*^{ts} allele was determined by automated DNA sequence analysis. Wild-type and *agv1*^{ts} mutant full-length genomic mutants were cut out of the pBG1 constructs by digestion with SmaI and cloned into the SmaI restriction site of pIRT2 (Hindley *et al*, 1987) with a *LEU2* selectable marker gene and the nucleotide sequence of both strands was determined by automated DNA sequencing analysis.

To isolate *agv1Δ* strains expressing *agv1*^{ts} alleles, single colonies of the heterozygous diploid strain, MZY214, were transformed with pIRT2+*agv1*$^{+}$, pIRT2+*agv1-1A1*, or pIRT2+*agv1-4A3*, induced to sporulate on ME plates for 3 days, and random sporulation analysis performed as described above. The resulting haploid strains, MZY504, MZY505, and MZY507 contain the ORF::*ura4*$^{+}$ allele and the pIRT2 plasmid with a *LEU2* gene.

Agv1^{ts} mutant strains were generated using targeted integration and homologous recombination as described by Keeney and Boeke, 1993. Haploid strains MZY504, MZY505, and MZY507 were grown overnight in YES media at 25°C,

plated onto multiple non-selective EMM plates containing 0.1% 5-fluoroorotic acid (5-FOA; Zymo Research) and grown at 25°C. Resulting single colonies were patched onto fresh non-selective EMM plates containing 0.1% 5-FOA plates. Haploid cells that had undergone gene conversion at the *agv1*$^{+}$ locus were isolated using auxotrophic complementation and temperature sensitivity screening at 36°C.

Temperature sensitivity assays and growth kinetics studies

For temperature sensitive assays, yeast strains were grown to mid-log phase (OD_{595nm} = 0.5/ml), collected at 1,400rpm for five minutes, resuspended in equal volume of media pre-warmed to the restrictive temperature of 36°C, and incubated at 36°C. Time-points post-temperature shift and fixation methods were performed according to experimental design.

For growth kinetic studies, yeast strains were grown to saturation at 25°C, diluted to an OD_{595nm} of 0.2/ml in media pre-warmed to 30°C or 36°C and incubated at the corresponding restrictive temperature. Aliquots were taken at 0, 4, 8, 12, 24, 36, 48, and 72 hours post-temperature shift and optical densities measured using spectrophotometry. Kinetic analysis of each *agv1*^{ts} strain was performed for 36°C shifts. The natural logarithm of the measured optical density for each strain during log phase growth (8-36 hours) was calculated and plotted. The slope of

each line was determined by linear regression and the slopes compared to the wild-type haploid strain YDM105 by analysis of variance. All temperature shifts were done in triplicate.

Antibody purification

An HPLC-purified peptide corresponding to amino acids 431-444 [CEDENEEGESSHRPD] of Agv1 was the antigen used for antibody production in rabbits (AnaSpec, Inc). Anti-Agv1 polyclonal antibodies (Ab1120) were purified by ammonium sulfate precipitation. An aliquot of the 3rd bleed for Ab1120 was collected at 3,000g for 30 minutes, precipitated by the slow addition of 41.49g of ammonium sulfate (final concentration of 30.5%), and stirred at 4°C overnight. The antibody was collected at 3,000g for 30 minutes and the supernatant precipitated by the slow addition of 0.87g of ammonium sulfate (final concentration of 50%), and stirred at 4°C overnight. The antibody was collected at 3,000g for 30 minutes and the supernatant discarded. The pellet was resuspended in 5ml of sterile 1X PBS, and dialyzed overnight in 1X PBS with three changes in dialysis solution. The antibody collected at 3,000g for 30 minutes to remove any remaining debris. The antibody solution was adjusted to pH 8.0 with 1M Tris pH 10.0 and passed through a 5ml Protein A bead column. The column was washed with 10 column volumes of 100mM Tris pH 8.0 followed by a wash with 10 column volumes of 10mM Tris pH 8.0. The antibody was

eluted with filter sterilized 100mM glycine pH 3.0 and the eluate collected in 1.5ml microcentrifuge tubes already containing 50μl of 1M Tris pH 8.0. The tubes were mixed gently to bring the pH back to neutral. Fractions were analyzed for total protein concentration by Bradford assay (Bradford, 1976) to determine peak fractions. The peak fractions were pooled and the total concentration determined by Bradford assay.

Microscopic Analyses

Intracellular localization studies in fission yeast using indirect immunofluorescence were performed according to Hagan and Ayscouth, 2000 with minor modifications. Cells were grown to mid-log phase (OD_{595nm} = 0.5/ml) at 25°C or 30°C, and fixed in RNase-free formaldehyde (4%v/v; Electron Microscopy Science) for 30 minutes at 25°C, or shifted to pre-warmed media for varying times and fixed in RNase-free formaldehyde (4% v/v; Electron Microscopy Science) for 30 minutes at 25°C. After fixation, the cells were collected at 1,400rpm for 5 minutes, resuspended in 1ml of PEM (100mM Pipes, 10mM $MgSO_4$, 1mM EGTA, adjusted to pH 6.9) and transferred to a 1.5ml microcentrifuge tube. In order to not lose any cells, a 5 second spin at 13,000rpm was performed with the tube hinge facing toward the central axis followed by a 5 second spin at 13,000rpm with the tube hinge facing away from the central axis. The pellets were washed with PEM, resuspended in 900μl of

PEMS (PEM + 1.2M Sorbitol), and incubated with 0.3% β-mercaptoethanol for 10 minutes at 25ºC, then incubated in digestion buffer [0.3mg/ml Zymolyase 100T (Seikagaku America) in PEMS] at 30˚C for 10 - 15 minutes to form spheroplasts. The progression of spheroplast formation was monitored by mixing 1μl of 10% SDS in a 6μl aliquot of cells on a glass slide and visualizing under the microscope. Cells forming spheroplasts are dark and matte instead of bright and glossy. If less than 70% of the cells had formed spheroplasts, the cells were returned to 30°C for another 5-10 minutes and checked again. Spheroplasts were permeabilized by resuspension in PEMST (PEMS + 1% Triton X-100) for 1 minute at 25°C. The cells were washed three times in PEM and equilibrated in 500μl PEMBAL (PEM + 1% bovine serum albumin, 0.1% NaN_3, 100mM lysine-HCl) for 10 minutes. 100μl of cells were transferred to a new tube, pelleted and resuspended in 100μl of 1° antibody [1:250 α-HA (12CA5 monoclonal; Roche), 1:200 α-Agv1 peptide antibody Ab1120 (AnaSpec); 1:250 α-hArf1p (Langille *et al*, 1999); 1:100 β-COP (Santa Cruz); 1:100 ε-COP (Santa Cruz); 1:100 γ-COP (Santa Cruz); 1:100 α-Adaptin (Santa Cruz); or 1:100 γ1-Adaptin (Santa Cruz)] in PEMBAL. Reactions were incubated on a tube roller overnight at 25°C. Secondary antibodies at a ratio of 1:500 in PEMBAL (Alexa Fluor® 488 donkey anti-goat IgG; Alexa Fluor® 488 goat anti-rabbit IgG; or Alexa Fluor® 594 goat anti-mouse IgG; Molecular Probes/Invitrogen) were reabsorbed overnight with 100μl of fixed and spheroplasted wild-type haploid cells (YDM105) to reduce

background levels. Cells were washed 3 times for 15 minutes each in 500μl of PEMBAL then resuspended in 100μl of the preabsorbed 2° antibody in PEMBAL and incubated on a tube roller overnight at 25°C. Cells were washed 3 times for 15 minutes each in 500μl of PEMBAL. For co-localization experiments using antibodies generated in goat (β-COP and γ-COP) with antibodies generated in rabbit or mouse, the goat primary antibody was detected with the donkey anti-goat secondary antibody before addition of the other antibody to avoid cross-reactivity of secondary antibodies. The cells were resuspended in 100μl of the second 1° antibody [1:250 α-HA (12CA5 monoclonal; Roche) or 1:200 α-Agv1 peptide antibody Ab1120 (AnaSpec)] in PEMBAL. Cells were washed 3 times for 15 minutes each in 500μl of PEMBAL then resuspended in 100μl of the preabsorbed 2° antibody (Alexa Fluor® 488 goat anti-rabbit IgG or Alexa Fluor® 594 goat anti-mouse IgG; Molecular Probes/Invitrogen) in PEMBAL and incubated on a tube roller overnight at 25°C. Cells were washed 3 times for 15 minutes each in 500μl of PEMBAL. Cells were resuspended in 100μl of PEMBAL and mounted on a cover slip pretreated with 0.1% hexadimethrine bromide by placing 20μl of the cell suspension on the cover slip and immediately removing as much of the suspension as possible by tilting the cover slip and pipetting the excess solution from the corner of the cover slip. Cells were left to dry in the dark for at least 30 minutes. Cover slips were mounted onto glass slides with 3μg/ml DAPI (Sigma) in Vectashield solution (Vector Laboratories, Inc). Antibody signals

were visualized using a Zeiss Axioplan2 microscope equipped with a 100x Apochromat objective. Images were acquired and analyzed using OpenLab 2.2.5 (Improvision).

For intracellular localization studies of Agv1 as well as coat proteins in mammalian cells using indirect immunofluorescence, Cos7 cells grown to 60% confluency in Dulbecco's Modified Eagle's Medium (DMEM; Invitrogen) supplemented with 10% fetal bovine serum (FBS) were transfected with 2μg of pLacZ and 6μg of pUC118, pHM6-*agv1*$^{+}$, or pHM6-*agv1-R52K* using ESCORT IV transfection reagent and incubated at 37°C and 5% CO_2. Twenty-four hours post-transfection, the cells were split onto three glass cover slips. Forty-eight hours post-transfection, the cells were rinsed 2 times for 10 minutes with 1X PBS to remove all media, fixed in ice-cold methanol for 5 minutes at -20°C, rinsed 2 times 10 minutes in 1X PBS, and stored in 70% ethanol overnight at 4°C. Cells were rinsed 2 times for 10 minutes in 1X PBS, incubated in 1% BSA (w/v) in 1X PBS for 30 minutes at RT, then incubated in 1°Ab (α-βCOP 1:100, or α-γCOP 1:100, or α-αAdaptin 1:100, or α-γ1Adaptin 1:100; Santa Cruz) in 1%BSA in 1X PBS gently rotating for 1 hour at RT. The cells were washed 3 times for 10 minutes in 0.1%BSA in 1XPBS, then incubated in 2° Ab (Alexa Fluor® 488 goat-α-Rabbit IgG 1:1500 or Alexa Fluor® 488 donkey-α-Goat IgG 1:1500; Molecular Probes/Invitrogen), in 1% BSA in 1X PBS covered with foil and gently rotated for

1 hour at RT. The cells were washed 3 times for 10 minutes in 0.1% BSA in 1X PBS, then incubated in 1°Ab (α-HA 1:500 or α-Agv1 1:250) in 1% BSA in 1X PBS covered in foil and gently rotated for 1 hour at RT. Cells were washed 3 times 10 minutes in 0.1% BSA in 1X PBS, then incubated in 2° Ab (Alexa Fluor® 594 goat-α-Mouse IgG 1:1500, or Alexa Fluor® 594 goat-α-Rabbit IgG 1:1500; Molecular Probes/Invitrogen) in 1% BSA in 1X PBS covered in foil and gently rotated for 1 hour at RT. The cells were washed 2 times for 5 minutes with 1X PBS and the cover slips allowed to air-dry in the dark for 30 minutes. Cover slips were mounted onto glass slides with 5μg/ml DAPI (Sigma) in Vectashield solution (Vector Laboratories, Inc). Antibodies were visualized using a Zeiss Axioplan2 microscope equipped with a 100x Apochromat objective. Images were acquired and analyzed using OpenLab 2.2.5 (Improvision).

For intracellular localization studies of RNA in fission yeast using RNA *in situ* hybridization, strains were grown 25°C to mid-log phase (OD_{595nm} = 0.5/ml). 10ml of cells were collected and fixed. The remaining cells were split into two aliquots: One placed at 25°C, and one placed at 37°C. At varying times, 10ml of cells were collected and fixed. Cells were fixed in 9ml of 1X PBS and 1.09ml of 37.7% ultra-pure RNAse-free paraformaldehyde (Electron Microscopy Sciences) for 40 minutes at RT rocking end over end. The cells were washed 2 times with 1X PBS and resuspended in 900μl of 1.2M sorbitol in 1X PBS. To partially digest

the cells walls, the cells were first incubated with 0.3% β-mercaptoethanol for 10 minutes at 25ºC, then incubated in 0.3mg/ml Zymolyase 100T (Seikagaku America) in 1.2M sorbitol in 1X PBS at 30˚C for 10 - 15 minutes to form spheroplasts. The progression of spheroplast formation was monitored by mixing 1μl of 10% SDS in a 6μl aliquot of cells on a glass slide and visualizing under the microscope. Cells forming spheroplasts are dark and matte instead of bright and glossy. If less than 70% of the cells had formed spheroplasts, the cells were returned to 30°C for another 5-10 minutes and checked again. Cells were washed 2 times with 1.2M sorbitol in 1X PBS, 2 times in 1X PBS, incubated 5 minutes in 0.1% NP-40 in 1X PBS to permeabilize the membranes, then finally washed once in 1X PBS. Cells were added to poly-lysine coated cover slips and left to adhere for 30 minutes at 4°C. Cells were rinsed in 1X PBS and dehydrated in 70% ethanol overnight at -20°C. The cells were rehydrated in 1X PBS for 10 minutes at RT, then prehybridized in 100μl pre-warmed 15% formamide hybridization solution (15% deionized formamide, 4X SSC, 1X Denhardts Solution, 125mg/ml tRNA, 10% dextran sulfate, 500mg/ml salmon sperm DNA) for one hour at 37°C. Cells were hybridized for one hour at 37°C with 200ng of Cy3-conjugated oligo(dT_{42}) probe [/C6dT/tt ttt ttt t/C6dT/t ttt ttt tt/C6dT/ ttt ttt ttt /C6dT/tt ttt ttt t/C6dT/t] or Alexa Fluor® 594-conjugated *S. pombe* 5S rRNA probe [/C6dT/cc aag cat agt ac/C6dT/ aac gag gcc c/C6dT/c aga cgc t/C6dT/a act gca gtg a/C6dT/c] with a glass cover slip covering the hybridization

reaction. Cells were washed in 2X SSC for 1 hour at RT, in 1X SSC for 1 hour at RT, in 0.5X SSC for 30 minutes at RT, and then rinsed in sterile 1X PBS and allowed to air dry in the dark at least 30 minutes. Cover slips were mounted onto glass slides with 3μg/ml DAPI (Sigma) in Vectashield solution (Vector Laboratories, Inc). The fluorochrome-labeled oligonucleotide signals were visualized using a Zeiss Axioplan2 microscope equipped with a 100x Apochromat objective. Images were acquired and analyzed using OpenLab 2.2.5 (Improvision).

For intracellular localization studies in fission yeast cells using GFP fusion proteins, strains were grown to mid-log phase (OD_{595nm} = 0.5/ml) in EMM with appropriate supplements at 25°C, shifted to EMM with appropriate supplements pre-warmed to 36°C, and aliquots taken after 0, 2, or 4 hours at 36°C. Cells were fixed in ice-cold methanol for 10 minutes at –20°C, rinsed in 1XPBS three times, equilibrated in PBAL (1% BSA w/v, 0.1%NaN_3 w/v, 100mM lysine-HCl in 1X PBS), resuspended in 50-100μl PBAL, and mounted onto glass cover slips pretreated with 0.1% hexadimethrine bromide by placing 20μl of the cell suspension on the cover slip and immediately removing as much of the suspension as possible by tilting the cover slip and pipetting the excess solution from the corner of the cover slip. Cells were left to dry in the dark for at least 30 minutes. Cover slips were mounted onto glass slides with 3μg/ml DAPI (Sigma)

in Vectashield solution (Vector Laboratories, Inc). GFP-fusion proteins were visualized using a Zeiss Axioplan2 microscope equipped with a 100x Apochromat objective. Images were acquired and analyzed using OpenLab 2.2.5 (Improvision).

For internalization studies in fission yeast cells using FM4-64 (Molecular Probes), strains were grown to mid-log phase (OD_{595nm} = 0.5/ml) in EMM with adenine, uracil, and leucine at 25°C. A 1ml aliquot of cells was collected at 13,000rpm for 1 minute, resuspended in EMM with adenine, uracil, leucine, and 50μM FM4-64 (from a 10mM stock in DMSO), and incubated for 15 minutes at 25°C. Cells were collected at 13,000rpm for 1 minute, washed by resuspension in 1ml of EMM with adenine, uracil, and leucine to remove free FM4-64, resuspended in 1ml of EMM with adenine, uracil, and leucine pre-warmed to 36°C, and incubated for 0, 15, 30, 45, and 60 minutes at 36°C. Cells were collected at 13,000rpm for 1 minute, resuspended in 100μl PBAL, and mounted on a cover slip pretreated with 0.1% hexadimethrine bromide by placing 20μl of the cell suspension on the cover slip and immediately removing as much of the suspension as possible by tilting the cover slip and pipetting the excess solution from the corner of the cover slip. Cells were left to dry in the dark for at least 30 minutes. Cover slips were mounted onto glass slides with 3μg/ml DAPI (Sigma) in Vectashield solution (Vector Laboratories, Inc). FM4-64 signal was visualized using a Zeiss

Axioplan2 microscope equipped with a 100x Apochromat objective. Images were acquired and analyzed using OpenLab 2.2.5 (Improvision).

For morphological studies of fission yeast cells using electron microscopy, YDM259, *agv1*$^{+}$, *agv1-1A1*, *agv1-4A3* strains were grown to mid-log phase (OD_{595nm} = 0.5/ml) in EMM with appropriate supplements at 25°C. A 1ml aliquot was collected. The remainder of the culture was pelleted at 1,400rpm for 4 minutes and resuspended in equal volume of EMM with appropriate supplements pre-warmed to 36°C and grown at 36°C for three hours. At three hours, a 1ml aliquot was collected. Both aliquots of each strain were fixed in 2.5% glutaraldehyde (Electron Microscopy Sciences) in 0.1M sodium cacodylate (SC) buffer (pH 7.2) for 30 minutes at 4°C, then washed three times in SC buffer. Cells were digested for 10 minutes at 25ºC in 0.15 mg/ml Zymolyase 100T, then washed four times for 5 minutes each in SC buffer. Cells were subsequently post-fixed in 1% osmium tetroxide/SC buffer, twice for 20 minutes each at 4°C, rinsed in SC buffer for 5 minutes at 25ºC, and incubated in SC buffer overnight at 4°C. Samples were gradually dehydrated in an ethanol series, rinsed in acetone, and incubated overnight in 1:1 acetone:Spurr's resin at 25ºC, then embedded in Spurr's hard resin. Ultrathin sections were stained with saturated uranyl acetate and 0.5% lead citrate. Images were taken on a Phillips CM10 transmission electron microscope (UMass Core Electron Microscopy Facility).

Protein Studies

To obtain denatured S. pombe protein extracts, 50ml aliquots of strains at an OD_{595nm} of about 0.4/ml were collected at 1,400rpm for 4 minutes, washed in 5 ml of ice-cold stop buffer (150mM NaCl, 50mM NaF, 10mM EDTA, 1mM NaN_3, pH 8), and the pellet drained. The pellet was resuspended in 50μl of RIPA buffer (10mM sodium phosphate, pH 7, 1% Triton X-100, 0.1% SDS, 2mM EDTA, 150mM NaCl, 50mM NaF, and 2X Complete EDTA-free protease inhibitor cocktail (Roche)) and transferred to a 2ml microcentrifuge tube containing about 0.2ml of 425-600 micron acid washed glass beads (Sigma, G-8772). Cells were lysed by 10 cycles of 1-minute vortexing followed by 1 minute on ice. 100μl of 1% SDS was added and the extracts boiled for 3 minutes. Supernatant was transferred to new 1.5ml microcentrifuge tubes. The beads were washed with 150μl of RIPA buffer and the wash added to the 1.5ml microcentrifuge tube. The extract was spun at 14,000rpm for 10 minutes at 4°C to remove the cell debris and the supernatant was transferred to a new 1.5ml microcentrifuge tube. The protein concentration was determined by Bradford Assay (BioRad).

The ability of Agv1 to interact with HIV-I Rev was determined by affinity chromatography and Western blot analysis. HA-Agv1-His_6 in BL21LysS cells were partially purified by lysing the cells and doing a 30% ammonium sulfate

precipitation. The partially purified HA-Agv1-His_6 was first coupled to Ni^{2+}-agarose resin by incubating 100μl of HA-Agv1-His6 lysate with 100μl of Ni^{2+}-agarose beads pre-equilibrated at a 1:1 ratio in binding buffer (50mM Tris-HCl, pH 7.4, 100mM NaCl, 20% glycerol, 2X Complete protease Inhibitor Cocktail with EDTA (Roche), 1mM β-mercaptoethanol) overnight at 4°C. To monitor the non-specific binding capacity of the resin, either 200μl of 1mg/ml acetylated BSA or 100μl of 14mg/ml GST-Rev was incubated with 100μl of Ni^{2+}-agarose beads in parallel. The protein-resin samples were centrifuged at 6,000rpm for 5 minutes and the supernatant transferred to new microcentrifuge tubes. The samples were spun again at 13,000rpm for 30 seconds and the residual liquid transferred to the corresponding supernatant tube. The protein coupled resins were washed three times in binding buffer with 0.01% Triton X-100, and 10mM β-mercaptoethanol, then resuspended in 100μl of gel resolving buffer (1.5M Tris, pH 8.8, 0.4% SDS). 25μl of the sample was combined with 7μl 5X SDS loading dye, heated to 100°C for 10 minutes, and resolved on a 10% SDS-polyacrylamide gel. One-fifth of the total HA-Agv1-His_6, BSA, or GST-Rev protein used in the coupling step was run out as an input control. One-twentieth of each corresponding supernatant was also analyzed by Western blot analysis using a monoclonal anti-6XHis antibody (1:250; Clontech) or a rabbit polyclonal anti-Rev antibody (1:750). 88.4% of the input Agv1-His_6 bound, indicating saturation of the agarose beads. 100μl of the Agv1-coupled beads were incubated with 200μl

of purified GST, GST-Rev, GST-RevM10, GST-WT-NES, or GST-M10-NES fusion protein (approximately 0.2-0.34mg/ml) overnight at 4°C. The protein-resin samples were centrifuged at 6,000rpm for 5 minutes and the supernatant transferred to new microcentrifuge tubes. The samples were spun again at 13,000rpm for 30 seconds and the residual liquid transferred to the corresponding supernatant tube. The protein-coupled resins were washed three times in binding buffer with 0.05% Triton X-100, and 10mM β-mercaptoethanol, with a final wash in 50mM Tris-HCl, pH 8.0, 2X Complete protease Inhibitor Cocktail with EDTA (Roche), and 10mM β-mercaptoethanol. The protein-coupled resin was resuspended in 60μl of gel resolving buffer and 12μl of 5X SDS loading buffer, heated at 100°C for 10 minutes, and resolved on a 10% SDS-polyacrylamide gel. One-fifth of total protein for each GST fusion protein used was run as an input control. One-twentieth of each corresponding supernatant was also analyzed by Western blot analysis using a polyclonal rabbit anti-Rev antibody (1:750).

Vesicular transport assays

To follow the processing of fission yeast Cpy1, *S. pombe* gene-converted strains *agv1*$^{+}$, *agv1-1A1*, and *agv1-4A3* were grown to mid-log phase (OD_{595nm} = 0.5/ml) in yeast nitrogen base (YNB) without ammonium sulfate with the addition of 37.84mM ammonium chloride and appropriate supplements at 25ºC to mid-log

phase. Cultures were then incubated at the semi-permissive temperature of 30°C for 30 minutes prior to isotopic labeling. Ten optical density equivalents at 595nm of a yeast culture were collected by centrifugation and resuspended in 0.5 ml SD media with 1 mg/ml bovine serum albumin and 500 μCi of Trans ^{35}S-label (MP Biomedicals, Inc.). Cells were labeled for 15 minutes at 30ºC and chased with excess unlabeled methionine and cysteine (4.67 μg/ml). Following a 10 or 30-minute incubation, isotopic labeling was terminated in 10nM NaN_3 and immediate immersion in liquid nitrogen. Cells were lysed in 200 μl of lysis buffer (50mM Tris pH 7.4, 1% SDS, 1X COMPLETE minus EDTA protease inhibitor tablet; Roche) using acid-washed glass beads (Sigma) by 10 vortex cycles (one minute vortex and one minute ice). Protein was solubilized by boiling for 5 minutes, diluted 2-fold with IP Dilution Buffer (1.25% Triton X-100, 190mM NaCl, 6mM EDTA, 60mM Tris pH 7.4), cleared by centrifugation, and immunoprecipitated with 3 μl anti-Cpy1 antibody (Tabuchi *et al*, 1997) rotating end over end overnight at 4°C. Protein A-Sepharose beads [Roche: 20% in IP Buffer (50mM Tris pH 7.5, 150mM NaCl, 0.5% Tween 20, 0.1mM EDTA)] were added to each sample and incubated for an additional 2 hours at 4°C. The beads were washed twice with IP buffer, then twice with IP buffer containing 2M Urea. The beads were incubated in Laemmli sample buffer (Laemmli, 1970) for 30 minutes at 55°C, DTT for 10 minutes at 100ºC, and resolved on a 10% denaturing polyacrylamide gel. The gel was fixed in 50% methanol/12% acetic

acid for 15 minutes, rinsed in ddH_2O for 15 minutes, fluorographed using Autofluor (National Diagnostics) for 90 minutes, dried for 2 hours at 80ºC and visualized by autoradiography.

To determine whether fission yeast Cpy1 is secreted in the *agv1^{ts}* strains, YDM259, *Δvps34*, *agv1^{+}*, *agv1-1A1*, and *agv1-4A3* cells from actively growing cultures were spotted onto YES plates and incubated overnight at 25°C. Plates were overlaid with nitrocellulose filters and shifted to the semi-permissive temperature of 30°C for 24 hours. The filters were scraped and rinsed in 1X PBS, UV irradiated at 1,200 *μ*joules x100, rinsing in 1X TBST (10mM Tris pH 7.8, 150mM NaCl, 0.05% Tween 20), blocked for 30 minutes at 25ºC in BLOTTO (10% powdered milk in 1X TBST), incubated overnight at 4°C with α-Cpy1 antibody 1:500 (Tabuchi *et al*, 1997) in BLOTTO, washed three times for fifteen minutes at RT in 1X TSBT, probed with α-rabbit-HRP secondary antibody 1:5000 in BLOTTO for 1 hour at RT. Secondary antibody was washed two times for twenty minutes in 1X TBST and visualized by ECL (Amersham).

TABLE 6-1: Plasmids Used in This Study

Plasmid Name	Vector and Insert	Source
pMZA490	pcDNA3 + *agv1*$^+$ cDNA	This Study
pMZA492	pKS + *agv1*$^+$ gDNA (-13 to +1597)	This Study
pMZA493	pSP72(minus EcoRI, EcoRV, & SmaI)	This Study
pMZA494	pSP72(minus EcoRI, EcoRV, & SmaI) + *agv1*$^+$ gDNA (-13 to +1597)	This Study
pMZA495	pSP72(minus EcoRI, EcoRV, & SmaI) + (-13 to +409) *agv1*$^+$ gDNA - *ura4*$^+$ - (+1319 to +1597) *agv1*$^+$ gDNA	This Study
pMZA496	pREP81X + *agv1*$^+$	This Study
pMZA497	pREPHA41X + *agv1*$^+$	This Study
pMZA498	pBG1(minus SacI) + genomic *agv1*$^+$ (-484 to +2403)	This Study
pMZA499	pBG1(minus SacI) + genomic *agv1-1A1* (-484 to +2403)	This Study
pMZA501	pBG1(minus SacI) + genomic *agv1-4A3* (-484 to +2403)	This Study
pMZA502	pHB6 + *agv1*$^+$ cDNA	This Study
pMZA505	pIRT2 + full-length genomic *agv1*$^+$	This Study
pMZA506	pIRT2 + full-length genomic *agv1-1A1*	This Study
pMZA508	pIRT2 + full-length genomic *agv1-4A3*	This Study
pMZA516	pREPHA41X + *agv1-R52K*	This Study
pMZA517	pHM6 + *agv1*$^+$ cDNA	This Study
pMZA518	pHM6 + *agv1*$^+$*-R52K* cDNA	This Study
pMZB562	pREP81X + hRIP cDNA	This Study
pMZB563	pREP41-HA-hRIP cDNA	This Study
pMZB564	pREPHA41X + hRIP(+4aa) cDNA	This Study
pMZB565	pREPHA41X + hRIP(+4aa)ΔNPF cDNA	This Study
pMZB566	pREPHA41X + hRIP(+4aa)W93* cDNA	This Study
pREP81X	pREP81X	K. Maundrell
pREPHA41X	pREPHA41X	K. Maundrell
pR1GEF1	pREP1X + GST-NES_{REV}-EGFP	M. Yoshida
pR1GLF2	pREP1X + GST-NLS_{SV40}-EGFP	M. Yoshida
nmt-GFP-13g6	pREP41 + GFP-13g6	W. Z. Cande
nmt-GFP-gma12	pREP41 + GFP-gma12	W. Z. Cande
pREP41EGFPC	pREP41EGFPC	I. Hagan
pREP42EGFPC	pREP42EGFPC	I. Hagan
pMZC125	pREP41-HA-Rev	This Study
pMZC126	pREP42-Rev-EGFP	This Study
pMZD701	pREP41EGFPC+*GLO3*	This Study
pMZD702	pREP41EGFPC+*glo3-R59K*	This Study
pMZD703	pREP42EGFPC+RnARFGAP1	This Study

pMZD704	pREP42EGFPC+*GCS1*	This Study
pMZD705	pREP42EGFPC + *AGE2*	This Study
pMZD706	pREP42EGFPC + *agv1*$^{+}$	This Study
pMZD707	pREP42EGFPC + *agv1-R52K*	This Study
pMZD708	pREP42EGFPC+*GLO3*	This Study
pMZD709	pREP42EGFPC+*glo3-R59K*	This Study
pMZD710	pREP41EGFPC+*GCS1*	This Study

TABLE 6-2: Strains Used in This Study

Strain	Genotype	Source
YDM105	*ade6-210 leu1-32 ura4-D18 h*$^{+}$	D. McCollum
YDM108	*ade6-216 leu1-32 ura4-D18 h*$^{-}$	D. McCollum
YDM258	*his3-D1 ade6-216 leu1-32 ura4-D18 h*$^{-}$	D. McCollum
YDM259	*his3-D1 ade6-216 leu1-32 ura4-D18 h*$^{+}$	D. McCollum
crm1-809	*leu1 crm1-809 h*$^{-}$	M. Yanagida
rae1-167	*leu1-32 ura4-D18 rae1-167 h*$^{-}$	R. Dhar
*vps34*Δ	*vps34*Δ*::ura4*$^{+}$ *leu1 his2 ura4 ade6-M216 h*$^{+}$	K. Takegawa
sns-A10	*leu1-32 ura4-D18 ade6-M216 h*$^{-}$	S. Sazer
MZY214	*agv1+/agv1*Δ*::ura4+ ade6-210/ade6-216 leu1-32/leu1-32 ura4-D18/ura4-D18 h*$^{+}$*/h*$^{-}$	This Study
MZY215	*agv1*Δ*::ura4*$^{+}$ *ade6-216 leu1-32 ura4-D18 h*$^{+}$ *[pREP81-agv1*$^{+}$*]*	This Study
MZY216	*agv1*Δ*::ura4*$^{+}$ *ade6-216 leu1-32 ura4-D18 h*$^{+}$ *[pREP41-HA-agv1*$^{+}$*]*	This Study
MZY217	*agv1+/agv1*Δ*::ura4+ ade6-210/ade6-216 leu1-32/leu1-32 ura4-D18/ura4-D18 h*$^{+}$*/h*$^{-}$ *[pREP81-hRIP]*	This Study
MZY218	*agv1+/agv1*Δ*::ura4+ ade6-210/ade6-216 leu1-32/leu1-32 ura4-D18/ura4-D18 h*$^{+}$*/h*$^{-}$ *[pREP41-HA-hRIP]*	This Study
MZY300	*ade6*-210 *leu1*-32 *ura4*-D18 h^{+}, pMZD563	This Study
MZY302	*agv1+/agv1*Δ*::ura4+ ade6-210/ade6-216 leu1-32/leu1-32 ura4-D18/ura4-D18 h*$^{+}$*/h*$^{-}$ *[pIRT2-agv1*$^{+}$*]*	This Study
MZY303	*agv1+/agv1*Δ*::ura4+ ade6-210/ade6-216 leu1-32/leu1-32 ura4-D18/ura4-D18 h*$^{+}$*/h*$^{-}$ *[pIRT2-agv1-1A1]*	This Study
MZY305	*agv1+/agv1*Δ*::ura4+ ade6-210/ade6-216 leu1-32/leu1-32 ura4-D18/ura4-D18 h*$^{+}$*/h*$^{-}$ *[pIRT2-agv1-4A3]*	This Study
MZY319	*leu1 crm1-809 h*$^{-}$ *[pREP1-GST-NES*$_{Rev}$*-EGFP]*	This Study
MZY320	*agv1*Δ*::ura4+::agv1+ ade6-216 leu1-32 ura4-D18* h^{-} *[pREP1-GST-NES*$_{Rev}$*-EGFP]*	This Study
MZY321	*agv1*Δ*::ura4+::agv1-1A1 ade6-216 leu1-32 ura4-D18 h*$^{-}$ *[pREP1-GST-NES*$_{Rev}$*-EGFP]*	This Study
MZY323	*agv1*Δ*::ura4+::agv1+ ade6-216 leu1-32 ura4-D18* h^{-} *[pREP1-GST-NLS*$_{SV40}$*-EGFP]*	This Study
MZY324	*agv1*Δ*::ura4+::agv1-1A1 ade6-216 leu1-32 ura4-D18 h*$^{-}$ *[pREP1-GST-NLS*$_{SV40}$*-EGFP]*	This Study
MZY326	*agv1*Δ*::ura4+::agv1+ ade6-216 leu1-32 ura4-D18* h^{-} *[pREP42-Rev-EGFP]*	This Study
MZY327	*agv1*Δ*::ura4+::agv1-1A1 ade6-216 leu1-32 ura4-D18 h*$^{-}$ *[pREP42-Rev-EGFP]*	This Study
MZY328	*agv1*Δ*::ura4+::agv1-4A3 ade6-216 leu1-32 ura4-D18 h*$^{+}$ *[pREP42-Rev-EGFP]*	This Study
MZY350	*agv1*Δ*::ura4+::agv1+ ade6-216 leu1-32 ura4-D18* h^{-} *[pREP41-HA-agv1+]*	This Study
MZY351	*agv1*Δ*::ura4+::agv1-1A1 ade6-216 leu1-32 ura4-D18 h*$^{-}$ *[pREP41-HA-agv1+]*	This Study

MZY352	*agv1Δ::ura4+::agv1-4A3 ade6-216 Leu1-32 ura4-D18 h$^+$ [pREP41-HA-agv1+]*	This Study
MZY353	*agv1Δ::ura4+::agv1+ ade6-216 leu1-32 ura4-D18* h$^-$ *[pREP41-HA- agv1-R52K]*	This Study
MZY354	*agv1Δ::ura4+::agv1-1A1 ade6-216 leu1-32 ura4-D18 h$^-$ [pREP41-HA- agv1-R52K]*	This Study
MZY355	*agv1Δ::ura4+::agv1-4A3 ade6-216 Leu1-32 ura4-D18 h$^+$ [pREP41-HA- agv1-R52K]*	This Study
MZY473	agv1Δ::ura4$^+$ *his3*-D1 *ade6*-210 *leu1*-32 *ura4*-D18 *h$^+$ [pREP81-agv1+]*	This Study
MZY500	*agv1Δ::ura4+::agv1+::EGFP-kanMX6 ade6-216 leu1-32 ura4-D18* h$^-$	This Study
MZY504	*agv1Δ::ura4+ ade6-216 Leu1-32 ura4-D18* h$^-$ *[pIRT2-agv1$^+$]*	This Study
MZY505	*agv1Δ::ura4+ ade6-216 Leu1-32 ura4-D18 h$^-$ [pIRT2-agv1-1A1]*	This Study
MZY507	*agv1Δ::ura4+ ade6-216 Leu1-32 ura4-D18 h$^+$ [pIRT2-agv1-4A3]*	This Study
MZY509	*agv1Δ::ura4+::agv1+ ade6-216 Leu1-32 ura4-D18* h$^-$	This Study
MZY510	*agv1Δ::ura4+::agv1-1A1 ade6-216 Leu1-32 ura4-D18 h$^-$*	This Study
MZY511	*agv1Δ::ura4+::agv1-4A3 ade6-216 Leu1-32 ura4-D18 h$^+$*	This Study
MZY512	*agv1Δ::ura4+::agv1+ ade6-216 Leu1-32 ura4-D18 h$^-$ [nmt-GFP-13g6]*	This Study
MZY513	*agv1Δ::ura4+::agv1-1A1 ade6-216 Leu1-32 ura4-D18 h$^-$ [nmt-GFP-13g6]*	This Study
MZY514	*agv1Δ::ura4+::agv1-4A3 ade6-216 Leu1-32 ura4-D18 h$^+$ [nmt-GFP-13g6]*	This Study
MZY515	*agv1Δ::ura4+::agv1+ ade6-216 Leu1-32 ura4-D18 h$^-$ [nmt-GFP-gma12]*	This Study
MZY516	*agv1Δ::ura4+::agv1-1A1 ade6-216 Leu1-32 ura4-D18 h$^-$ [nmt-GFP-gma12]*	This Study
MZY517	*agv1Δ::ura4+::agv1-4A3 ade6-216 Leu1-32 ura4-D18 h$^+$ [nmt-GFP-gma12]*	This Study
MZY524	*agv1Δ::ura4+::agv1+ ade6-216 Leu1-32 ura4-D18 h$^-$ [pREP42-EGFPC]*	This Study
MZY525	*agv1Δ::ura4+::agv1-1A1 ade6-216 Leu1-32 ura4-D18 h$^-$ [pREP42-EGFPC]*	This Study
MZY526	*agv1Δ::ura4+::agv1-4A3 ade6-216 Leu1-32 ura4-D18 h$^+$ [pREP42-EGFPC]*	This Study
MZY527	*agv1Δ::ura4+::agv1+ ade6-216 Leu1-32 ura4-D18 h$^-$ [pREP41-glo3$^+$-EGFP]*	This Study
MZY528	*agv1Δ::ura4+::agv1-1A1 ade6-216 Leu1-32 ura4-D18 h$^-$ [pREP41-glo3+-EGFP]*	This Study
MZY529	*agv1Δ::ura4+::agv1-4A3 ade6-216 Leu1-32 ura4-D18 h$^+$ [pREP41-glo3$^+$-EGFP]*	This Study
MZY530	*agv1Δ::ura4+::agv1+ ade6-216 Leu1-32 ura4-D18 h$^-$ [pREP41-glo3-R59K-EGFP]*	This Study
MZY531	*agv1Δ::ura4+::agv1-1A1 ade6-216 Leu1-32 ura4-D18 h$^-$ [pREP41-glo3-R59K-EGFP]*	This Study
MZY532	*agv1Δ::ura4+::agv1-4A3 ade6-216 Leu1-32 ura4-D18 h$^+$ [pREP41-glo3-R59K-EGFP]*	This Study
MZY533	*agv1Δ::ura4+::agv1+ ade6-216 Leu1-32 ura4-D18 h$^-$ [pREP42-ArfGAP1-EGFP]*	This Study
MZY534	*agv1Δ::ura4+::agv1-1A1 ade6-216 Leu1-32 ura4-D18 h$^-$ [pREP42-ArfGAP1-EGFP]*	This Study
MZY535	*agv1Δ::ura4+::agv1-4A3 ade6-216 Leu1-32 ura4-D18 h$^+$ [pREP42-ArfGAP1-EGFP]*	This Study
MZY536	*agv1Δ::ura4+::agv1+ ade6-216 Leu1-32 ura4-D18 h$^-$ [pREP42-gcs1$^+$-EGFP]*	This Study
MZY537	*agv1Δ::ura4+::agv1-1A1 ade6-216 Leu1-32 ura4-D18 h$^-$ [pREP42-gcs1+-EGFP]*	This Study
MZY538	*agv1Δ::ura4+::agv1-4A3 ade6-216 Leu1-32 ura4-D18 h$^+$ [pREP42-gcs1$^+$-EGFP]*	This Study
MZY539	*agv1Δ::ura4+::agv1+ ade6-216 Leu1-32 ura4-D18 h$^-$ [pREP42-age2$^+$-EGFP]*	This Study

MZY540	*agv1Δ::ura4+::agv1-1A1 ade6-216 Leu1-32 ura4-D18 h⁻ [pREP42-age2+-EGFP]*	This Study
MZY541	*agv1Δ::ura4+::agv1-4A3 ade6-216 Leu1-32 ura4-D18 h⁺ [pREP42-age2⁺-EGFP]*	This Study
MZY542	*agv1Δ::ura4+::agv1+ ade6-216 Leu1-32 ura4-D18 h⁻ [pREP41-EGFPC]*	This Study
MZY543	*agv1Δ::ura4+::agv1-1A1 ade6-216 Leu1-32 ura4-D18 h⁻ [pREP41-EGFPC]*	This Study
MZY544	*agv1Δ::ura4+::agv1-4A3 ade6-216 Leu1-32 ura4-D18 h⁺ [pREP41-EGFPC]*	This Study
MZY545	*agv1Δ::ura4+::agv1+ ade6-216 Leu1-32 ura4-D18 h⁻ [pREP41-glo3⁺-EGFP and pREP42-gcs1⁺-EGFP]*	This Study
MZY546	*agv1Δ::ura4+::agv1-1A1 ade6-216 Leu1-32 ura4-D18 h⁻ [pREP41-glo3+-EGFP and pREP42-gcs1+-EGFP]*	This Study
MZY547	*agv1Δ::ura4+::agv1-4A3 ade6-216 Leu1-32 ura4-D18 h⁺ [pREP41-glo3⁺-EGFP and pREP42-gcs1⁺-EGFP]*	This Study
MZY548	*agv1Δ::ura4+::agv1+ ade6-216 Leu1-32 ura4-D18 h⁻ [pREP41-glo3⁺-EGFP and pREP42-age2⁺-EGFP]*	This Study
MZY549	*agv1Δ::ura4+::agv1-1A1 ade6-216 Leu1-32 ura4-D18 h⁻ [pREP41-glo3+-EGFP and pREP42-age2+-EGFP]*	This Study
MZY550	*agv1Δ::ura4+::agv1-4A3 ade6-216 Leu1-32 ura4-D18 h⁺ [pREP41-glo3⁺-EGFP and pREP42-age2⁺-EGFP]*	This Study
MZY551	*agv1Δ::ura4+::agv1+ ade6-216 Leu1-32 ura4-D18* h⁻ *[pREP42-agv1⁺-EGFP]*	This Study
MZY552	*agv1Δ::ura4+::agv1-1A1 ade6-216 Leu1-32 ura4-D18 h⁻ [pREP42-agv1+-EGFP]*	This Study
MZY553	*agv1Δ::ura4+::agv1-4A3 ade6-216 Leu1-32 ura4-D18 h⁺ [pREP42-agv1+-EGFP]*	This Study
MZY554	*agv1Δ::ura4+::agv1+ ade6-216 Leu1-32 ura4-D18* h⁻ *[pREP42-agv1-R52K-EGFP]*	This Study
MZY555	*agv1Δ::ura4+::agv1-1A1 ade6-216 Leu1-32 ura4-D18 h⁻ [pREP42-agv1-R52K-EGFP]*	This Study
MZY556	*agv1Δ::ura4+::agv1-4A3 ade6-216 Leu1-32 ura4-D18 h⁺ [pREP42-agv1-R52K-EGFP]*	This Study
MZY557	*agv1Δ::ura4+::agv1+ ade6-216 Leu1-32 ura4-D18 h⁻ [pREP42-glo3⁺-EGFP]*	This Study
MZY558	*agv1Δ::ura4+::agv1-1A1 ade6-216 Leu1-32 ura4-D18 h⁻ [pREP42-glo3+-EGFP]*	This Study
MZY559	*agv1Δ::ura4+::agv1-4A3 ade6-216 Leu1-32 ura4-D18 h⁺ [pREP42-glo3⁺-EGFP]*	This Study
MZY560	*agv1Δ::ura4+::agv1+ ade6-216 Leu1-32 ura4-D18 h⁻ [pREP42-glo3-R59K-EGFP]*	This Study
MZY561	*agv1Δ::ura4+::agv1-1A1 ade6-216 Leu1-32 ura4-D18 h⁻ [pREP42-glo3-R59K-EGFP]*	This Study
MZY562	*agv1Δ::ura4+::agv1-4A3 ade6-216 Leu1-32 ura4-D18 h⁺ [pREP42-glo3-R59K-EGFP]*	This Study
MZY563	*agv1Δ::ura4+::agv1+ ade6-216 Leu1-32 ura4-D18 h⁻ [pREP41-gcs1⁺-EGFP]*	This Study
MZY564	*agv1Δ::ura4+::agv1-1A1 ade6-216 Leu1-32 ura4-D18 h⁻ [pREP41-gcs1+-EGFP]*	This Study
MZY565	*agv1Δ::ura4+::agv1-4A3 ade6-216 Leu1-32 ura4-D18 h⁺ [pREP41-gcs1⁺-EGFP]*	This Study
MZY566	*agv1Δ::ura4+::agv1+ ade6-216 Leu1-32 ura4-D18 h⁻ [pREP41-gcs1⁺-EGFP and pREP42-glo3⁺-EGFP]*	This Study
MZY567	*agv1Δ::ura4+::agv1-1A1 ade6-216 Leu1-32 ura4-D18 h⁻ [pREP41-gcs1+-EGFP and pREP42-glo3+-EGFP]*	This Study

MZY568	*agv1Δ::ura4+::agv1-4A3 ade6-216 Leu1-32 ura4-D18 h^{+} [pREP41-gcs1+-EGFP and pREP42-glo3+-EGFP]*	This Study
MZY569	*agv1Δ::ura4+::agv1+ ade6-216 Leu1-32 ura4-D18 h^{-} [pREP41-gcs1^{+}-EGFP and pREP42-age2^{+}-EGFP]*	This Study
MZY570	*agv1Δ::ura4+::agv1-1A1 ade6-216 Leu1-32 ura4-D18 h^{-} [pREP41-gcs1+-EGFP and pREP42-age2+-EGFP]*	This Study
MZY571	*agv1Δ::ura4+::agv1-4A3 ade6-216 Leu1-32 ura4-D18 h^{+} [pREP41-gcs1+-EGFP and pREP42-age2+-EGFP]*	This Study
MZY600	*leu1-32 ura4-D18 ade6-M216 h- [nmt-GFP-13g6]*	This Study
MZY601	*leu1-32 ura4-D18 ade6-M216 h-[nmt-GFP-gma12]*	This Study

BIBLIOGRAPHY

Adachi Y and Yanagida M (1989) Higher order chromosome structure is affected by cold-sensitive mutations in a Schizosaccharomyces pombe gene *crm1*$^{+}$, which encodes a 115-kD protein preferentially localized in the nucleus and at its periphery. *J Cell Biol* **108**: 1195-1207.

Antonny B, Huber I, Paris S, Chabre M, and Cassel D (1997) Activation of ADP-ribosylation factor 1 GTPase-activating protein by phosphatidylcholine-derived diacylglycerols. *J Biol Chem* **272**:30848-30851.

Aoe T, Huber I, Vasudevan C, Watkins SC, Romero G, Cassel D, and Hsu VW (1999) The KDEL receptor regulates a GTPase-activating protein for ADP-ribosylation factor 1 by interacting with its non-catalytic domain. *J Biol Chem* **274**: 20545-20549.

Aoe T, Cukierman E, Lee A, Cassel D, Peters PJ, and Hsu VW (1997) The KDEL receptor, ERD2, regulates intracellular traffic by recruiting a GTPase-activating protein for ARF1. *EMBO J* **16**: 7305-7316.

Aridor M, Bannykh SI, Rowe T, and Balch WE (1995) Sequential coupling between COPII and COPI vesicle coats in endoplasmic reticulum to Golgi transport. *J Cell Biol* **131**: 875-893.

Basi G, Schmid E, and Maundrell K (1993) TATA box mutations in the *Schizosaccharomyces pombe nmt1* promoter affect transcription efficiency but not the transcription start point of thiamine repressibility. *Gene* **123**:131-136.

Basyuk E, Boulon S, Pederson FS, Bertrand E, and Rasmussen SV (2005) The packaging signal of MLV is an integrated module that mediates intracellular transport of genomic RNAs. *J Mol Biol* **354**: 330-339.

Basyuk E, Galli T, Mougel M, Blanchard J-M, Sitbon M, and Bertrand E (2003) Retroviral genomic RNAs are transported to the plasma membrane by endosomal vesicles. *Dev Cell* **5**: 161-174.

Béthune J, Wieland F, and Moelleken J (2006) COPI-mediated transport. *J Memb. Biol* **211**:65-79.

Bharathi A, Ghosh A, Whalen WA, Yoon JH, Pu R, Dasso M, and Dhar R (1997) The human RAE1 gene is a functional homologue of *Schizosaccharomyces*

pombe rae1 gene involved in nuclear export of poly(A^+) RNA. *Gene* **198**: 251-258.

Bigay J, Casella J-F, Drin G, Mesmin B, and Antonny B (2005) ARFGAP1 responds to membrane curvature through the folding of a lipid packing sensor motif. *EMBO J* **24**:2244-2253.

Bigay J, Gounon P, Robineau S, and Antonny B (2003) Lipid packing sensed by ArfGAP1 couples COPI coat disassembly to membrane bilayer curvature. *Nature* **426**: 563-566.

Blader IJ, Cope MJTV, Jackson TR, Profit AA, Greenwood AF, Drubin DG, Prestwich GD, and Theibert AB (1999) *GCS1*, an Arf guanosine triphosphate-activating protein in *Saccharomyces cerevisiae*, is required for normal actin cytoskeletal organization *in vivo* and stimulates actin polymerization *in vitro*. *Mol Biol Cell* **10**: 581-596.

Boeke JD, Truheart J, Natsoulis G, and Fink GR (1987) 5-Fluoroototic Acid as a selective agent in yeast molecular genetics. *Methods Enzymol* **154**: 164-175.

Bogerd HP, Fridell RA, Madore S, and Cullen BR (1995) Identification of a novel cellular cofactor for the Rev/Rex class of retroviral regulatory proteins. *Cell* **82**: 485-494.

Bradford MM (1976) A rapid and sensitive method for the quantitation of microgram quantities of protein utilizing the principle of protein-dye binding. *Anal Biochem* **72**: 248-254.

Brazer SW, Williams HP, Chappell TG, and Cande WZ (2000) A fission yeast kinesin affects Golgi membrane recycling. *Yeast* **16**: 149-166.

Brown JA, Bharathi A, Ghosh A, Whalen W, Fitzgerald E, and Dhar R (1995) A mutation in the *Schizosaccharomyces pombe rae1* gene causes defects in poly(A^+) RNA export and in the cytoskeleton. *J Biol Chem* **270**: 7411-7419.

Burke JD and Gould KL (1994) Molecular cloning and characterization of the *Schizosaccharomyces pombe his3* gene for use as a selectable marker. *Mol Gen Genet* **242**:169-176.

Chappell TG, Hajibagheri MAN, Ayscough K, Pierce M, and Warren G. (1994) Localization of an α-1,2 galactosyltransferase activity to the Golgi apparatus of *Schizosaccharomyces pombe*. *Mol Biol Cell* **5**: 519-526.

Craven RA, Griffiths DJF, Sheldrick KS, Randall RE, Hagan IM, and Carr AM (1998) Vectors for the expression of tagged proteins in Schizosaccharomyces pombe. *Gene* **221**:59-68.

Cukierman E, Huber I, Rotman M, and Cassel D (1995) The ARF1 GTPase-activating protein: zinc finger motif and Golgi complex localization. *Science* **270**: 1999-2002.

D'Souza and Summers (2005) How retroviruses select their genomes. *Nature Reviews* **3**:643-655.

D'Souza-Schorey C and Chavier P (2006) ARF proteins: roles in membrane traffic and beyond. *Mol Cell Biol* **7**: 347-358.

Dogic D, de Chassey B, Pick E, Cassel D, Lefkir Y, Hennecke S, Cosson P, and Letourneur F (1999) The ADP-ribosylation factor GTPase-activating protein Glo3p is involved in ER retrieval. *Euro J Cell Biol* **78**: 305-310.

Donaldson JG and Honda A (2005) Localization and function of Arf family GTPases. *Biochem Soc Trans* **33**:639-642.

Drebot MA, Johnston GC, and Singer RA (1987) A yeast mutant conditionally defective for reentry into the mitotic cell cycle from stationary phase. *Proc Natl Acad Sci USA* **84**: 7948-7952.

Drin G, Casella J-F, Gautier R, Boehmer T, Schwartz TU, and Antonny B (2007) A general amphipathic α-helical motif for sensing membrane curvature. *Nat Struct Mol Biol* **14**: 138-146.

Doria M, Salcini AE, Colombe E, Parslow TG, Pelicci PG, and Di Fiore PP (1999) the Eps15 homology (EH) domain-based interaction between Eps15 and Hrb connects the molecular machinery of endocytosis to that of nucleocytoplasmic transport. *J Cell Biol* **147**: 1379-1384.

Duden R (2003) ER-to-Golgi transport: COPI and COPII function. *Mol Mem Biol* **20**: 197-207.

Erickson FL, Hannig EM, Krasinskas A and Kahn RA (1993) Cloning and sequence of ADP-ribosylation Factor 1 (ARF1) from *Schizosaccharomyces pombe*. *Yeast* **9**: 923-927.

Eugster A, Frigerio G, Dale M, Duden R (2000) COPI domains required for coatomer integrity, and novel interactions with ARF and ARF-GAP. *EMBO J* **19**: 3905-3917.

Fabre E and Hurt E (1997) Yeast genetics to dissect the nuclear pore complex and nucleocytoplasmic trafficking. *Annu Rev Genet* **31**: 277-313.

Felber BK, Hadzopoulou-Cladaras M, Cladaras C, Copeland T, and Pavlakis GN (1989) Rev protein of human immunodeficiency virus type 1 affects the stability and transport of the viral mRNA. *Proc Natl Acad Sci USA* **86**: 1495-1499.

Fischer U, Huber J, Boelens SC, Mattaj IW, and Lührmann R (1995) The HIV-1 Rev activation domain is a nuclear export signal that accesses an export pathway used by specific cellular RNAs. *Cell* **82**: 475-483.

Fischer U, Meyer S, Teufel M, Heckel C, Lührmann R, and Rautmann G (1994) Evidence that HIV-1 Rev directly promotes the nuclear export of unspliced RNA. *EMBO J* **13**: 4105-4112.

Frankel AD and Young JAT (1998) HIV-1: Fifteen proteins and an RNA. *Annu Rev Biochem* **67**:1-25.

Fridell RA, Bogerd HP, and Cullen BR (1996) Nuclear export of late HIV-1 mRNAs occurs via a cellular protein export pathway. *Proc Natl Acad Sci USA* **93**: 4421-4424.

Fritz CC and Green MR (1996) HIV Rev uses a conserved cellular protein export pathway for the nucleocytoplasmic transport of viral RNAs. *Curr Biol* **6**: 848-854.

Fritz CC, Zapp ML, and Green MR (1995) A human nucleoporin-like protein that specifically interacts with HIV Rev. *Nature* **376**: 530-533.

Fukuda M, Asano S, Nakamura T, Adachi M, Yoshida M, Yanagida M, and Nishida E (1997) CRM1 is responsible for intracellular transport mediated by the nuclear export signal. *Nature* **390**: 308-311.

Garrus JE, von Schwedler UK, Pornillos OW, Morham SG, Zavitz KH, Wang HE, Wettstein DA, Stray KM, Cote M, Rich RL, Myszka DG, and Sundquist WI (2001) Tsg101 and the vacuolar protein sorting pathway are essential for HIV-1 budding. *Cell* **107**: 55-65.

Gaynor EC, Graham TR, and Emr SD (1998) COPI in ER/Golgi and intra-Golgi transport: do yeast COPI mutants point the way? *Biochim et Biophys Acta* **1404**: 33-51.

Grimm C, Kohli J, Murray J and Maundrell K (1988) Genetic engineering of *Schizosaccharomyces pombe*: a system fro gene disruption and replacement using the ura4 gene as a selectable marker. *Mol Gen Genet* **215:** 81-86.

Hagan IM and Ayscouth KR (2000) Fluorescence Microscopy in Yeast. In Allan,V.J. (ed), *Protein Localization of Fluorescence Microscopy: A Practical Approach*. Oxford University Press, Oxford, UK, pp.179-206.

Henderson BR and Percipalle P (1997) Interactions between HIV Rev and nuclear import and export factors: The Rev nuclear localization signal mediates specific binding to human Importin-β. *J Mol Biol* **274**: 693-707.

Hindley J, Phear G, Stein M, and Beach D (1987) *suc1*$^{+}$ encodes a predicted 13-kd protein that is essential for cell viability and is directly involved in the division cycle of *S. pombe*. *Mol Cell Biol* **7**: 504-511.

Hosobuchi M, Kreis T, and Schekman R (1992) SEC21 is a gene required for ER to Golgi protein transport that encodes a subunit of a yeast coatomer. *Nature* **360**: 603-605.

Ireland LS, Johnston GC, Drebot MA, Dhiiion N, DeMaggio AJ, Hoekstra MF, and Singer RA (1994) A member of a novel family of yeast 'Zn-finger' proteins mediates the transition from stationary phase to cell proliferation. *EMBO J* **13**: 3812-3821.

Jung G, Ueno H, and Hayashi R (1999) Carboxypeptidase Y: Structural basis for protein sorting and catalytic triad. *J Biochem* **126**: 1-6.

Kahn RA and Gillman AG (1986) The protein cofactor necessary for ADP ribosylation of Gs by cholera toxin is itself a GTP binding protein. *J Bio Chem* **261**: 7906-7911.

Kang-Decker N, Mantchev GT, Juneja SC, McNiven MA and van Deursen JMA (2001) Lack of Acrosome Formation in Hrb-Deficient Mice. *Science* **294**:1531-1533.

Kaufer NF, Simanis V, and Nurse P (1985) Fission yeast Schizosaccharomyces pombe correctly excises a mammalian RNA transcript intervening sequence. *Nature* **318**: 78-80.

Keeney JB and Boeke JD (1994) Efficient targeted integration at *leu1-32* and *ura4-294* in *Schizosaccharomyces pombe*. *Genetics* **136**: 849-856.

Kostrub CF, Lei EP and Enoch T (1998) Use of gap repair in fission yeast to obtain novel alleles of specific genes. *Nucleic Acids Research* **26**: 4783-4784.

Kudo N, Wolff B, Sekimoto T, Schreiner EP, Yoneda Y, Yanagida M, Horinouchi S, and Yoshida M (1998) Leptomycin B inhibition of signal-mediated nuclear export by direct binding to crm1. *Exp Cell Research* **242**: 540-547.

Laemmli UK (1970) Cleavage of structural proteins during the assembly of the head of bacteriophage T4. *Nature* **227**: 680-685.

Langille SE, Patki V, Klarlund JK, Buxton JM, Holik JJ, Chawla A, Corvera S, and Czech MP (1999) ADP-ribosylation factor 6 as a target of guanine nucleotide exchange factor GRP1. *J Biol Chem* **274**: 27099-27104.

Lewis SM, Poon PP, Singer RA, Johnston GC, and Spang RA (2004) The ArfGAP Glo3 is required for the generation of COPI vesicles. *Mol Biol Cell* **15**: 4064-4072.

Liu X, Zhang C, Xing G, Chen Q, and He F (2001) Functional characterization of novel human ARFGAP3. *FEBS* **490**: 79-83.

Makler V, Cukierman E, Rotman M, Admon A, and Cassel D (1995) ADP-ribosylation factor-directed GTPase-activating protein: purification and partial characterization. *J Biol Chem* **270**: 5232-5237.

Malim MH, McCarn DF, Tiley LS, and Cullen BR (1991) Mutational Definition of the human immunodeficiency virus type 1 Rev activation domain. *J Virol* **65**: 4248-4254.

Malim MH, Hauber J, Le S-Y, Maizel JV, and Cullen BR (1989a) The HIV-1 *rev trans*-activator acts through a structured target sequence to activate nuclear export of unspliced viral mRNA. *Nature* **338**: 254-257.

Malim MH, Bohnlein S, Hauber J, and Cullen BR (1989b) Functional dissection of the HIV-1 Rev trans-activator-derivation of a trans-dominant repressor of Rev function. *Cell* **58**: 205-214.

Mandiyan V, Andreev J, Schlessinger J, and Hubbard SR (1999) Crystal structure of the ARF-GAP domain and ankyrin repeats of PYK2-associated protein beta. *EMBO J* **18:** 6890-6898.

Matynia A, Salus SS, and Sazer S (2001) Three proteins required for early steps in the protein secretory pathway also affect nuclear envelope structure and cell cycle progression in fission yeast. *J Cell Science* **115**: 421-431.

Maundrell K (1993) Thiamine-repressible expression vectors pREP and pRIP for fission yeast. *Gene* **123**:127-130.

Maundrell K (1990) *nmt1* in fission yeast. *J. Biol Chem* **265**: 10857-10864.

Mesmin B, Drin G, Levi S, Rawet M, Cassel D, Bigay J, and Antonny B (2007) Two lipid-packing sensor motifs contribute to the sensitivity of ARFGAP1 to membrane curvature. *Biochem* **46**: 1779-1790.

Meyer BE and Malim MH (1994) The HIV-1 Rev trans-activator shuttles between the nucleus and the cytoplasm. *Genes & Dev* **8**: 1538-1547.

Moreno S, Klar A and Nurse P (1991) Molecular genetic analysis of fission yeast, *Schizosaccharomyces pombe*. In Guthrie,C. and Fink,G.R. (ed), *Methods in Enzymology*. Academic Press, Inc., San Diego, CA, pp. 795-823.

Moss J and Vaughan M (1998) Molecules in the ARF orbit. *J Bio Chem* **273**: 21431-21434.

Neville M, Stutz F, Lee L, David LI, and Rosbash M (1997) The importin-beta family member Crm1p bridges the interaction between Rev and the nuclear pore complex during nuclear export. *Curr Biol* **7**: 767-775.

Nie Z, Hirsch DS, Luo R, Jian X, Stauffer S, Cremesti A, Andrade J, Lebowitz J, Marino M, Ahvazi B, Hinshaw JE, and Randazzo PA (2006) A BAR domain in

the N terminus of the Arf GAP ASAP1 affects membrane structure and trafficking of epidermal growth factor receptor. *Curr Biol* **16**: 130-139.

Nie Z and Randazzo PA (2006) Arf GAPs and membrane traffic. *J Cell Sci* **119**: 1203-1211.

Nie Z, Hirsch DS, and Randazzo PA (2003) Arf and its many interactors. *Cur Opin Cell Biol* **15**:396-404.

Pearson WR and Lipman DJ (1988) Improved tools for biological sequence comparison. *Proc Natl Acad Sci USA* **85**: 2444-2448

Pei J and Grishin NV (2007) PROMALS: towards accurate multiple sequence alignments of distantly related proteins. *Bioinformatics* **23**: 802-808.

Pepperkok R, Scheel J, Horstmann H, Hauri HP, Griffiths G, and Kreis TE (1993) Beta-COP is essential for biosynthetic membrane transport from the endoplasmic reticulum to the Golgi complex in vivo. *Cell* **74**: 71-82.

Peter BJ, Kent HM, Mills IG, Vallis Y, Butler PJG, Evans PR, and McMahon HT (2004) BAR domains as sensors of membrane curvature: the amphiphysin BAR structure. *Science* **303**: 495-499.

Pollard VW and Malim MH (1998) The HIV-1 Rev protein. *Annu Rev Microbiol* **52**: 491-532.

Poon PP, Nothwehr SF, Singer RA, and Johnston GC (2001) The Gcs1 and Age2 ArfGAP proteins provide overlapping essential function for transport from the yeast trans-Golgi network. *J Cell Biol* **155**: 1239-1250.

Poon PP, Cassel D, Sprang A, Rotman M, Pick E, Singer RA, and Johnston GC (1999) Retrograde transport from the yeast Golgi is mediated by two ARF GAP proteins with overlapping function. *EMBO J* **18**: 555-564.

Poon PP, Wang X, Rotman M, Huber I, Cukierman E, Cassel D, Singer RA, and Johnston GC (1996) *Saccharomyces cerevisiae* Gcs1 is an ADP-ribosylation factor GTPase-activating protein. *Proc Natl Acad Sci* **93**: 10074-10077.

Randazzo PA, Andrade J, Miura K, Brown MT, Long YQ, Stauffer S, Roller P, and Cooper JA (2000) The Arf GTPase-activating protein ASAP1 regulates the actin cytoskeleton. *Proc Natl Acad Sci* **97**: 4011-4016.

Rein U, Andag U, Duden R, Schmitt HD, and Spang A (2002) ARF-GAP-mediated interaction between the ER-Golgi v-SNAREs and the COPI coat. *J Cell Biol* **157**: 395-404.

Robinson M, Poon PP, Schindler C, Murray LE, Kama R, Gabriely G, Singer RA, Spang A, Johnston GC, and Gerst JE (2006) The Gcs1 ARF-GAP mediates Snc1,2 v-SNARE retrieval to the Golgi in yeast. *Mol Biol Cell* **17**:1845-1858.

Rothman JE (1994) Mechanisms of intracellular protein transport. *Nature* **372**: 55-63.

Salcini AE, Confalonieri S, Doria M, Santolini E, Tassi E, Minenkova O, Cesareni G, Pelicci PG, Di Fiore PP (1997) Binding specificity and in vivo targets of the EH domain, a novel protein-protein interaction module. *Genes Dev* **11**:2239-2249.

Sambrook J, Fritsch EF and Maniatis T (1989) *Molecular Cloning: A Laboratory Manual*. 2nd edn. Cold Spring Harbor Laboratory Press, Cold Spring Harbor, NY.

Sánchez-Velar N, Udofia EB, Yu Z, and Zapp ML (2004) hRIP, a cellular cofactor for Rev function, promotes release of HIV RNAs from the perinuclear region. *Genes & Dev* **18**:23-34.

Stack JH, DeWald DB, Takegawa K, and Emr SD (1995) Vesicle-mediated protein transport: regulatory interactions between the Vps15 protein kinase and the Vps34 PtdIns 3-kinase essential for protein sorting to the vacuole in yeast. *J Cell Biol* **129**: 321-334.

Stade K, Ford CS, Guthrie C, and Weis K (1997) Exportin 1 (Crm1p) is an essential nuclear export factor. *Cell* **90**:1041-1050.

Stearns T, Kahn RA, Botstein D, and Hoyt MA (1990) ADP ribosylation factor is an essential protein in Saccharomyces cerevisiae and is encoded by two genes. *Mol Cell Biol* **10**: 6690-6699.

Stephens DJ, Lin-Marq N, Pagano A, Pepperkok R, and Paccaud J-P (2000) COPI-coated ER-to-Golgi transport complexes segregate from COPII in close proximity to ER exit sites. *J Cell Sci* **113**: 2177-2185.

Stutz F, Kantor J, Zhang D, McCarthy T, Neville M, and Rosbash M (1997) The yeast nucleoporin Rip1p contributes to multiple export pathways with no essential role for its FG-repeat region. *Genes & Dev* **11**: 2857-2868.

Stutz F, Neville N, and Rosbash M (1995) Identification of a novel nuclear pore-associated protein as a functional target of the HIV-1 rev protein in yeast. *Cell* **82**: 495-506.

Szafer E, Rotman M, and Cassel D (2001) Regulation of GTP hydrolysis on ADP-ribosylation factor-1 at the Golgi membrane. *J Biol Chem* **276**: 47834-47839.

Tabuchi M, Iwaihara O, Ohtani Y, Ohuchi N, Sakurai J-I, Morita T, Iwahara S, and Takegawa K (1997) Vacuolar protein sorting in fission yeast: cloning, biosynthesis, transport, and processing of Carboxypeptidase Y from *Schizosaccharomyces pombe*. *J Bact* **179**: 4179-4189.

Takegawa K, DeWald DB, and Emr SD (1995) Schizosaccharomyces pombe Vps34p, a phosphatidylinositol-specific PI 3-kinase essential for normal cell growth and vacuole morphology. *J Cell Sci* **108**: 3745-3756.

Thompson JD, Higgins DG, and Gibson TJ (1994) CLUSTAL W: improving the sensitivity of progressive multiple sequence alignment through sequence weighting, position-specific gap penalties and weight matrix choice. *Nucleic Acids Res* **22**: 4673-4680.

Toyama R, Bende SM, and Dhar R (1992) Transcriptional activity of the human immunodeficiency virus-1 LTR promoter in fission yeast Schizosaccharomyces pombe. *Nucl Acid Res* **20**: 2591-2596.

Trautwein M, Dengjel J, Schirle M, and Spang A (2004) Arf1p provides an unexpected link between COPI vesicles and mRNA in *Saccharomyces cerevisiae*. *Mol Bio Cell* **15**: 5021-5037.

Vida TA and Emr SD (1995) A new vital stain for visualizing vacuolar membrane dynamics and endocytosis in yeast. *J Cell Biol* **128**: 779-792.

Ward TH, Polishchuk RS, Caplan S, Hirschberg K, and Lippincott-Schwartz J (2001) Maintenance of Golgi structure and function depends on the integrity of ER export. *J Cell Biol* **155**: 498-499.

Watson PJ, Frigerio G, Collins BM, Duden R, and Owen DJ (2004) γ-COP appendage domain – structure and function. *Traffic* **5**: 79-88.

Wood V, Gwilliam R, Rajandream MA, Lyne M, Lyne R, Stewart A, Sgouros J, Peat N, Hayles J, Baker S, Basham D, Bowman S, Brooks K, Brown D, Brown S, Chillingworth T, Churcher CM, Collins M, Connor R, Cronin A, Davis P, Feltwell T, Fraser A, Gentles S, Goble A, Hamlin N, Harris D, Hidalgo J, Hodgson G, Holroyd S, Hornsby T, Howarth S, Huckle EJ, Hunt S, Jagels K, James K, Jones L, Jones M, Leather S, McDonald S, McLean J, Mooney P, Moule S, Mungall K, Murphy L, Niblett D, Odell C, Oliver K, O'Neil S, Pearson D, Quail MA, Rabbinowitsch E, Rutherford K, Rutter S, Saunders D, Seeger K, Sharp S, Skelton J, Simmonds M, Squares R, Squares S, Stevens K, Taylor K, Taylor RG, Tivey A, Walsh SV, Warren T, Whitehead S, Woodward J, Volckaert G, Aert R, Robben J, Grymonprez B, Weltjens I, Vanstreels E, Rieger M, Schaefer M, Mueller-Auer S, Gabel C, Fuchs M, Fritzc C, Holzer E, Moestl D, Hilbert H, Borzym K, Langer I, Beck A, Lehrach H, Reinhardt R, Pohl TM, Eger P, Zimmermann W, Wedler H, Wambutt R, Purnelle B, Goffeau A, Cadieu E,

Dreano S, Gloux S, Lelaure V, Mottier S, Galibert F, Aves SJ, Xiang Z, Hunt C, Moore K, Hurst SM, Lucas M, Rochet M, Gaillardin C, Tallada VA, Garzon A, Thode G, Daga RR, Cruzado L, Jimenez J, Sanchez M, del Rey F, Benito J, Dominguez A, Revuelta JL, Moreno S, Armstrong J, Forsburg SL, Cerrutti L, Lowe T, McCombie WR, Paulsen I, Potashkin J, Shpakovski GV, Ussery D, Barrell BG and Nurse P (2002) The genome sequence of Schizosaccharomyces pombe. *Nature* **415**: 871-880.

Yahara N, Sato K, and Nakano A (2006) The Arf1p GTPase-activating protein glo3p executes its regulatory function through a conserved repeat motif at its C-terminus. *J Cell Biol* **119**: 2604-2612.

Yanagisawa LL, Marchena J, Xie Z, Li X, Poon PP, Singer RA, Johnston GC, Randazzo PA, and Bankaitis VA (2002) Activity of specific lipid-regulated ADP ribosylation factor-GTPase-activating proteins is required for Sec14p-dependent Golgi secretory function in yeast. *Mol Biol Cell* **13**: 2193-2206.

Yang, J-S, Yee SY, Gao M, Bourgoin S, Randazzo PA, Premont RT, and Hsu VW (2002) ARFGAP1 promotes the formation of COPI vesicles, suggesting function as a component of the coat. *J Cell Biol* **159**: 69-78.

Yoon JH, Whalen WA, Bharathi A, Shen R, and Dhar R (1997) Npp106p, a *Schizosaccharomyces pombe* nucleoporin similar to *Saccharomyces cerevisiae* Nic96p, functionally interacts with Rae1p in mRNA export. *Mol Cell Biol* **17**: 7047-7060.

Yu Z, Sánchez-Velar N, Catrina IE, Kittler ELW, Udofia EB, and Zapp ML (2005) The cellular HIV-1 Rev cofactor hRIP is required for viral replication. *Proc Natl Acad Sci* **102**: 4027-4032.

Zhang C, Yu Y, Zhang S, Liu M, Xing G, Wei H, Bi J, Liu X, Zhou G, Dong C, Hu Z, Zhang Y, Luo L, Wu C, Zhao S, He F (2000) Characterization, chromosomal assignment, and tissue expression of a novel human gene belonging to the ARF GAP family. *Genomics* **63**: 400-408.

Zhang C-J, Bowzard JB, Anido A, and Kahn RA (2003) Four ARF GAPs in *Saccharomyces cerevisiae* have both overlapping and distinct functions. *Yeast* **20**: 315-330.

Zhang C-J, Cavenagh MM, and Kahn RA (1998) A family of Arf effectors defined as suppressors of the loss of Arf function in the yeast Saccharomyces cerevisiae. *J Biol Chem* **273**: 19792-19796.

Zhao Y, Cao J, O'Gorman MRG, Yu M, and Yogev R (1996) Effect of human immunodeficiency virus type 1 protein R (vpr) gene expression on basic cellular function of fission yeast Schizosaccharomyces pombe. *J Virol* **70**: 5821-5826.

Zhao Y and Lieberman HB (1995) Schizosaccharomyces pombe: a model for molecular studies of eukaryotic genes. *DNA Cell Biol* **14**: 359-371.

Zimmerberg J and McLaughlin S (2004) Membrane curvature: How BAR domains bend bilayers. *Curr Biol* **14**: R250-R252.

SUPPLEMENTAL SECTION

A yeast two-hybrid screen identified the human Rev Interacting Protein (hRIP) as a cellular co-factor for HIV-1 Rev, specifically the ability to interact with the Rev nuclear export signal (NES; Fritz *et al*, 1995; Bogerd *et al* 1995). In addition, a correlation was established between the loss of hRIP binding to Rev NES mutants and the loss of Rev function, suggesting hRIP could play a role in the export of Rev-directed viral RNAs (Fritz *et al*, 1995; Bogerd *et al*, 1995). However, the hRIP-Rev interaction is indirect, suggesting that a cellular transport factor mediates this interaction (Henderson & Percipalle, 1997). Experiments with NESs from cellular proteins Protein Kinase Inhibitor (PKI) and Inhibitor of Nuclear Factor κB (IκB) were also shown to interact with hRIP in yeast two-hybrid screens. Specifically, fusion of the PKI-NES or the IκB-NES to the RNA-binding domain of Rev generates a fully functional Rev protein, suggesting that Rev protein export uses a cellular export pathway (Fritz and Green 1996). The cellular factor thought to bridge the Rev-hRIP interaction is CRM1 (Neville *et al*, 1997). Here we describe the use of the *agv1*^{ts} strains to study the possible role of Agv1 in nucleocytoplasmic transport pathways and to determine a possible interaction between HIV-1 Rev and Agv1.

Poly (A^+) RNA export is not affected in *agv1^{ts}* strains at restrictive temperature.

A correlation between loss of Rev-binding and loss of Rev function suggests hRIP could play a role in the export of Rev-directed viral RNAs (Fritz *et al*, 1995; Bogerd *et al*, 1995). We investigated the role of Agv1 in mRNA export by RNA *in situ* hybridization using a Cy3-conjugated oligo dT50 probe. Strains MZY504, MZY505, and MZY507 were grown in EMM supplemented with adenine to mid-log phase and then shifted to the restrictive temperature of 36°C for one hour. To validate the assay, an *S. pombe rae1-167* temperature sensitive strain was used as a positive control for the nuclear accumulation of poly(A)$^+$ RNA (Yoon *et al*, 1997). *Rae1$^+$* is essential for the general export of mRNA in fission yeast and loss of Rae1 activity results in an accumulation of poly(A)$^+$ RNA in the nucleus within five minutes and a complete block in export of poly(A)$^+$ RNA within 30 minutes (Brown *et al*, 1995). At permissive temperature, the poly(A)$^+$ RNA can be seen distributed throughout both the nucleus and the cytoplasm in all strains tested (Figure S-1, Panels E-H). As expected, after 1 hour at restrictive temperature, the poly (A)$^+$ RNA accumulates in the nucleus of all the *rae1-167* cells (Figure S-1, Panel I). On the contrary, after 1 hour at restrictive temperature, the poly (A)$^+$ RNA is distributed throughout the nucleus and the cytoplasm of the MZY504 deletion strain expressing wild-type *agv1$^+$* (Figure S-1, Panel J) as well as the MZY505 and MZY507 deletion strains expressing the *ts*

mutant alleles *1A1* and *4A3* (Figure S-1, Panels K & L), suggesting that Agv1 does not play a direct role in the general mRNA export pathway.

Agv1 does not play a role in leucine rich NES-mediated Protein Export

To investigate the possible role of Agv1 in NES-mediated nuclear protein export, the localization of an *nmt1* promoter-driven GST-NES_{Rev}-EGFP reporter construct (Kudo *et al*, 1998) was determined at restrictive temperature by GFP fluorescence microscopy. Strains MZY320 and MZY321 were grown in EMM supplemented with adenine and uracil to mid-log phase, shifted to restrictive temperature and localization of the GFP-fusion protein determined at 36°C. At 0 hours, the GST-NES_{Rev}-EGFP reporter construct localizes in the cytoplasm in all strains (Figure S-2, Panels A, E, & I). Following 1, 2, or 3 hours at either 18°C or 36°C, the GST-NES_{Rev}-EGFP reporter construct still localizes in the cytoplasm in all strains (Figure S-2, Panels B-D, F-H, & J-L), suggesting that Agv1 does not play a direct role in leucine rich NES-mediated protein export. However, the *crm1-AC1* cold-sensitive strain (Adachi and Yanagida, 1989) expressing the GST-NES_{Rev}-GFP construct (Fukuda *et al*, 1997) used as a positive control (Strain MZY319) does not show a cold-sensitive phenotype at the restrictive temperature of 18°C (Figure S-2, Panels A-D).

Agv1 does not play a direct role in NLS-Mediated Protein Import

To investigate the possible role of Agv1 in NLS-mediated nuclear protein export, the localization of an *nmt1* promoter-driven GST-NLS_{SV40}-EGFP reporter construct (Kudo *et al*, 1998) was determined at restrictive temperature by GFP fluorescence microscopy. Strains MZY323 and MZY324 were grown in EMM supplemented with adenine and uracil to mid-log phase, shifted to restrictive temperature and localization determined at 36°C. There was no known mutant of a nuclear import protein to use as a positive control to validate this experiment. At 0 hours, the GST-NLS_{SV40}-EGFP reporter construct localizes in the nucleus in all strains (Figure S-3, Panels B & F). Following 1, 2, or 3 hours at 36°C, the GST-NLS_{SV40}-EGFP reporter construct still localizes in the nucleus of all strains (Figure S-3, Panels C-E & G-I), suggesting that Agv1 does not play a direct role in general NLS-mediated protein import. However, there was no known fission yeast protein import mutant to use as a positive control for this experiment.

Agv1 interacts with the nuclear export signal of REV

hRIP has been shown to interact with the NES signal of HIV-1 Rev, but not the NES mutant, Rev M10 (Fritz *et al*, 1995). We determined whether Agv1 could interact with Rev by affinity chromatography. Specifically, HA-Agv1-His_6 partially purified protein, or binding buffer alone, was coupled to Ni^{2+}-agarose beads, and one fifth of each resulting complex was resolved on a 10% SDS-

polyacrylamide gel and probed with a mouse monoclonal α-His antibody to determine HA-Agv1-His_6 coupling (88.4% of input protein bound to beads). The remaining resin:HA-Agv1-His_6 complex was incubated with different glutathione S-transferase (GST)-Rev fusion proteins: GST-Rev is GST fused to full length wild-type Rev (37.2kDa); GST-RevM10 is GST fused to full length Rev with point mutations in the leucine rich NES (37.2kDa); GST-WT-NES is GST fused to three tandemized copies of just the wild-type NES of Rev (27.7kDa); GST-M10-NES is GST fused to three tandemized copies of just the NES of RevM10 (27.7kDa); GST is GST alone (25kDa). The resulting protein-resin complexes were resolved on a 10% SDS-polyacrylamide gel and probed with a rabbit polyclonal α-Rev antibody. The results indicate that Agv1 interacts with GST-Rev and GST-WT-NES (Figure S-4, Lanes 2 & 5) but not with GST alone (Figure S-4, Lane 4). Moreover, Agv1 does not interact with GST-RevM10 or GST-M10-NES (Figure S-4, Lanes 3 & 6). These results indicate that Agv1 interacts with the NES of HIV-1 Rev and suggest that *S. pombe* could possibly support Rev function.

Rev localization is altered in *agv1^{ts}* strains at restrictive temperature

Given the fact that Agv1 and Rev interact *in vitro*, a pREP42-Rev-GFP fusion protein was transformed into the gene-converted strains, *agv1^{+}*, *agv1-1A1*, and *agv1-4A3* in order to generate a Rev assay. The localization of Rev at restrictive temperature was determined by GFP fluorescence microscopy.

Strains MZY326, MZY327, and MZY328 were grown to mid-log phase in EMM supplemented with adenine and leucine, shifted to restrictive temperature, and Rev localization determined at 36°C. At permissive temperature, Rev-GFP localizes predominantly in the nucleus with some cytoplasmic staining in all strains (Figure S-5, Panels A-C). This observation is consistent with Rev steady-state nuclear localization in mammalian cells (Felber *et al*, 1989). After 2 hours at 36°C, Rev-GFP continues to have a predominantly nuclear localization (Figure S-5, Panels D-F). However, after 4 hours at 36°C, the nuclear localization of Rev-GFP becomes less predominant in the wild-type gene-converted strain, *agv1*$^{+}$ (Figure S-5, Panel G). Alternatively, Rev-GFP remains predominantly nuclear in the > 90% of the *agv1*^{ts} gene-converted cells (Figure S-5, Panels H & I). These results suggest the possibility that Rev-GFP is unable to shuttle between the nucleus and the cytoplasm in the absence of Agv1 function.

5S rRNA localization is altered in *agv1*^{ts} strains.

Studies injecting Rev NES peptides conjugated to bovine serum albumin (BSA) into the nuclei of *Xenopus* oocytes and HeLa cells, indicate that wild-type Rev NES (BSA-R) blocks the nuclear export of 5S rRNA (Fischer *et al*, 1995). To investigate a possible role for Agv1 in 5S rRNA export, 5S rRNA localization was determined by RNA *in situ* hybridization using an ALEXA-594-conjugated oligonucleotide probe complementary to 5S rRNA. Strains MZY509, MZY510,

and MZY511 were grown in EMM supplemented with adenine, uracil, and leucine to mid-log phase and then shifted to the restrictive temperature of 36°C. At permissive temperature, 5S rRNA has a predominantly diffuse cytoplasmic localization in all strains (Figure S-6, Panels A-C). Following 2 or 4 hours at restrictive temperature, 5S rRNA localization remains predominantly diffuse in the cytoplasm in the *agv1*$^{+}$ strain (Figure S-6, Panel D & G). However, in the *agv1*^{ts} strains, the 5S rRNA begins to accumulate on a tubular structure in the cytoplasm (Figure S-6, Panels E, F, H, & I), suggesting that Agv1 could be involved in the transport of 5S rRNA to a discrete cytoplasmic localization.

DISCUSSION

Studies have previously demonstrated that Rev is essential for the export of unspliced and partially spliced HIV-1 RNA from the nucleus (Fischer *et al*, 1994). Moreover, studies showed that a Rev-hRIP interaction directly correlates with Rev function (Fritz *et al*, 1995; Bogerd *et al*, 1995). However the Rev interaction with hRIP is indirect (Henderson and Percipalle, 1997). Crm1 mediates the Rev-hRIP interaction (Neville *et al*, 1997), and *S. cerevisiae crm1* mutants accumulate poly(A)$^{+}$ RNA and NES-containing proteins in the nucleus (Stade *et al*, 1997), suggesting that hRIP and Agv1 could play a direct role in nucleocytoplasmic transport. However, our data indicates that Agv1 is not directly involved in general mRNA export, leucine rich NES-mediated protein

export, or NLS-mediated protein import. Our results do not demonstrate a block of poly(A)$^+$ RNA in the nucleus in the *agv1^{ts}* strains. Preliminary investigation of the possible role of Agv1 in other nuclear RNA export pathways, suggests that 5S rRNA accumulates in tubular structures in the cytoplasm.

The lack of functional positive controls for either the NES-mediated protein export or the NLS-mediated protein import assays do suggest caution in interpreting the results. However, given the growth curves of the *agv1^{ts}* strains at restrictive temperature and the striking localization of the reporter constructs, it appears that Agv1 is not directly involved in the general NES-mediated protein export or the general NLS-mediated protein import pathways. These results are consistent with studies using the dominant negative hRIP mutant, hRIPΔN360, which causes mislocalization of Rev-directed RNAs to the perinuclear region but does not affect general mRNA export, general NES-dependent protein export, or general NLS-dependent protein import (Sánchez-Velar *et al*, 2004).

The ability of Agv1 to interact with the Rev NES suggests the possibility that Rev may have similar function in fission yeast as in mammalian cells. Additionally, there appears to be a stronger nuclear accumulation of Rev-GFP in *agv1^{ts}* strains compared to wild-type at restrictive temperature. Our results indicate that Agv1 does not play a direct role in nuclear import or nuclear export. However, they do suggest that Agv1 might play a role in RNA transport in the cytoplasm.

Figure S-1. Agv1 does not play a direct role in export of poly(A)$^+$ RNA export. The strains *rae1-167*, MZY504, MZY505, and MZY507 were grown to mid-log phase (OD_{595nm} = 0.5/ml) in EMM supplemented with adenine at 25°C, shifted to EMM with adenine pre-warmed to 36°C, and an aliquot of cells fixed in 4% paraformaldehyde at 0 and 1 hour at 36°C. Localization of poly(A)$^+$ RNA was detected by RNA *in situ* hybridization using a Cy3-conjugated oligo (dT50) probe.

(A-D) Negative controls of strains *rae1-167* (A), MZY504 (B), MZY505 (C), and MZY507 (D) containing no Cy3-conjugated oligo (dT50) probe.

(E-H) Poly(A)$^+$ RNA localization in strains *rae1-167* (E), MZY504 (F), MZY505 (G), and MZY507 (I) at 25°C.

(I-L) Poly(A)$^+$ RNA localization in strains *rae1-167* (I), MZY504 (J), MZY505 (K), and MZY507 (L) following 1 hour at 36°C.

Figure S-2. Agv1 does not play a direct role in NES-mediated protein export. The strains MZY319, MZY320, and MZY321 were grown to mid-log phase (OD_{595nm} = 0.5/ml) in EMM supplemented with adenine and uracil at 30°C (MZY319) or 25°C (MZY320 and MZY321), shifted to EMM supplemented with adenine and uracil chilled to 18°C (MZY319) or pre-warmed to 36°C (MZY320 and MZY321). Cells were fixed in ice-cold methanol after 0 or 3 hours at 18°C or 36°C. GST-NES_{Rev}-GFP fusion protein localization was detected by GFP fluorescence microscopy.

(A-D) GST-NES_{Rev}-GFP localization in the strain MZY319 at 30°C (A), or following 1 (B), 2 (C), or 3 (D) hours at 18°C.

(E-H) GST-NES_{Rev}-GFP localization in the strain MZY320 at 25°C (E), or following 1 (F), 2 (G), or 3 (H) hours at 36°C.

(I-L) GST-NES_{Rev}-GFP localization in the strain MZY321 at 25°C (I), or following 1 (J), 2 (K), or 3 (L) hours at 36°C.

Figure S-3. Agv1 does not play a direct role in NLS-mediated protein import. The strains MZY323 and MZY324 were grown to mid-log phase (OD_{595nm} = 0.5/ml) in EMM supplemented with adenine and uracil at 25°C, shifted to EMM supplemented with adenine and uracil pre-warmed to 36°C. Cells were fixed in ice-cold methanol after 0, 2, or 3 hours at 36°C. GST-NLS_{SV40}-GFP fusion protein localization was detected by GFP fluorescence microscopy.

(A) *Agv1*$^{+}$ strain with no GFP fusion protein as a negative control for background.

(B-E) GST-NLS_{SV40}-GFP localization in the strain MZY323 at 25°C (B) or following 1 (C), 2 (D), or 3 (E) hours at 36°C.

(F-I) GST-NLS_{SV40}-GFP localization in the strain MZY324 at 25°C (F), or following 1 (G), 2 (H), or 3 (I) hours at 36°C.

Figure S-4. Agv1 interacts with HIV-1 Rev. Partially purified HA-Agv1-His_6 conjugated to Ni^{2+}-agarose beads, incubated at 4°C with GST-fusion proteins, resolved on 10% SDS polyacrylamide gel, and the complexes detected using an a rabbit polyclonal Rev antibody (1:750). Lane 1 is buffer alone, Lane 2 is GST-Rev (37.2kDa), Lane 3 is GST-RevM10 (37.2kDa), Lane 4 is GST (25kDa), Lane 5 is GST-WT-NES (27.7kDa), and Lane 6 is GST-M10-NES (27.7kDa).

Figure S-5. Rev remains in the nucleus in *agv1^{ts}* strains at restrictive temperature. Strains *agv1^{+}*, *agv1-1A1*, and *agv1-4A3* were grown to mid-log phase (OD_{595nm} = 0.5/ml) in EMM supplemented with adenine and leucine at 25°C, shifted to EMM supplemented with adenine and leucine pre-warmed to 36°C. Cells were fixed in ice-cold methanol following 0, 2, or 4 hours at 36°C. Rev-GFP fusion protein localization was detected by GFP fluorescence microscopy.

(A-C) Rev-GFP localization in the strains *agv1^{+}* (A), *agv1-1A1* (B), and *agv1-4A3* (C) at 25°C.

(D-F) Rev-GFP localization in the strains *agv1^{+}* (D), *agv1-1A1* (E), and *agv1-4A3* (F) following 2 hours at 36°C.

(G-I) Rev-GFP localization in the strains *agv1^{+}* (G), *agv1-1A1* (H), and *agv1-4A3* (I) following 4 hours at 36°C.

Figure S-6. 5S rRNA accumulates in the cytoplasm in *agv1*^{ts} strains at restrictive temperature. The strains *agv1*$^{+}$, *agv1-1A1*, and *agv1-4A3* were grown in mid-log phase (OD_{595nm} = 0.5/ml) in EMM supplemented with adenine, uracil, and leucine at 25°C, shifted to EMM supplemented with adenine, uracil, and leucine pre-warmed to 36°C. Cells were fixed in 4% paraformaldehyde after 0, 2, and 4 hours at 36°C. 5S rRNA localization was detected by RNA *in situ* hybridization using an ALEXA 594 fluorochrome-conjugated probe to 5S rRNA. White arrows indicate tubular structures in the cytoplasm.

(A-C) 5S rRNA localization in the strains *agv1*$^{+}$ (A), *agv1-1A1* (B), and *agv1-4A3* (C) at 25°C.

(D-F) 5S rRNA localization in the strains *agv1*$^{+}$ (D), *agv1-1A1* (E), and *agv1-4A3* (F) following 2 hours at 36°C.

(G-I) 5S rRNA localization in the strains *agv1*$^{+}$ (G), *agv1-1A1* (H), and *agv1-4A3* (I) following 4 hours at 36°C.

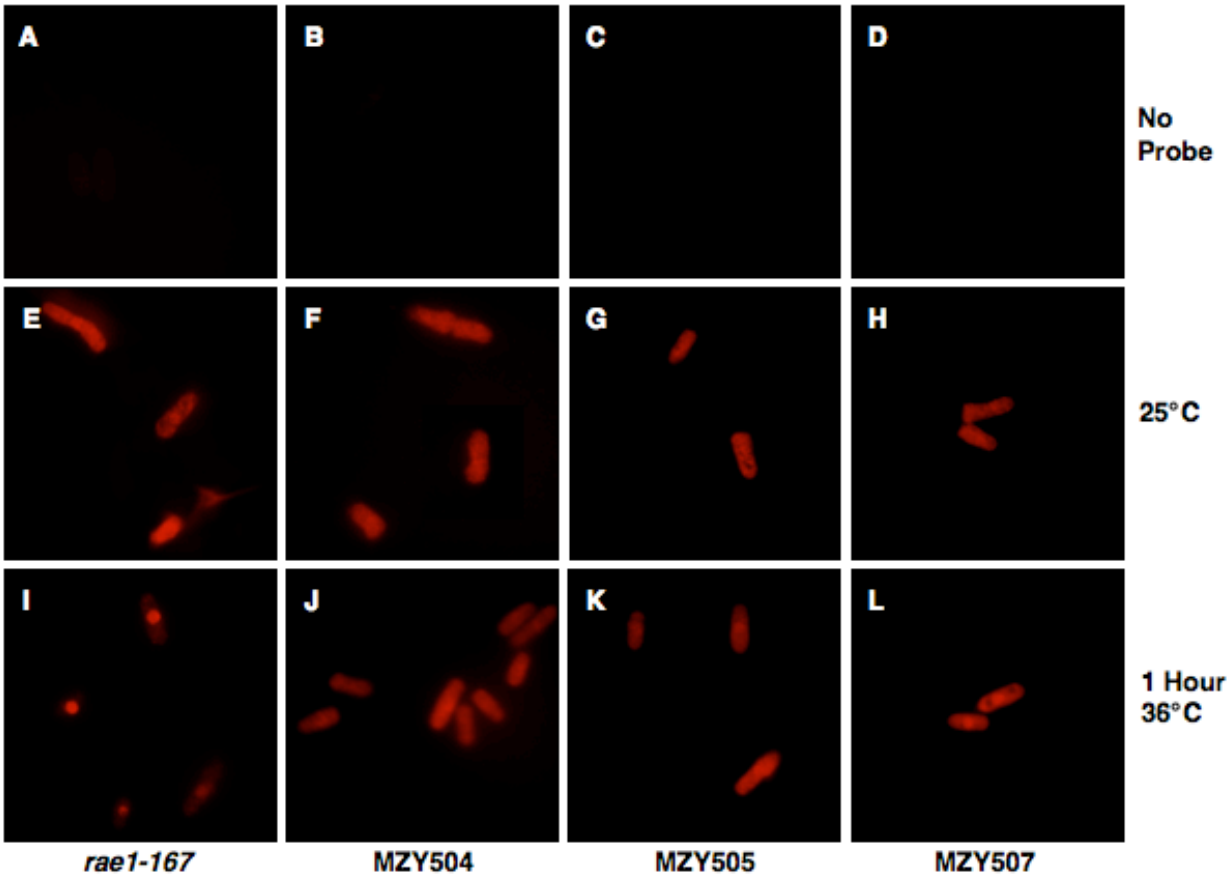
A
B
C
D
No Probe
E
F
G
H
25°C
I
J
K
L
1 Hour 36°C
rae1-167
MZY504
MZY505
MZY507

Figure S-1

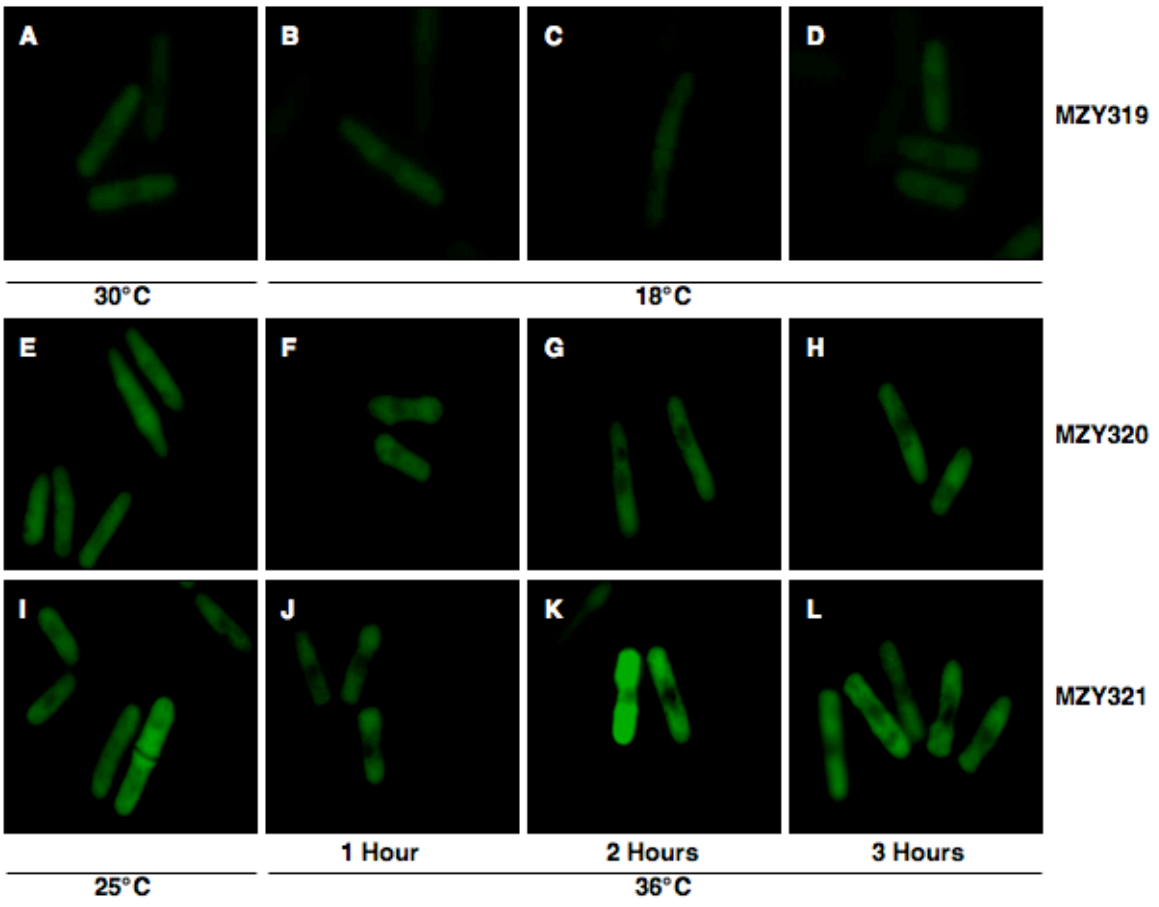
A
B
C
D
MZY319
30°C
18°C
E
F
G
H
MZY320
I
J
K
L
MZY321
1 Hour
2 Hours
3 Hours
25°C
36°C

Figure S-2

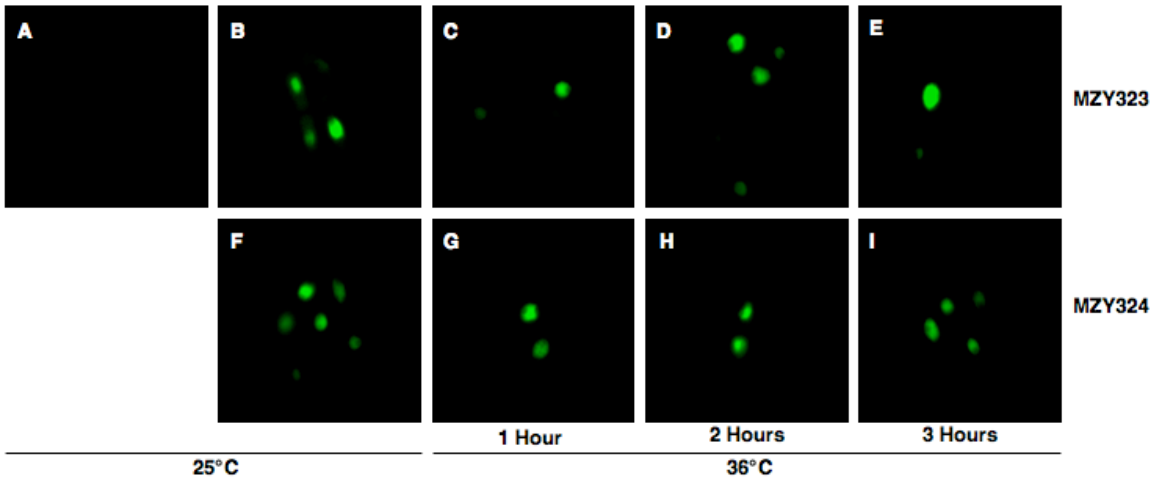

Figure S-3

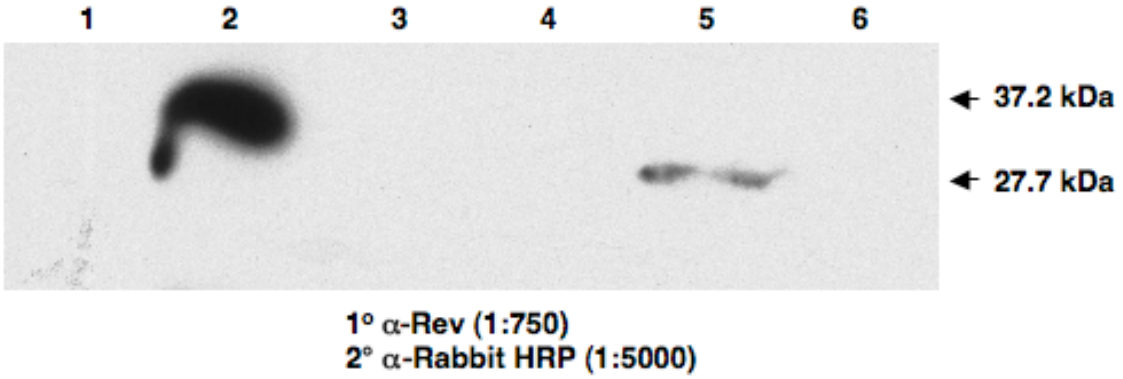

Figure S-4

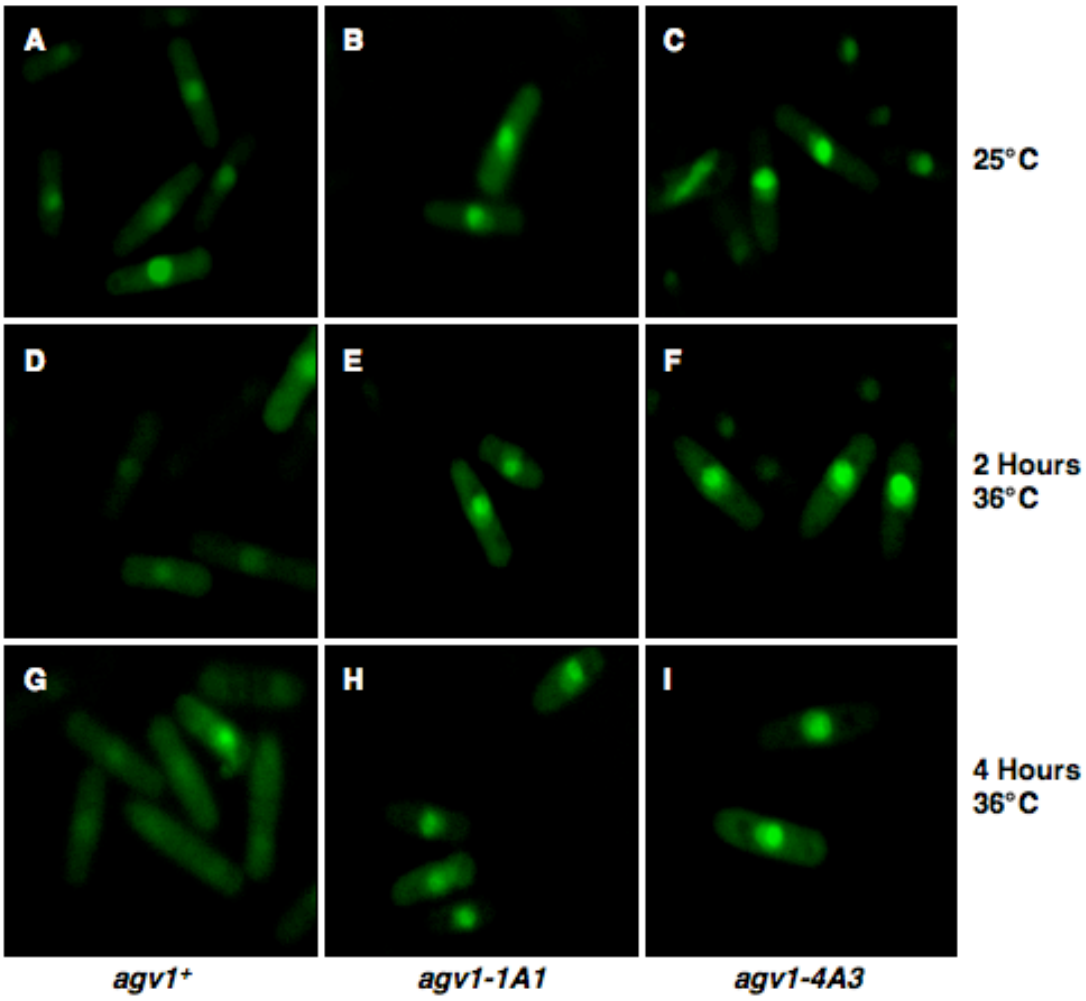

Figure S-5

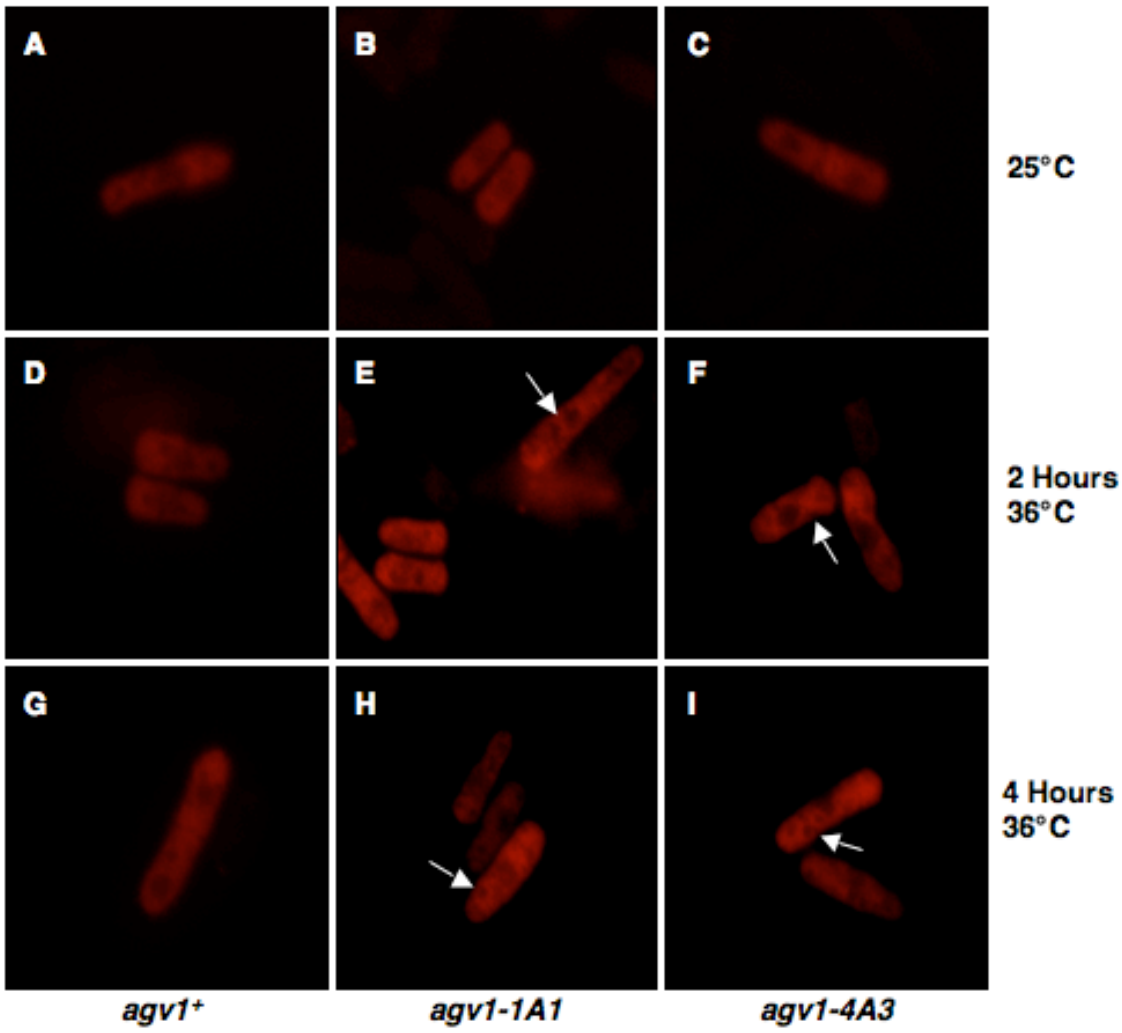

Figure S-6